Radio Astronomy

MSc. course

Lecture 8a,8b (of 14)

Calibration and Advanced radio interferometry

Prof. Mike Garrett
(ASTRON/Leiden/Swinburne)

Acknowledgements

I've tried to steal the best ideas and bring them together into a coherent picture that broadly covers radio astronomy - the technique and the science.

I acknowledge the following sources of information for this particular (2 x 45 min) lecture:

Publications (in order of usefulness):

Very Long Baseline Interfermetry Techniques and Applications, Marcello Felli, Ralph E. Spencer, Publisher: Kluwer - see in particular lectures by Peter WIlkinson and Craig Walker.

Astronomical Society of the Pacific Conference series Volume 180, Synthesis Imaging in Radio Astronomy II, G.B. Taylor, R.A. Perley, Publisher: Astronomical Society of the Pacific Conference

Very Long Baseline Interferometry and the VLBA: Napier, Diamond & Zensus., ASP Conf series, Vol 82, 1995.

Interferometry and Synthesis in Radio Astronomy (Second Edition), A.R. Thompson, J.M. Moran, G.W. Swenson Jr., Publisher: Wiley-VCH.

Presentations in the public domain (some acquired via google):

"Essential Radio Astronomy," Condon & Ransom (www.nrao.edu/course/astr534/Interferometers1.html)

Interacademiaal 2006 - Interferometry, Tom Oosterloo & Huib Jan van Langevelde, http://www.jive.nl/iac06/wiki/

Propogation effects, Steve Tingay SKADS School, Bologna.

Peeling - Tom Oosterloo, SKADS school.

MERLIN User Guide. Thomason et al.

Dan Briggs PhD thesis, 1995.

Tom Muxlow - wide-field imaging - ERIS school 2007.

If you want back-issues of lectures mail me!

Course overview

Each lecture (practcal session) is 2 x 45 minutes long. 15 minute break between each lecture.

Location: Oort 431

Time: Thursday at 1:45 - 2.30 pm and 2.45-3.30 pm
In February: 5/2, 12/2, 19/2. 26/2
In March: 5/3 (guest lecture), 12/3 (practical), 19/3, 26/3 (incl. 1 guest lecture Richard Schilizzi)
In April: 2/4, 9/4 (guest lecture, polarisation, Marijke Haverkorn), 16/4 (practical), 23/4 (N.B. no lectures on 30/4 Konningendag)
In May: 7/5 (guest lecture, HI, Raffaella Morganti, 14/5, (N.B. 21 May public holiday)

N.B. Field trip: visit to ASTRON, Westerbork and Exloo (date: 26 May!!!), no lecture that week.

Exam: by oral examination of the material - details to follow.

Course wiki page

www.astron.nl/~mag/dokuwiki/doku.php?id=radio_astronomy_course_description

- this is where you can find the most up-to-date course information - you can also find PDF copies of the lecture notes here and the overall content of the course.

Phase stability

In Lecture 4, we did not considered problems introduced by the distortions of the incoming wavefront as it passes through the Earth's atmosphere (troposhere and ionosphere). These introduce phase errors across the wave front that rapidly vary with time and across the radio telescope array.

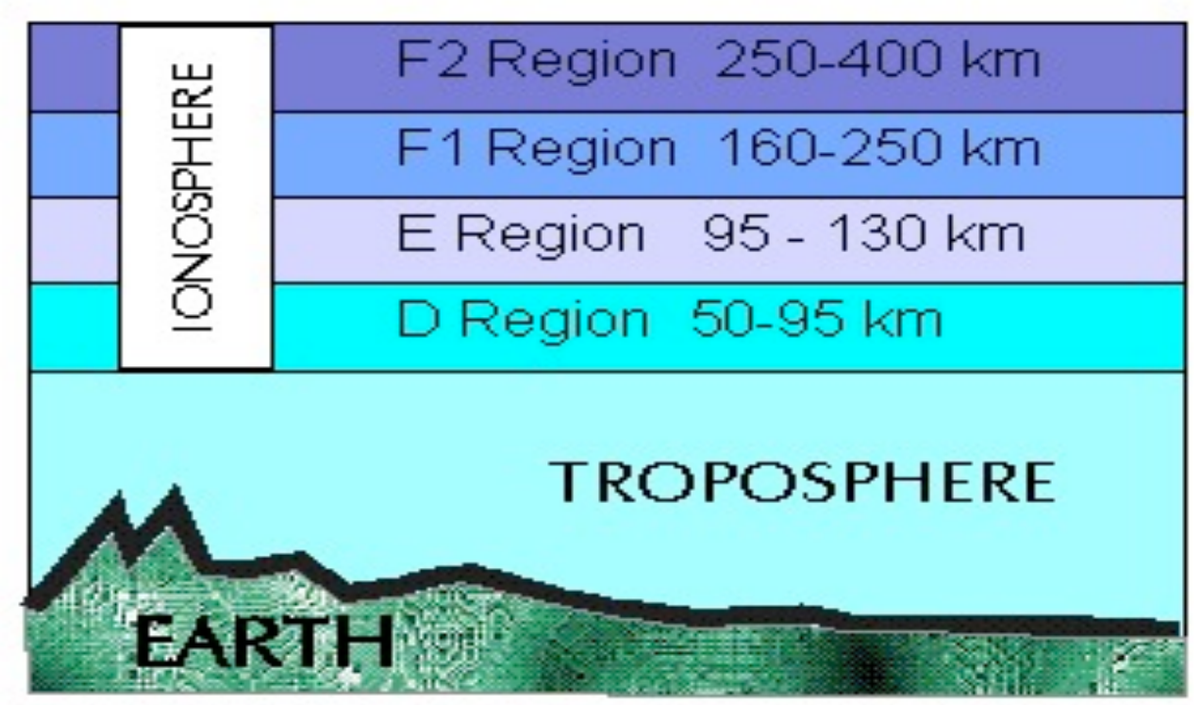

ionosphere

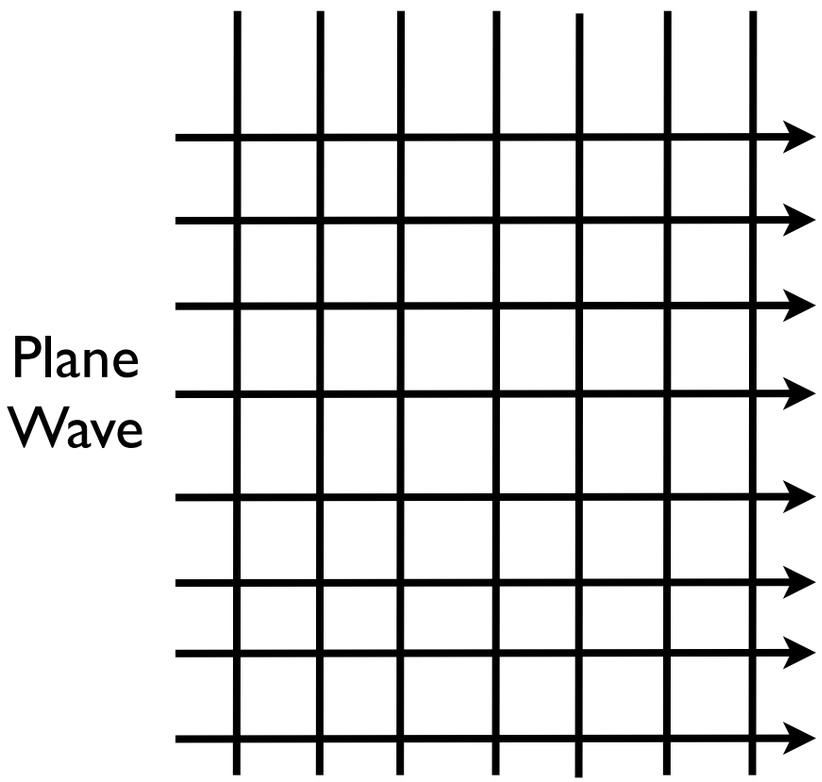

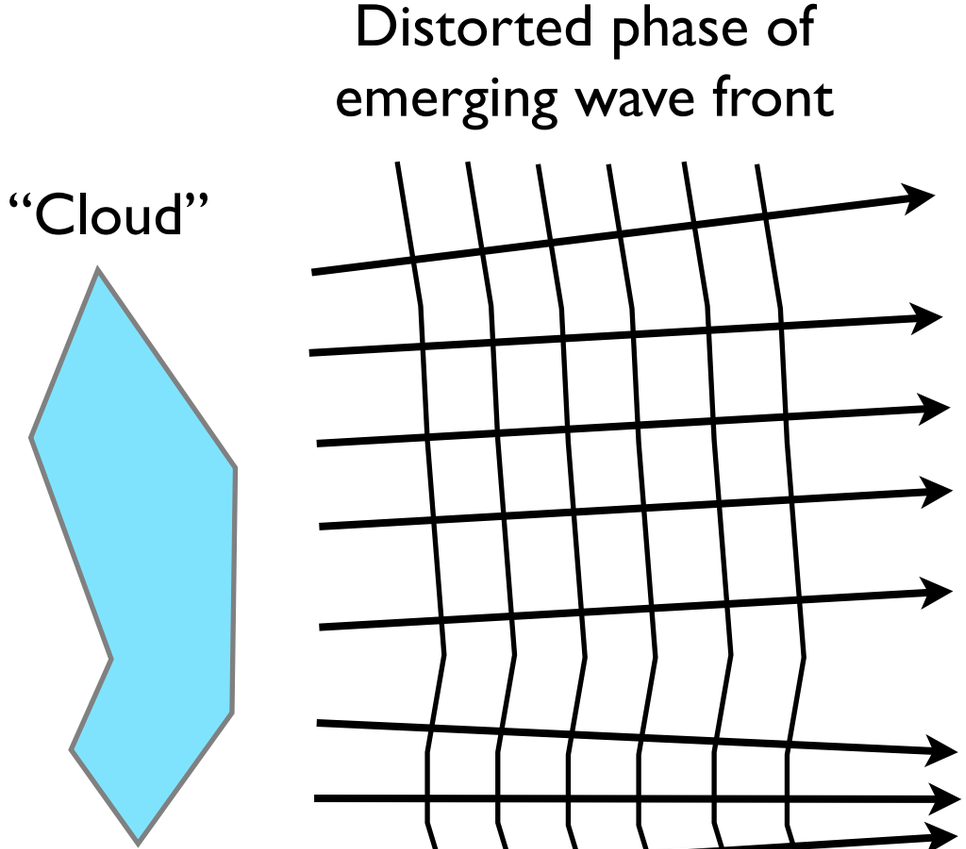

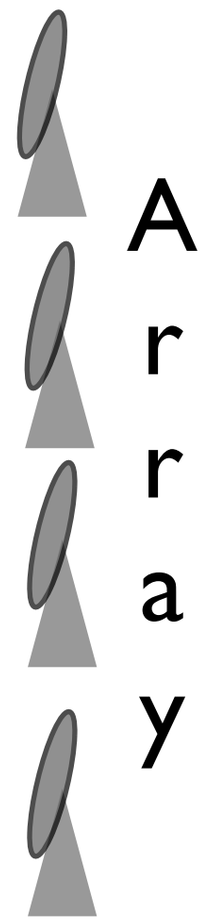

In radio astronomy the atmosphere can be stable over relatively long periods.

Coherence times (phase change < 1 radian in incoming wavefront) can be as long as ~ 10 minutes at cm wavelengths (mainly effected by water vapour in the troposphere) or as short as a few seconds at longer metre wavelengths (due to the fluctuations in the ionosphere's electron content) and millimetre/sub-millimetre wavelengths (again the troposphere):

Typical coherence times are:

Frequency	Good	Bad conditions
151 MHz	3 min	15 sec
480 MHz	10 min	45 sec
2 GHz	45 min	3 min
5 GHz	40 min	10 min
22 GHz	3 min	10 secs
200 GHz	0.5min	1 sec

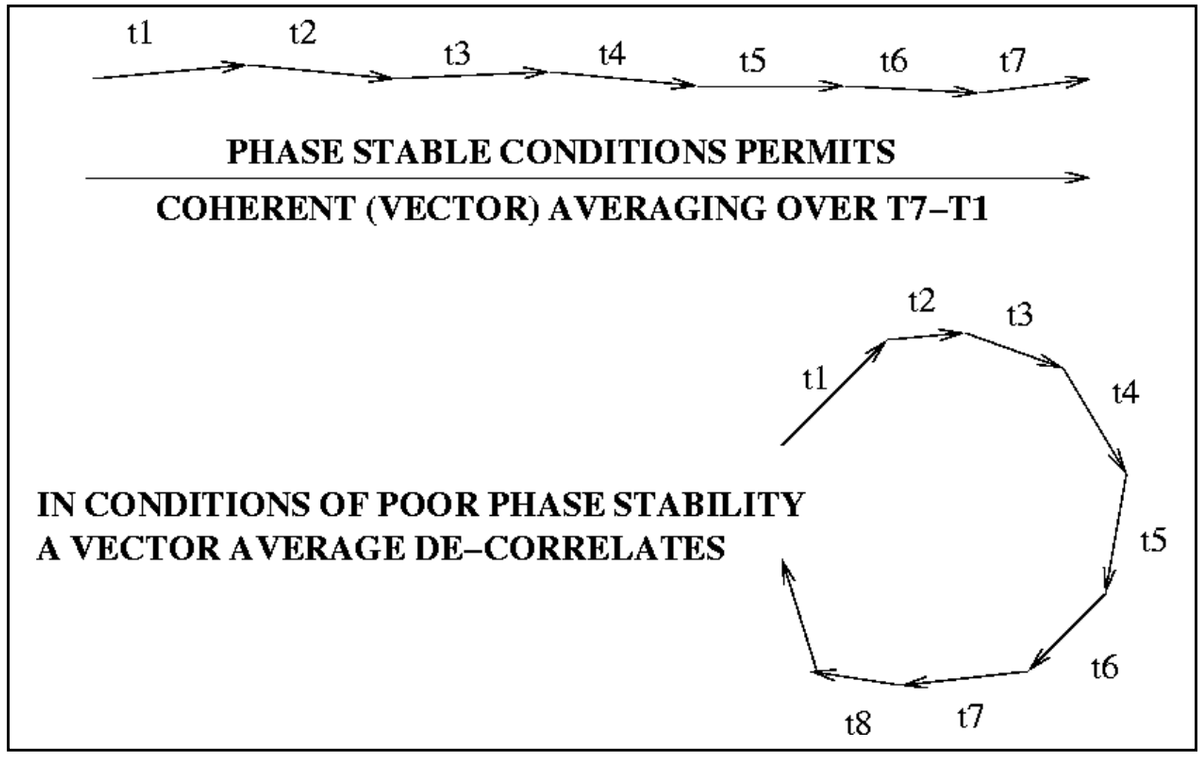

Stability at metre wavelengths is strongly dependent on solar cycle, time of day.

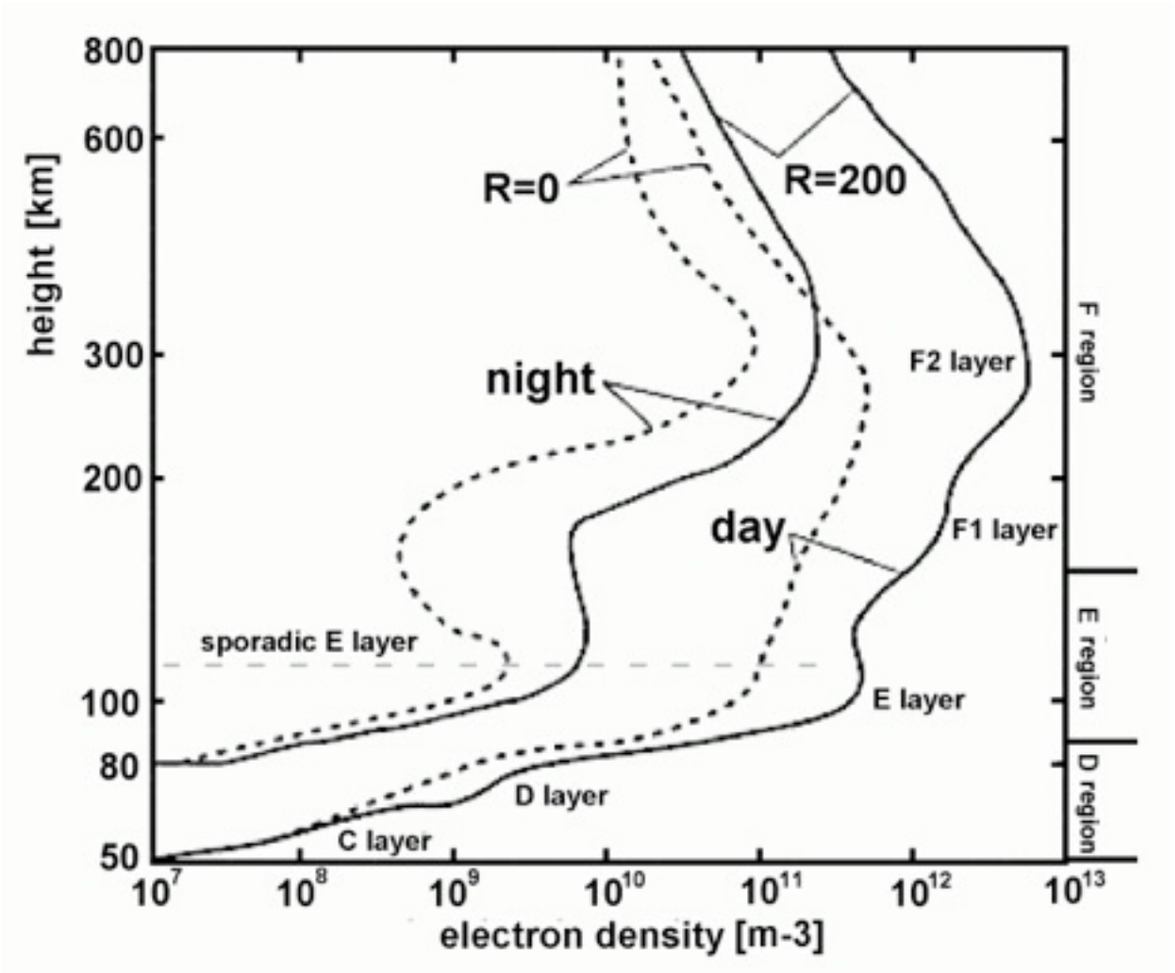

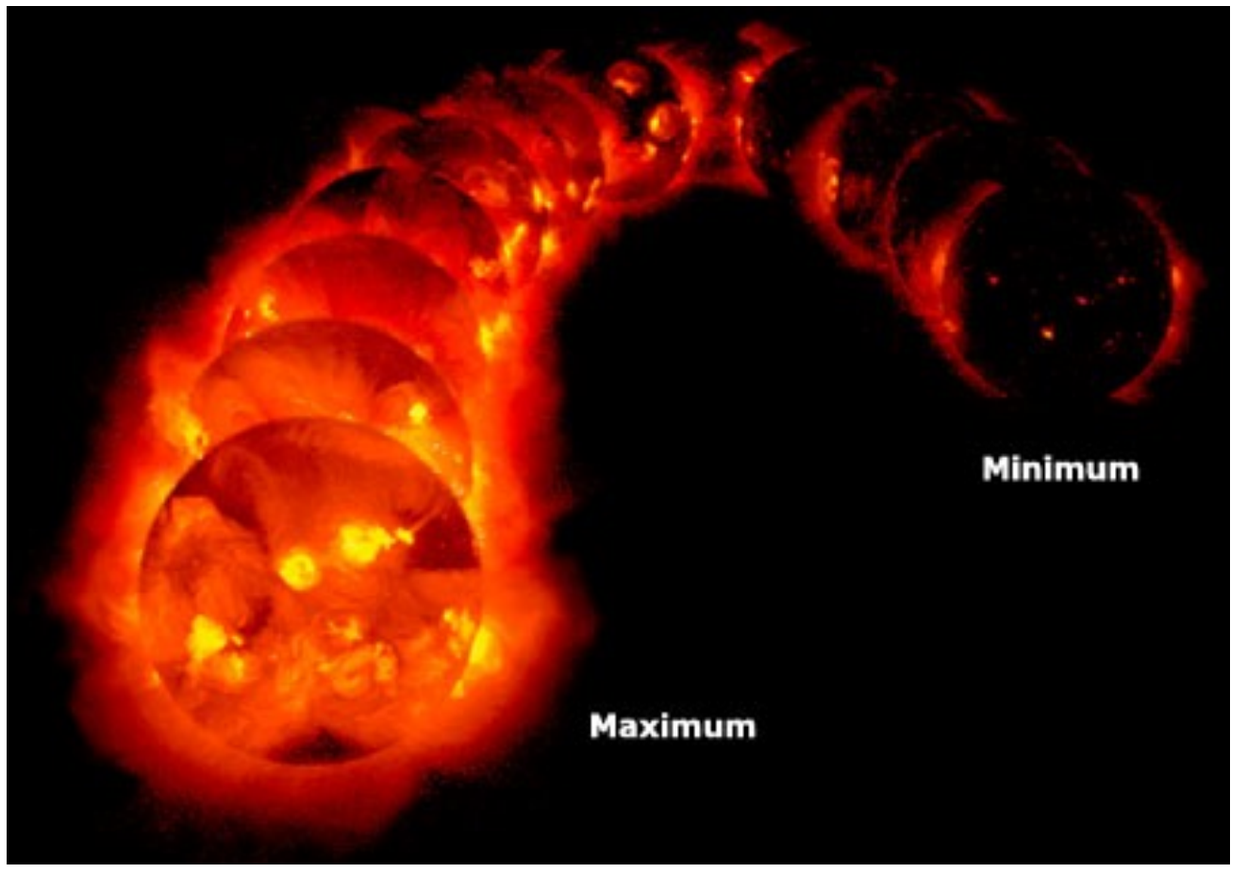

Next solar maximum is expected to peak in 2011 - sun expected to become active soon - worst possible timing for LOFAR! However, the most recent predictions suggest it may be the weakest solar maximum for 100 years (fingers crossed!).

Atmospheric path lengths

The chemical composition of the troposphere is essentially uniform, with the notable exception of water vapor. The water vapour is not well mixed with the rest of the troposphere and we refer to the "dry" and "wet" component.

The excess path length introduced by the troposhere is:

$$L_{trop} \sim \underbrace{0.228P_o}_{\text{dry cpt}} + \underbrace{6.3w}_{\text{wet cpt}} \quad \text{(cm)}$$

P_o = total atmospheric pressure at surface of Earth millibars
w = water vapour content above array (cm)

Typical values of L ~ 2 metres (8ns time delay). The dry component depends only on P_o and dominates L - however, it can be modeled to ~ 0.05cm. The wet part can only me modeled to ~ 2cm ==> wet component dominates phase errors.

Note that the troposphere path length is not a function of frequency (non-dispersive).

The ionosphere has three main layers (D, E, F) - ionisation state depends on solar uv and changes with time of day, season, latitude and solar activity. The excess path length at zenith introduced by the ionosphere is proportional to the Vertical Total Electron Content (VTEC):

$$L_{iono} \sim (40.3/\nu^2)\,VTEC \qquad \text{(metres)}$$

The TEC (column density) is in units of 10^{18} m^{-2} - typical values are ~ $5x10^{17}$ m^{-2} (max, day time), 5 x 10^{16} m^{-2} (min, night). At GHz frequencies L_{iono} ~ metres. TEC can be monitored via dual frequency GPS satellite signals (below). ν is in GHz.

The line of sight TEC goes as cos(ξ): $L_{iono} \sim (40.3/(\nu^2 \cos\xi))$ TEC => observations of source close to the horizon should be avoided.

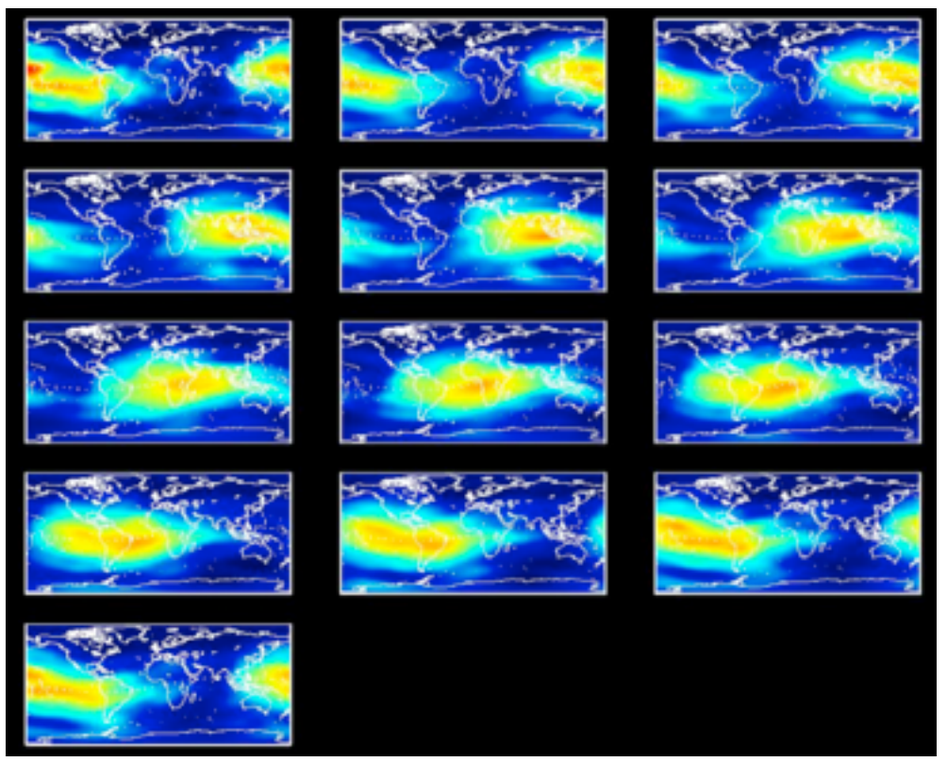

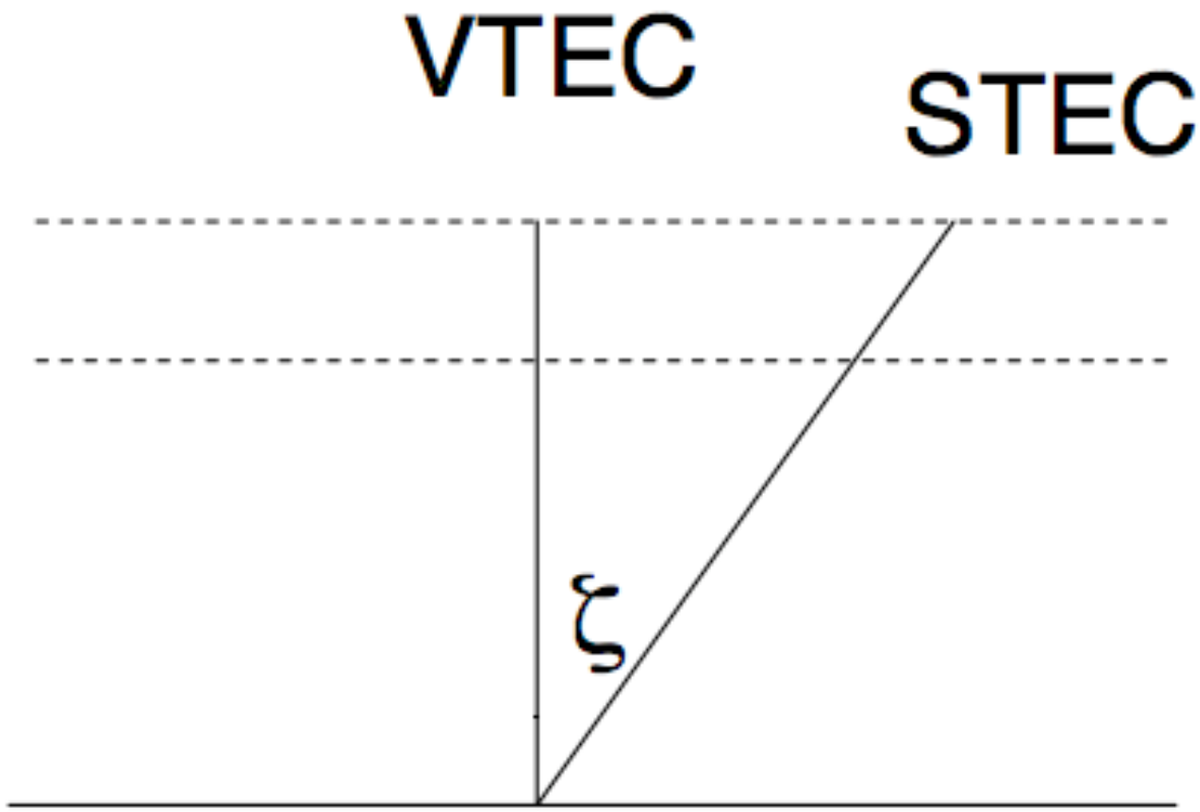

Since phase goes as: $\Phi \sim 2\pi\nu\tau \sim 2\pi\nu L/c$ .....

For ionosphere, $L \alpha \nu^{-2} \Rightarrow \Phi_{iono} \alpha \nu^{-1}$

For troposphere, $L \alpha \nu^{0} \Rightarrow \Phi_{trop} \alpha \nu$

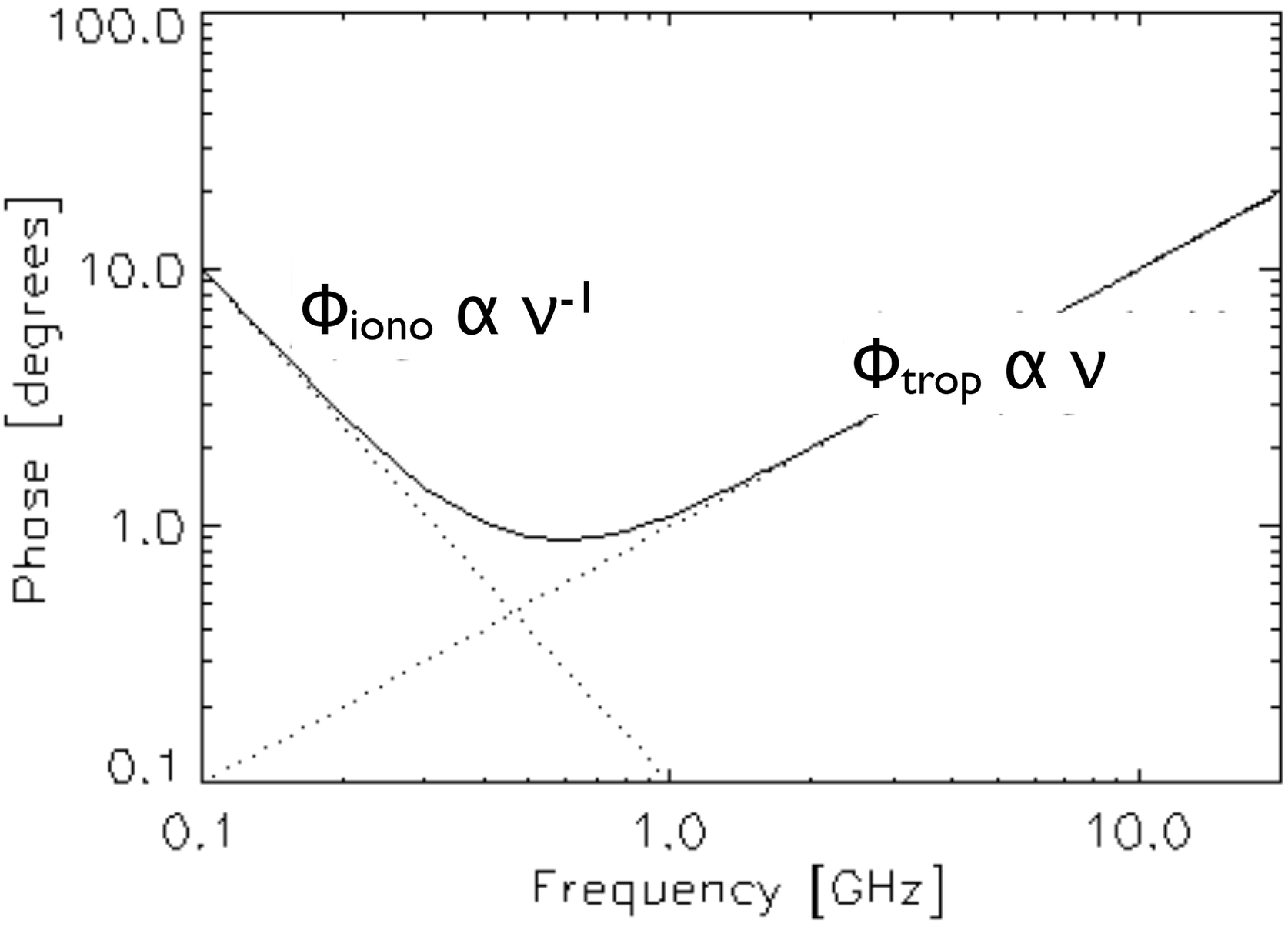

It turns out that the frequency at which phase errors are minimised is around 1 GHz (left).

Consider three telescopes observing the same source on the sky. Lets ignore small (uncorrelated) thermal noise errors associated with each telescope. Since the telescopes are all well separated from each other (e.g. > 1 km) they each look through a different part of the Earth's atmosphere:

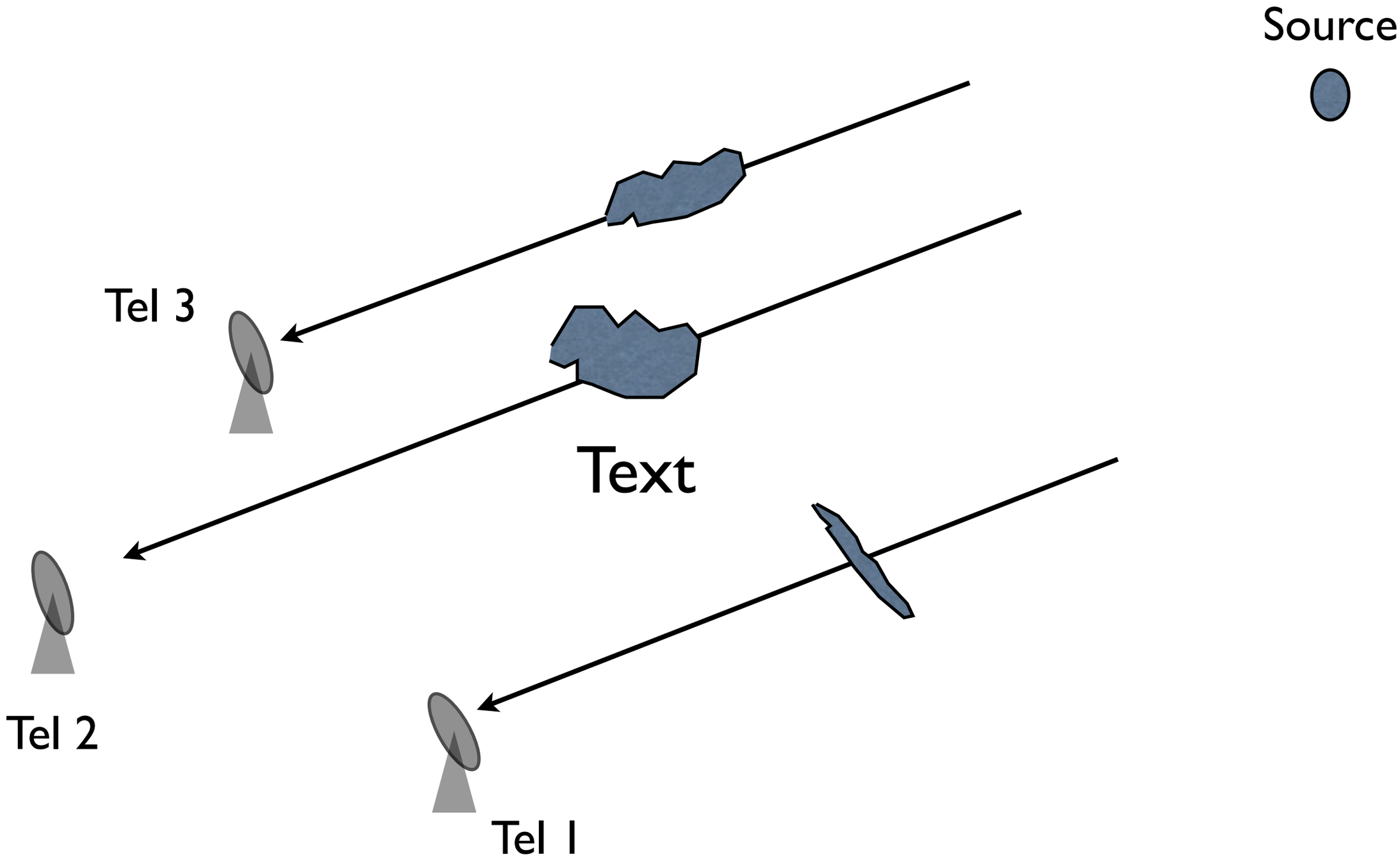

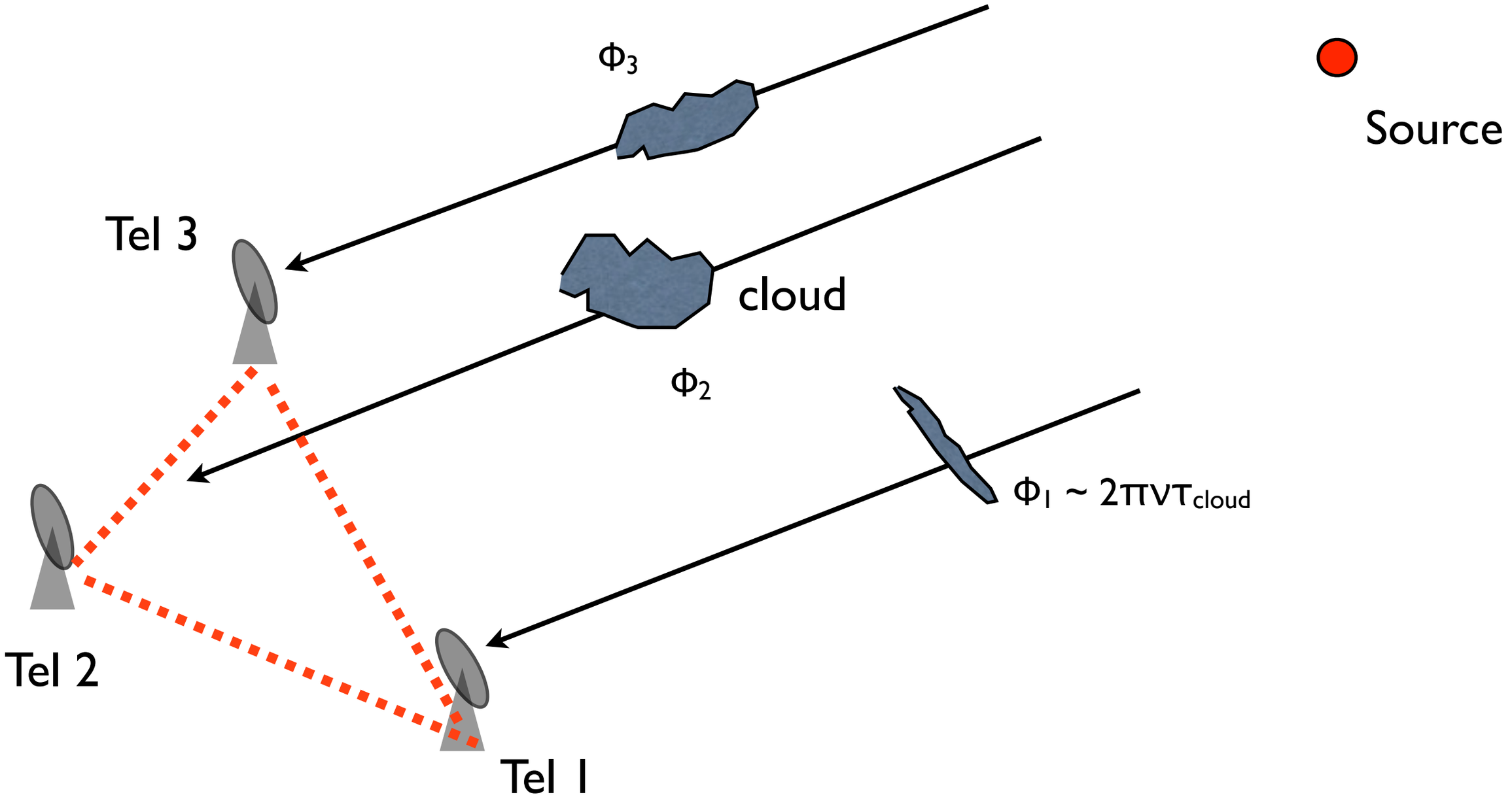

The measured visibility phase on baseline "12" is then: $\Phi_{12} = \varphi_{12} + \phi_1 - \phi_2$ [1]

where φ_{12} is the true source visibility on baselines 1-2, Φ_1 are phase offsets introduced by the clouds above each telescope.

So:

$$\Phi_{12} = \varphi_{12} + \phi_1 - \phi_2$$
$$\Phi_{23} = \varphi_{23} + \phi_2 - \phi_3 \qquad [2a]$$
$$\Phi_{31} = \varphi_{31} + \phi_3 - \phi_1$$

Clearly if we add these relations together:

$$\Phi_{12} + \Phi_{23} + \Phi_{31} = \varphi_{12}+\varphi_{23} + \varphi_{31} +(\phi_1 - \phi_1) +(\phi_2 - \phi_2)+(\phi_3 -\phi_3)$$

closure phase $$= \varphi_{12}+\varphi_{23} + \varphi_{31} \qquad [2b]$$

This formulation of adding together the observed visibility phases together of any 3 telescopes is known as forming a "closure triangle". [2b] is known as the closure phase for these 3 telescopes.

N.B. the important thing to note is that the closure phase contains information only on the true visibility of the source itself, i.e. its brightness distribution - ALL other telescope based errors cancel out (e.g. atmosphere, cable lengths, electronics etc.).

The concept of closure phase was first discovered by Roger Jennison:

A PHASE SENSITIVE INTERFEROMETER TECHNIQUE FOR THE MEASUREMENT OF THE FOURIER TRANSFORMS OF SPATIAL BRIGHTNESS DISTRIBUTIONS OF SMALL ANGULAR EXTENT

R. C. Jennison

MNRAS 1958

(Communicated by A. C. B. Lovell)

(Received 1958 February 21)

Summary

A method is described whereby the amplitude and phase of the complex Fourier transform of a spatial brightness distribution of small angular extent may be uniquely determined from a series of measurements with a triple interferometer system. Absolute measurement of the amplitude function is available, whilst measurements of phase are relative to a datum obtained at short aerial spacings. A practical radio frequency interferometer incorporating the principle is described and its operation is discussed.

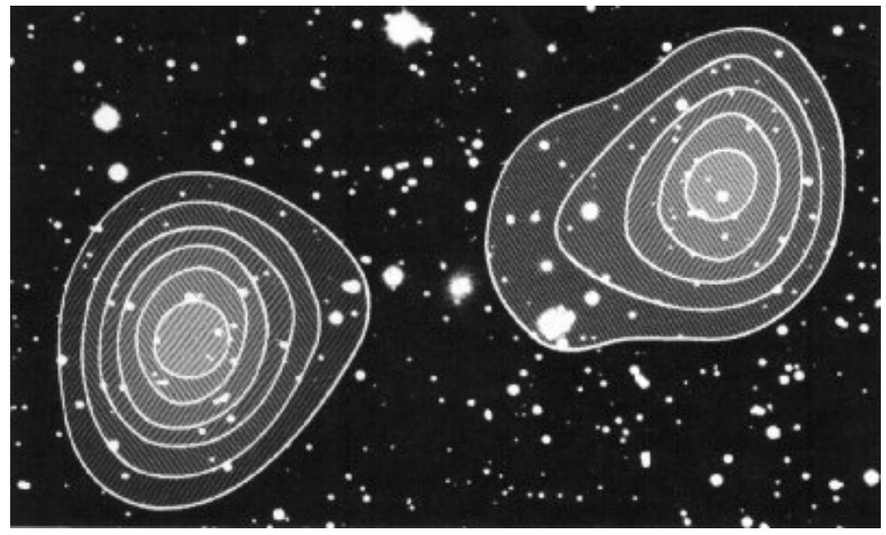

Jennison discovered closure phase while performing the first interferometry experiments at Jodrell Bank, using the mobile telescope. The technique made it possible to infer double structure in Cyg-A.

The concept of Closure Phase is important not only in radio astronomy but forms the basis for ALL interferometry calibration at IR and optical wavelengths.

For a given array of N telescopes, there are:

(N-1)(N-2)/2 independent closure phases [3]

e.g. for N=4 there are 3 *independent* closure relations.

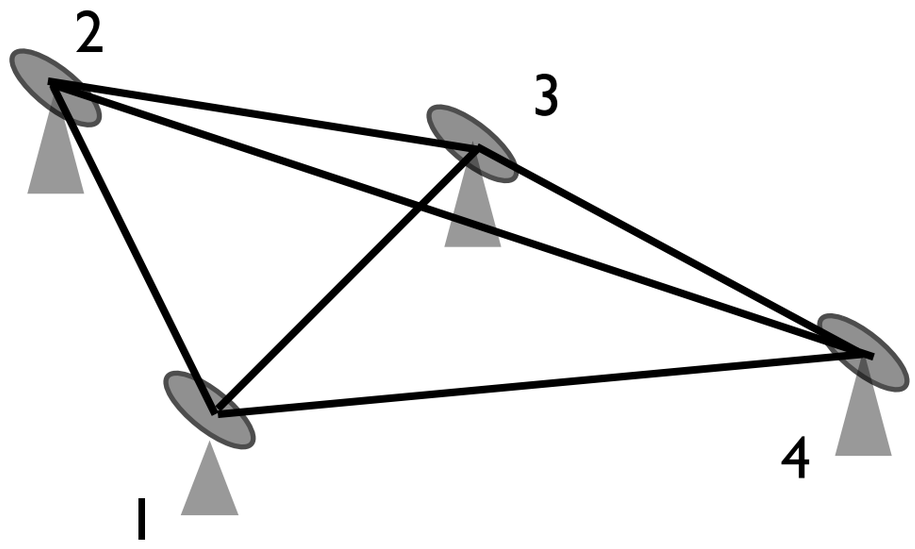

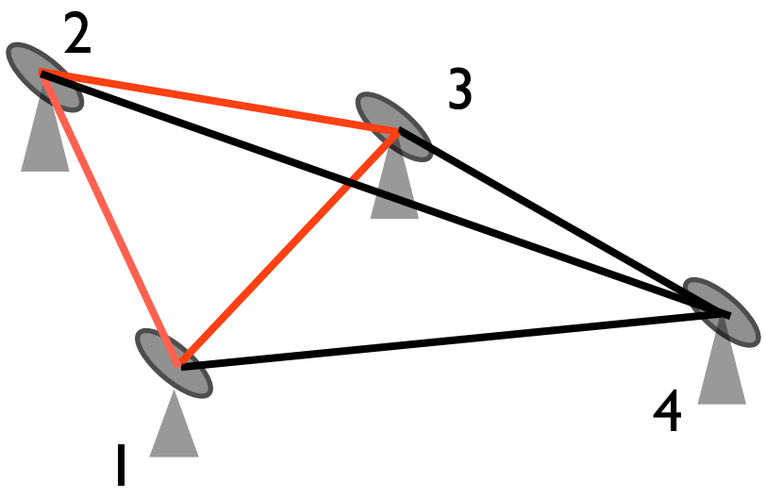

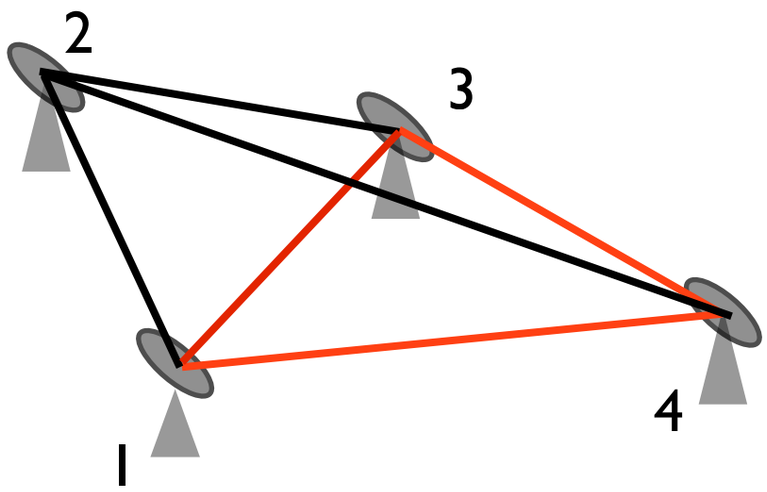

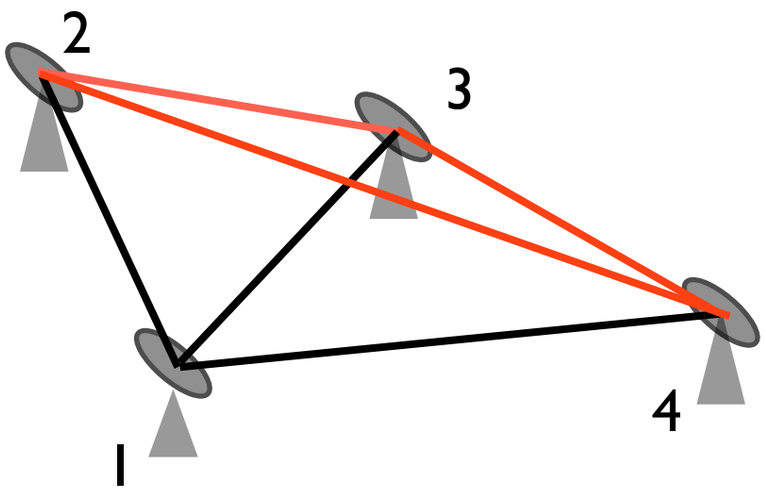

Visibility phase plotted for 3 telescopes of the VLBA (not fully calibrated):

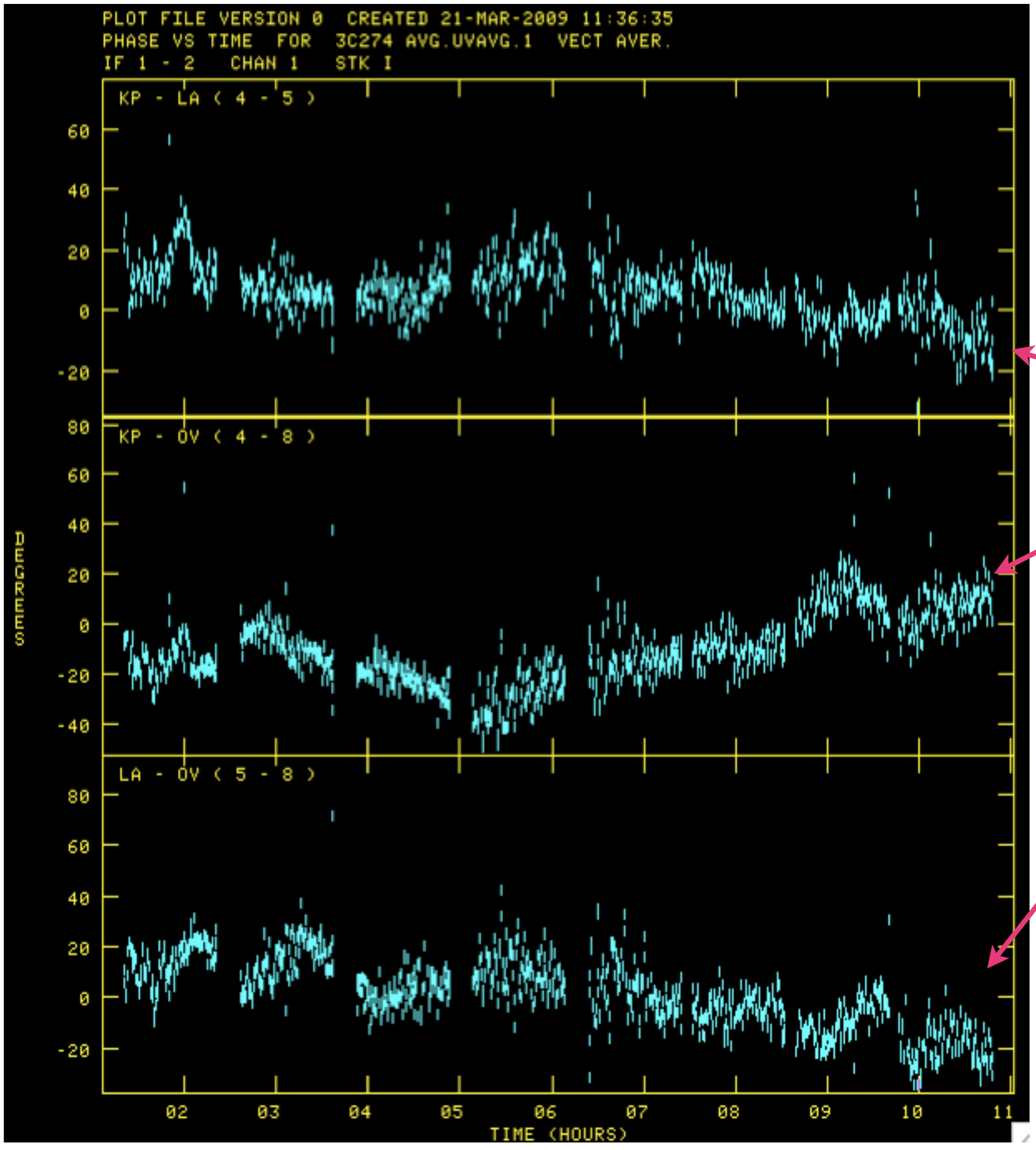

Tells us something about the source visibility phase, plus the atmospheric induced phase distortions, telescope electronic gain changes etc. etc.

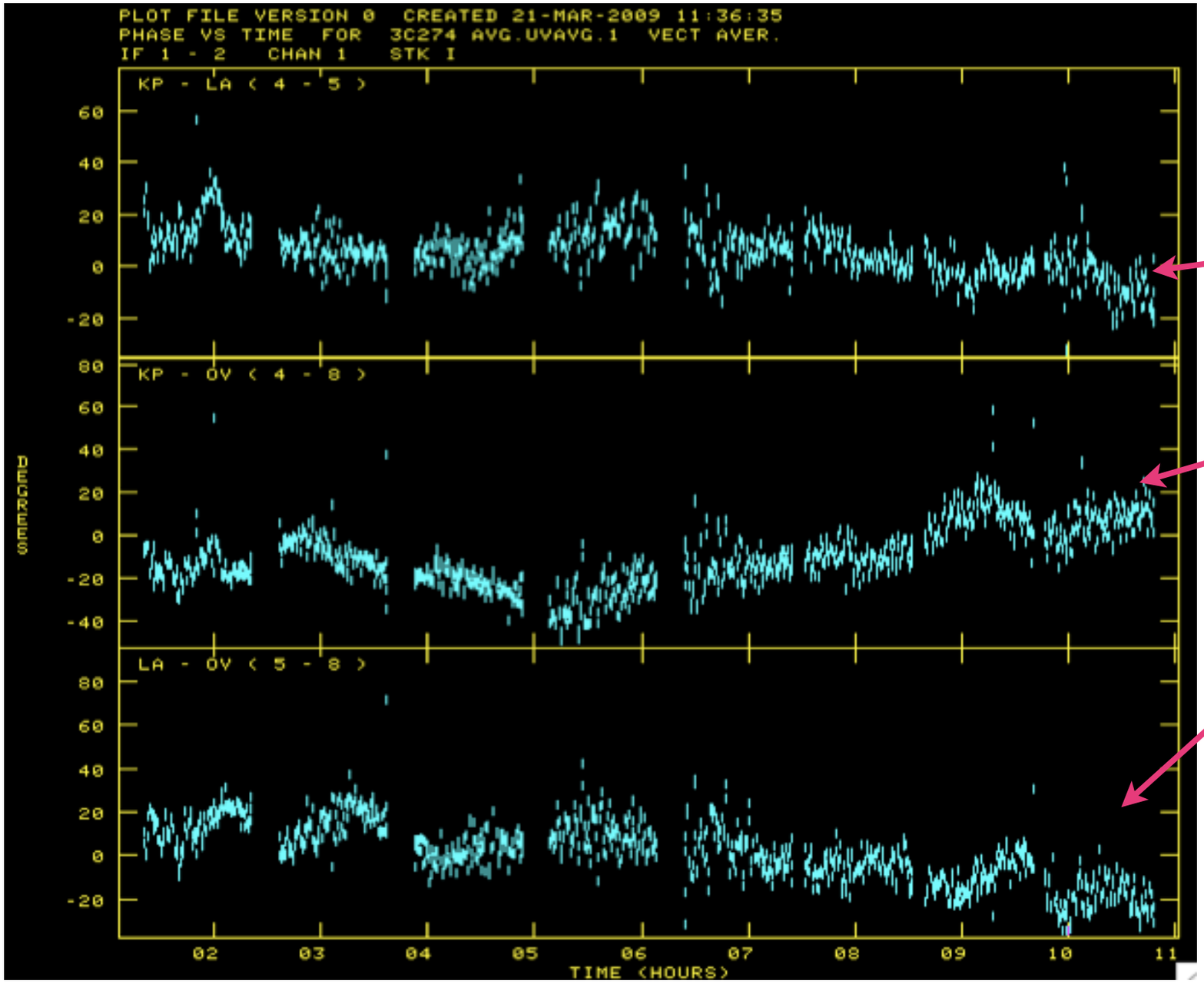

Tells us something about the source visibility phase, the atmospheric induced distortions to the phase, telescope electronic etc.

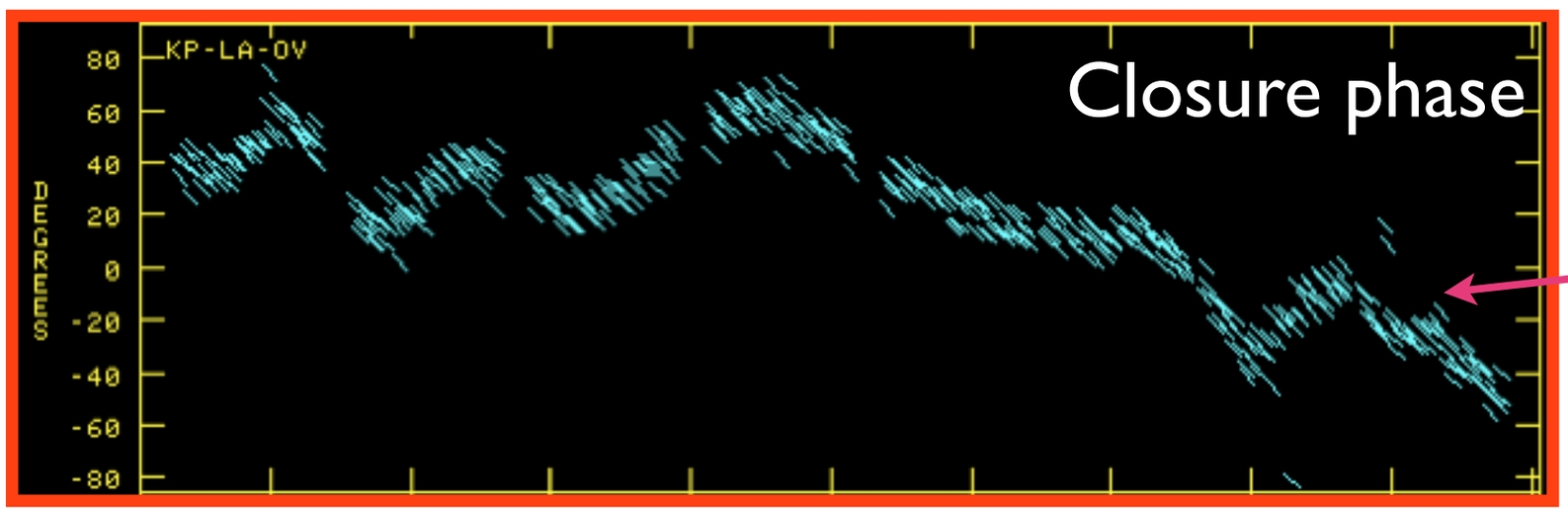

Closure phase

Closure phase: tells us something about the source visibility alone!

So from the closure relations we have (N-1)(N-2)/N good observables (measurements).

However, there are N telescope unknowns. We can reduce this to (N-1) unknowns if we make one of the telescopes the "reference antenna" (i.e. set the phase error to zero for this telescope).

Note that the ratio of *good observables/unknowns* (see eqn[3]) is then just:

$$(N-2)/N \quad [4]$$

So for N=3 we have only 33% of the information we need.

But for N=27 (the case of the VLA) we have 93% of the information we need.

==> *in general the reliability of Interferometric images favours large-N telescope arrays (e.g. see SKA, ALMA and SKA pathfinders) - calibration is more robust and uv-coverage more complete.*

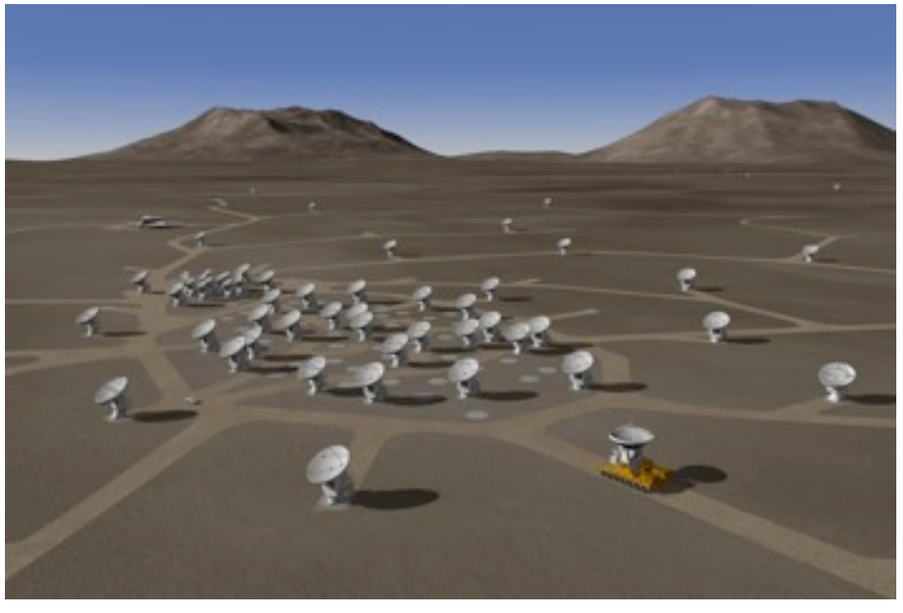

Even in the case of large-N, some extra a-priori information must be used to make progress, in the calibration of interferometry data. In particular, we make a few assumptions:

(i) the sky is positive

(ii) the brightness distribution the interferometer is sensitive to is of limited extent.

With these assumptions in place, we can begin to make progress.

Recall eqn [1]:

$$\Phi_{12} = \varphi_{12} + \phi_1 - \phi_2$$

We can generalise this to:

$$\Phi_{ij} = \varphi_{ij} + \phi_i - \phi_j \qquad \text{for any telescope pair i,j}$$

The phase error associated with telescope j is then, Φ_j such that:

$$\phi_j = \Phi_{ij} - \varphi_{ij} - \phi_i$$

For any given array we can, for one of the telescopes in the array (the so-called reference telescope), set $\phi_i = 0$. All measurements then become made relative to this telescope. (N.B. one consequence of this is that information about absolute position is lost).

In this case,

$$\phi_j = \Phi_{ij} - \varphi_{ij} \quad [5]$$

Now the cheeky part - the astronomer guesses what the source looks like, i.e. we define a trial map: φ_{ij}^{trial} then [5] becomes:

$$\phi_j = \Phi_{ij} - \varphi_{ij}^{trial} \quad [6]$$

In this way we can make guestimates of the various telescope based errors.

Usually the trial model is a simple point source.

This process of estimating the telescope errors is called *self-calibration*. The "self" refers to the fact that we use the source itself (and the associated data) to solve for the telescope errors. See the article by Peter Wilkinson for more details (see acknowledgements).

The entire process of making the best possible image is called *"hybrid mapping"*. The first trial model (usually a point source) provides the first estimate of the telescope errors. Once corrections are applied to the telescopes, the first "real" map is produced (e.g. via CLEAN). This becomes the new trial map for a new (and hopefully improved) set of telescope corrections. A new map is then again produced and this iterative cycle continues until the map (image) no longer improves (e.g. the thermal noise in the image does not decrease).

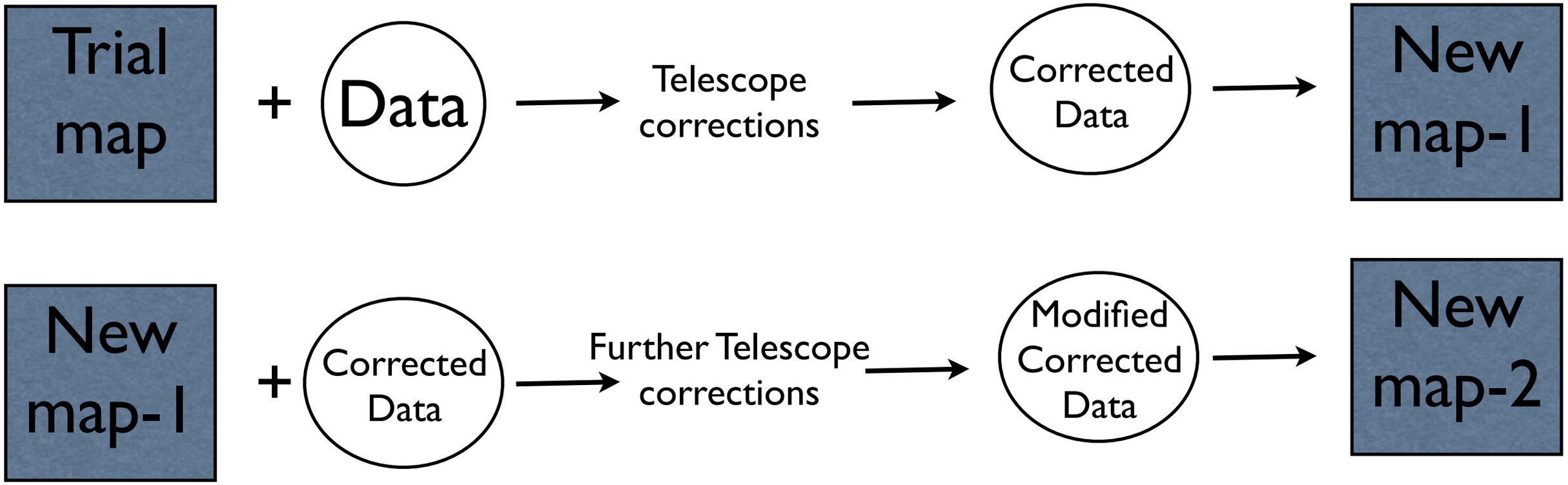

and so it continues... until the map converges.

Telescope errors do not only effect the phase of the visibility. The amplitude can also be degraded. However, phase errors usually dominate (at least at cm wavelengths where attenuation by the atmosphere is a relatively small effect).

In order to consider how self-calibration can be used to correct for amplitude errors, we must use a complex formalism:

$$V_{ij}^{obs}(t) = g_i(t)\, g^*_j(t)\, V_{ij}^{true}(t) \qquad [7]$$

where V_{ij} are the measured and true visibilities, and $g_i(t)\, g^*_j(t)$ are known as the complex gains of the telescopes i,j

The gains contain corrections to both the amplitude and phase of the visibility:

e.g. $g_i(t)=a_i(t)e^{i\phi_i(t)}$

In this formalism the observed and true Visibility can be written as:

$$V_{ij}^{obs}(t) = a_i(t)\, a_j(t)e^{i(\phi_i - \phi_j)}\, A_{ij}(t)e^{i\,\varphi ij(t)} \qquad [8] \qquad **$$

$$V_{ij}^{true}(t) = A_{ij}(t)\, e^{i\,\varphi ij(t)} \qquad [9]$$

Note that by taking the ratios of eqns such as [7] we arrive at the "closure quantities". e.g.

$$V_{12}^{obs}(t) = g_1(t)\, g_2(t)\, V_{12}^{true}(t) = a_1(t)e^{i\phi_1(t)}\, a_2(t)e^{-i\phi_2(t)}\, A_{12}(t)\, e^{i\,\varphi_{12}(t)}$$

$$V_{23}^{obs}(t) = g_2(t)\, g_3(t)\, V_{23}^{true}(t) = a_2(t)e^{i\phi_2(t)}\, a_3(t)e^{-i\phi_3(t)}\, A_{23}(t)\, e^{i\,\varphi_{23}(t)}$$

$$V_{13}^{obs}(t) = g_1(t)\, g_3(t)\, V_{13}^{true}(t) = a_1(t)e^{i\phi_1(t)}\, a_3(t)e^{-i\phi_3(t)}\, A_{13}(t)\, e^{i\,\varphi_{13}(t)}$$

If we consider the phase terms only and implicitly accept time dependance:

$$V_{12}^{obs}\, V_{23}^{obs} / V_{13}^{obs} = e^{i(\phi_1-\phi_2+\varphi_{12}+\phi_2-\phi_3+\varphi_{23})}\, e^{-i(\phi_1-\phi_3+\varphi_{13})}$$

$$= e^{i(\varphi_{12}+\varphi_{23}-\varphi_{13})} \quad [10]$$

Note that [10] is just the equivalent of our original closure phase presented in eqn[2b]

If we consider only the amplitude terms, we can see that for some combination of observed visibilities, the amplitude gains will cancel:

$$V_{12}^{obs}V_{34}^{obs}/(V_{13}^{obs}V_{24}^{obs}) = \frac{A_{12}A_{34}\,a_1a_2a_3a_4}{A_{13}A_{24}\,a_1a_2a_3a_4} = \frac{A_{12}A_{34}}{A_{13}A_{24}} \qquad [11]$$

Such ratios are known as "closure amplitudes" and require *at least 4* telescopes to be formed.

Like closure phases, closure amplitude is a "good observable", since it is not sensitive to measurement error. The closure amplitude and closure phase relations can be exploited in the hybrid mapping algorithm (see earlier slides).

In the early days of hybrid mapping the closure phases and amplitudes were explicitly used to constrain the hybrid mapping process. In the era of the VLA it was no longer computationally efficient to calculate all the closure quantities. More sophisticated algorithms were constructed but they are all roughly equivalent to the original method. Modern algorithms seek to minimise the difference between the observed data and the predicted data:

$$S = \Sigma_{ij,\, i<j} w_{ij} \left| V_{ij}^{obs} - g_i g^*_j V_{ij}^{true} \right| \qquad [12]$$

The w_{ij} reflect the fact that some data are higher weighted than other data (e.g. especially for VLBI arrays where all the telescopes have different sensitivities).

Algorithms using eqn [12] seek to minimise S by changing only the N-1 complex gains of the telescopes via a least squares approach. This is known as "self-calibration". In this formulation the problem can be considered to be over constrained (there are N(N-1)/2 measurements and only (N-1) unknowns).

The output of the algorithm is a list of telescope corrections (i.e. phase and amplitude = $g_i(t)$) as a function of time.

Note that by only modifying the telescope gains g_i (i.e. a_i , ϕ_i) the corrected data is always consistent with the closure quantities.

Hybrid mapping in practice

Here we will try and demonstrate hybrid mapping in practice via a VLBA data set.

The observing frequency is 327 MHz (as low as the VLBA goes and an area of the spectrum that has a lot of RFI, ionospheric disturbances also make it a potentially difficult data set to calibrate).

The observing bandwidth is 16 MHz, so the data rate (per telescope) is:

16E6 x 2 (Nyquist sampling) x 2 polarisations x 2-bits = 128 Mbits/sec.

The target source is 3C274 (also known as Virgo-A, M87 - AGN - lies only 16 Mpc away):

3C274 - VLA 90cm

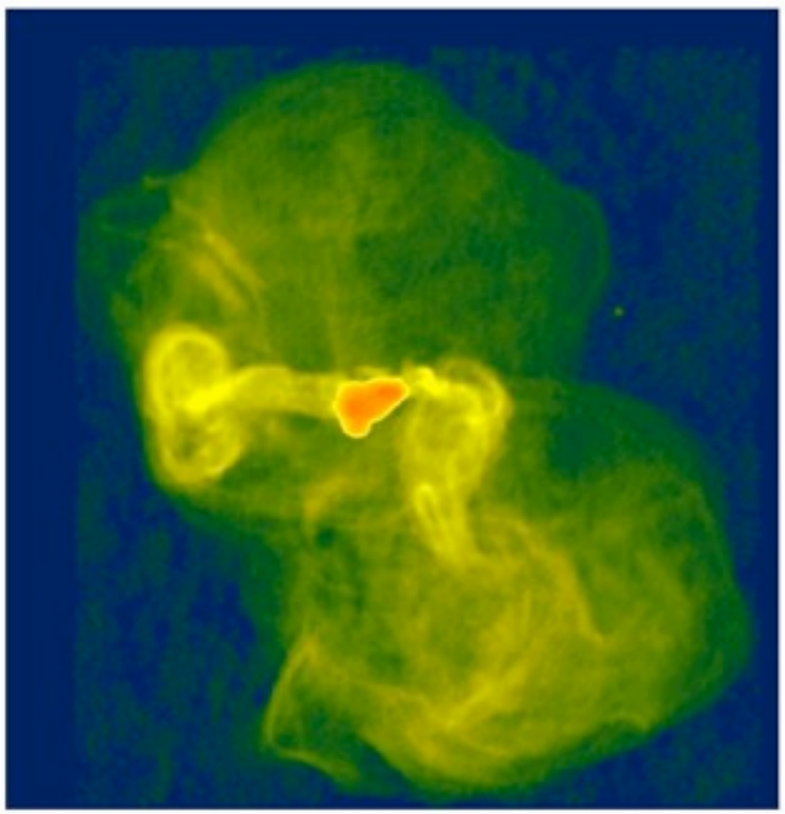

Plot of the original data (baselines to PT)

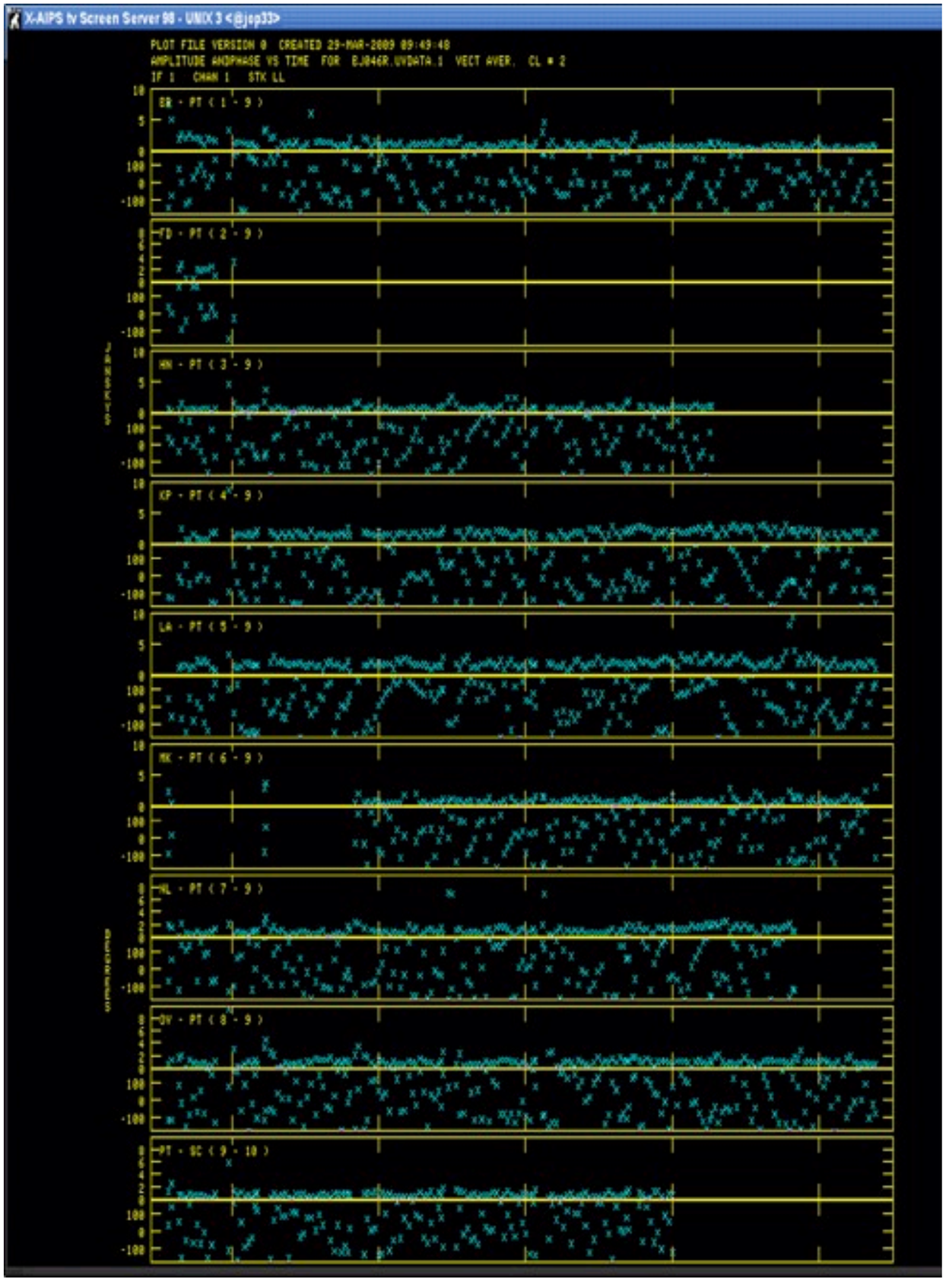

Plot of the antenna phase corrections after self-cal (LA is the reference antenna)

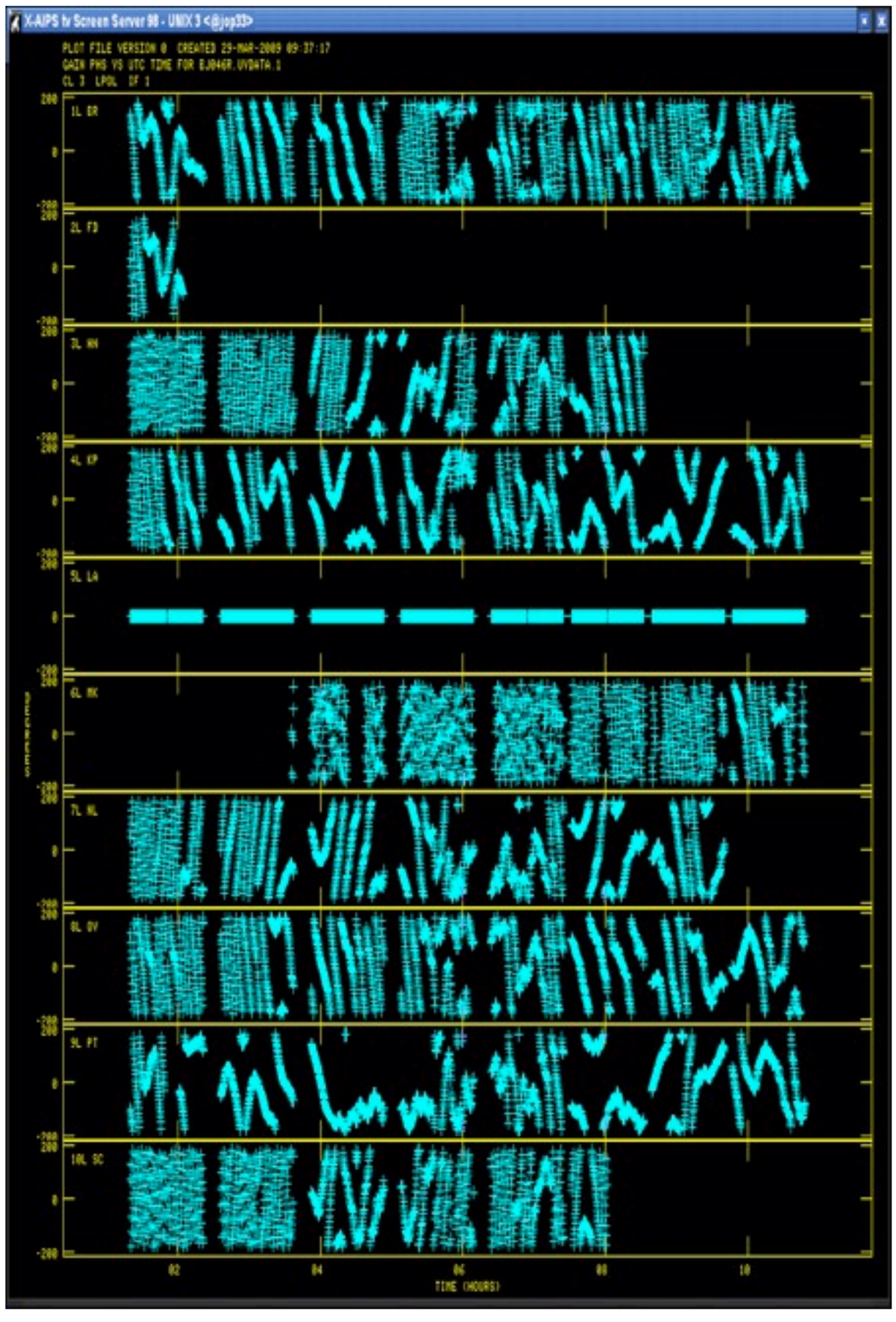

Plot of the original data (baselines to PT)

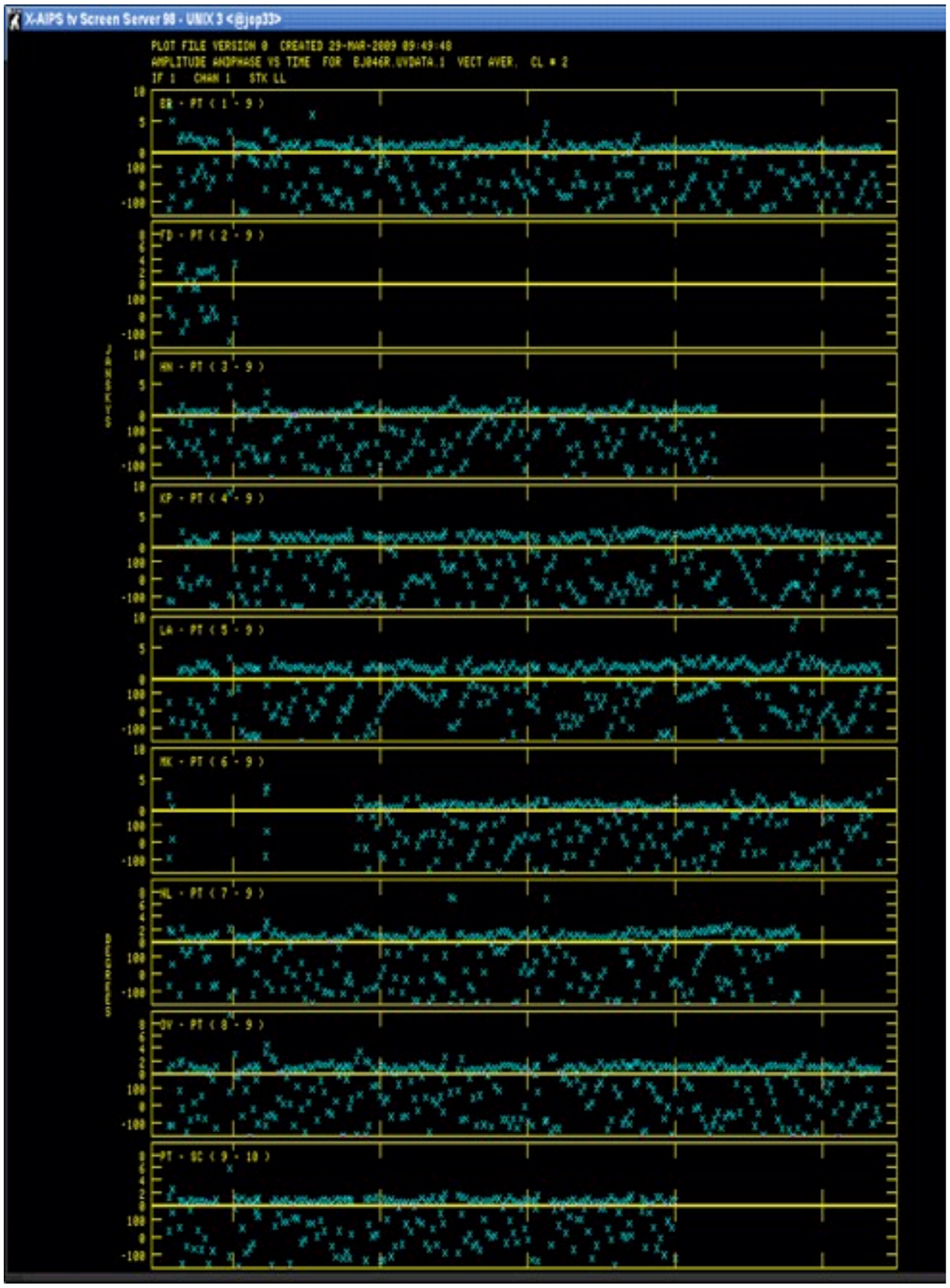

Plot of the data after applying self-cal corrections (baselines to PT only shown) - note data is now much more coherent.

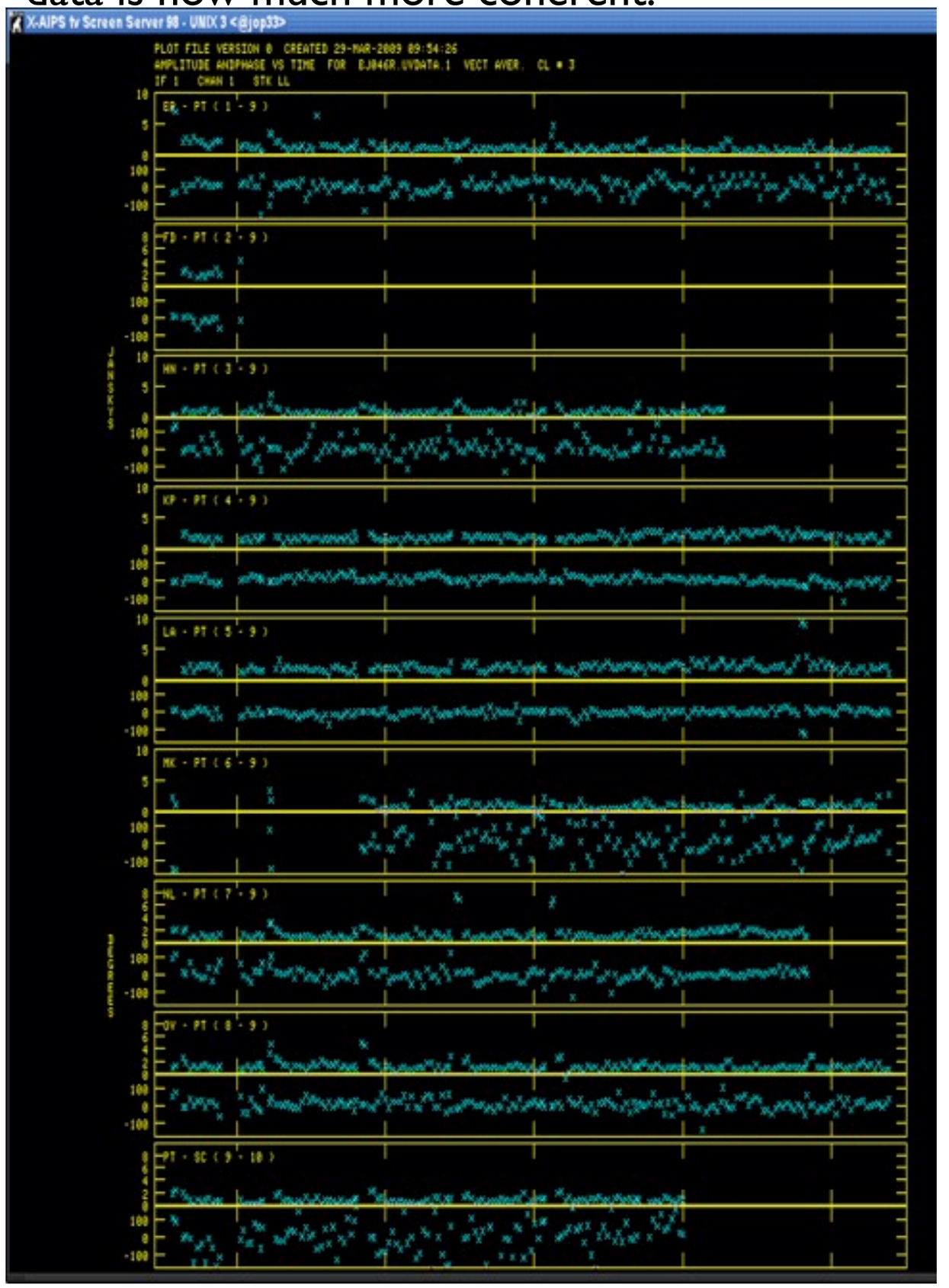

First Dirty map:

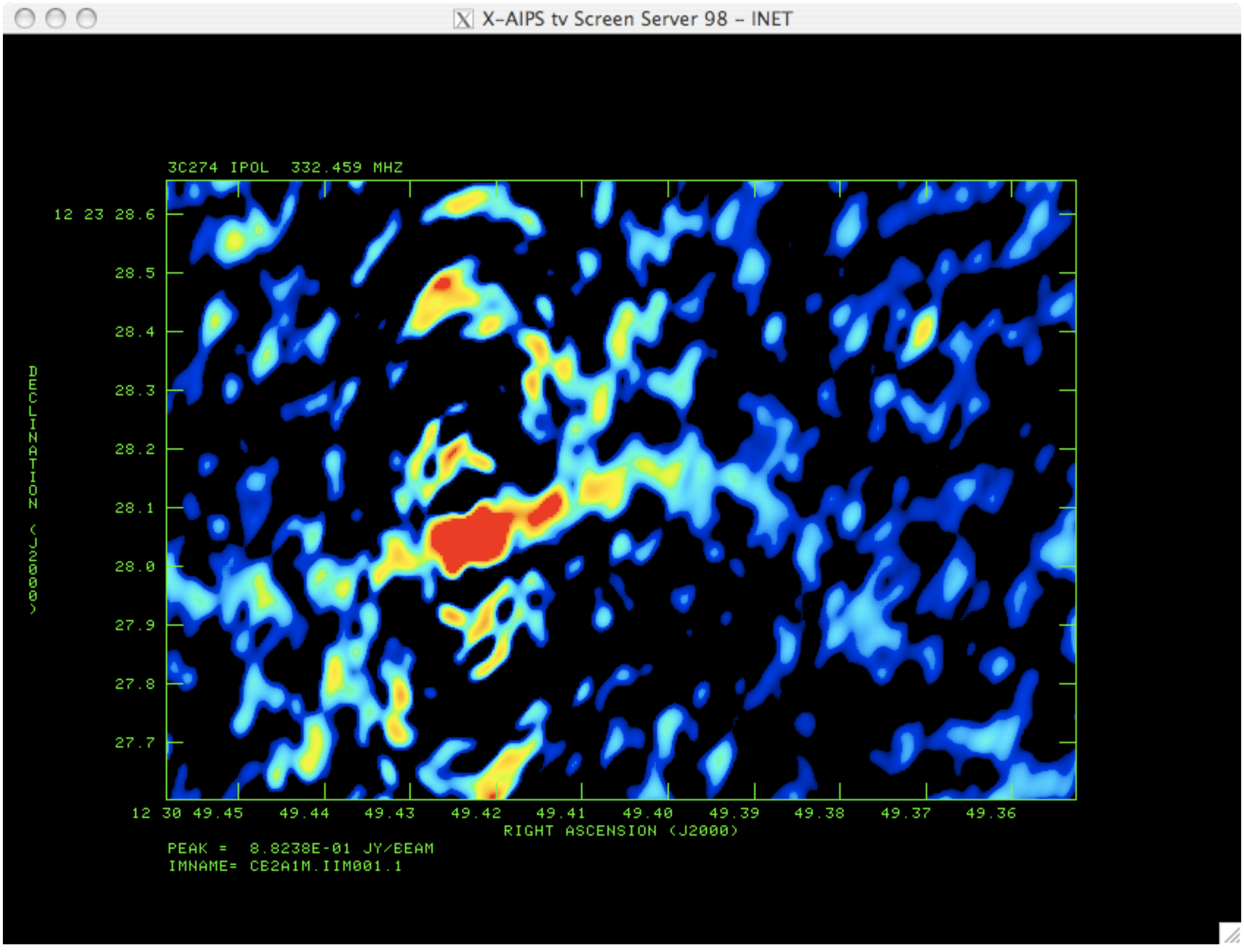

First CLEAN map:

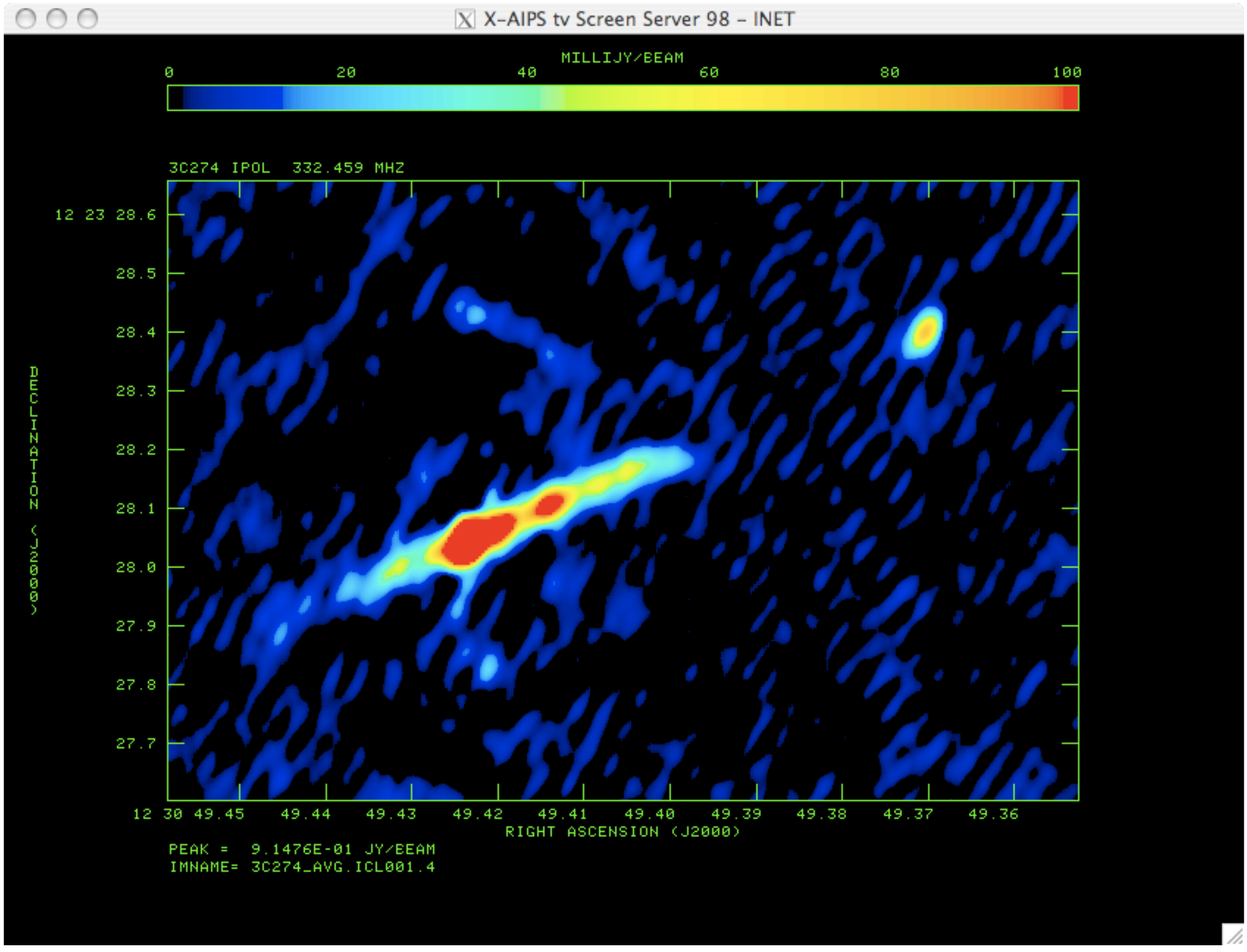

Plot of the 2nd round of *phase only* correction using previous CLEAN map as a model - note the corrections are now quite small (most of the corrections were made in the first self-cal). Large corrections still seen telescopes with long baselines (MK and SC) - note different scales!

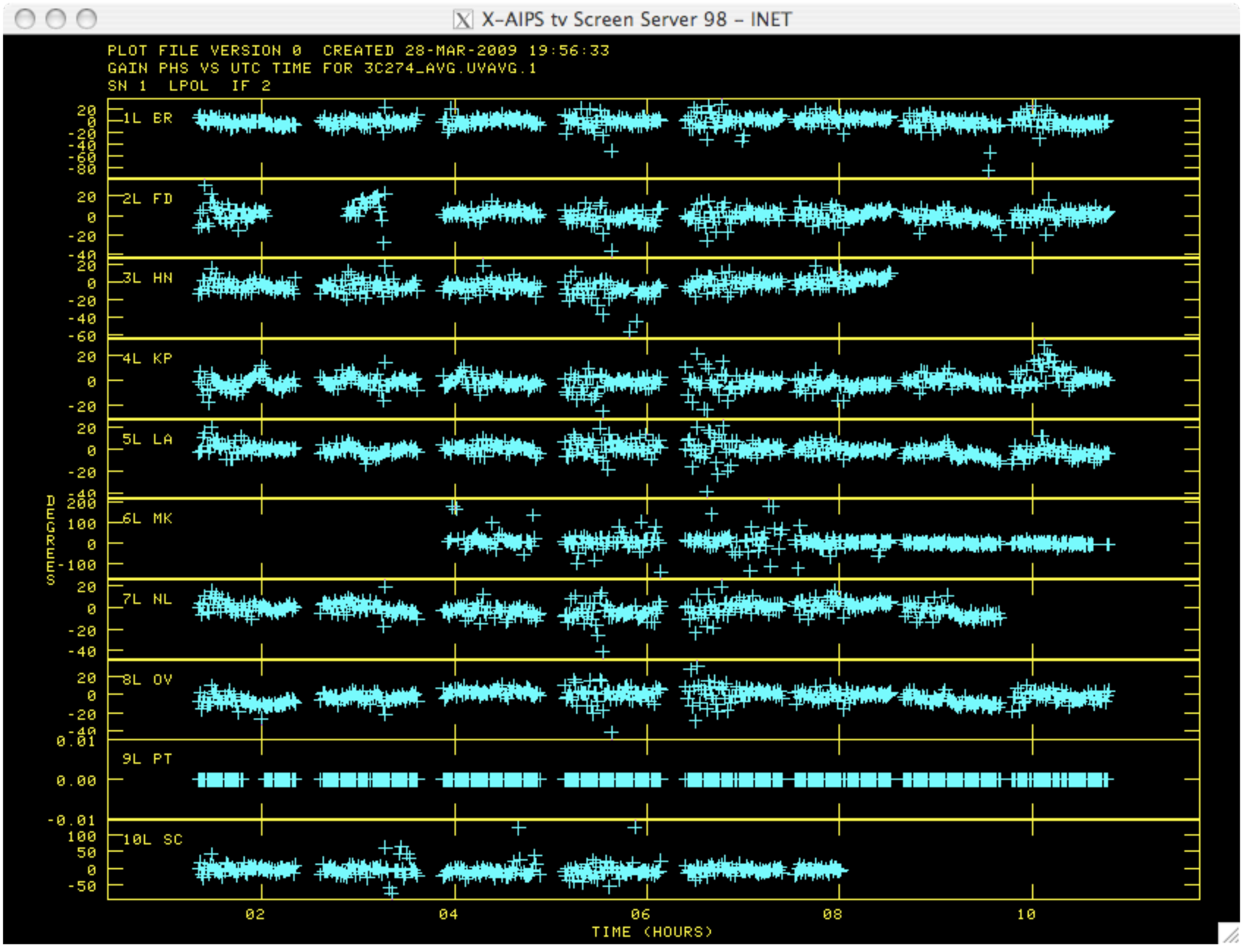

The improvement in the maps is also not so impressive:

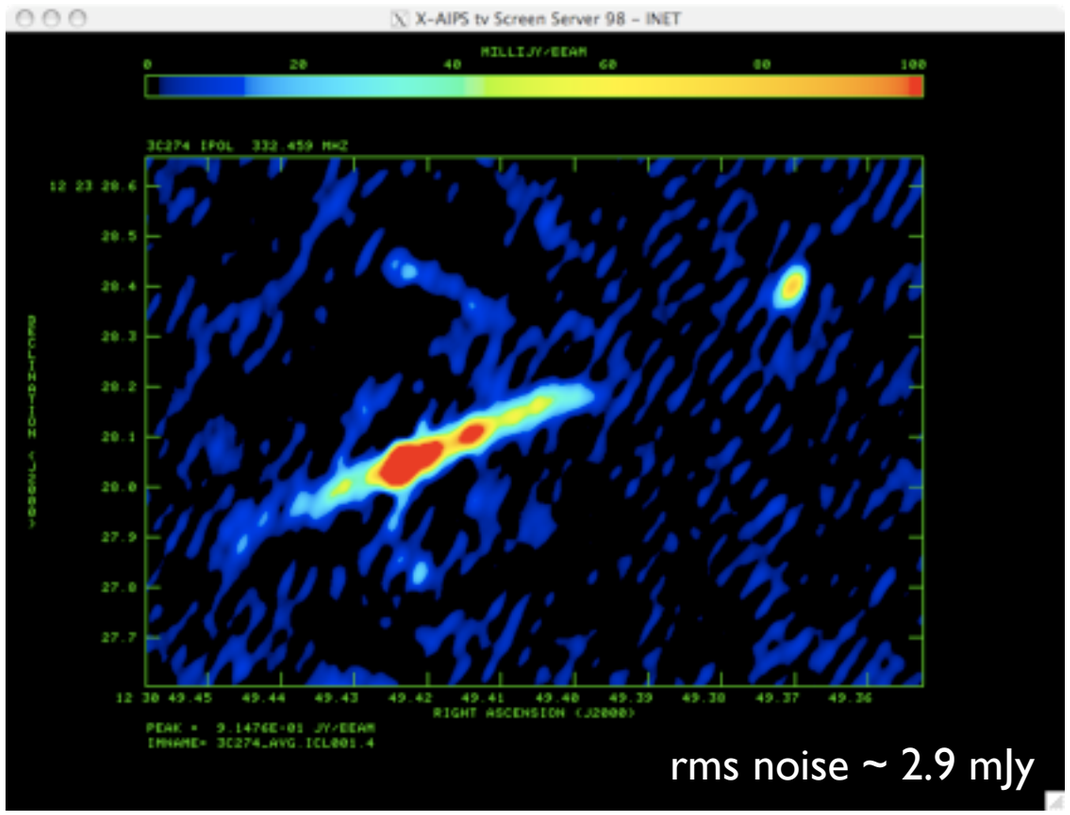

rms noise ~ 2.9 mJy

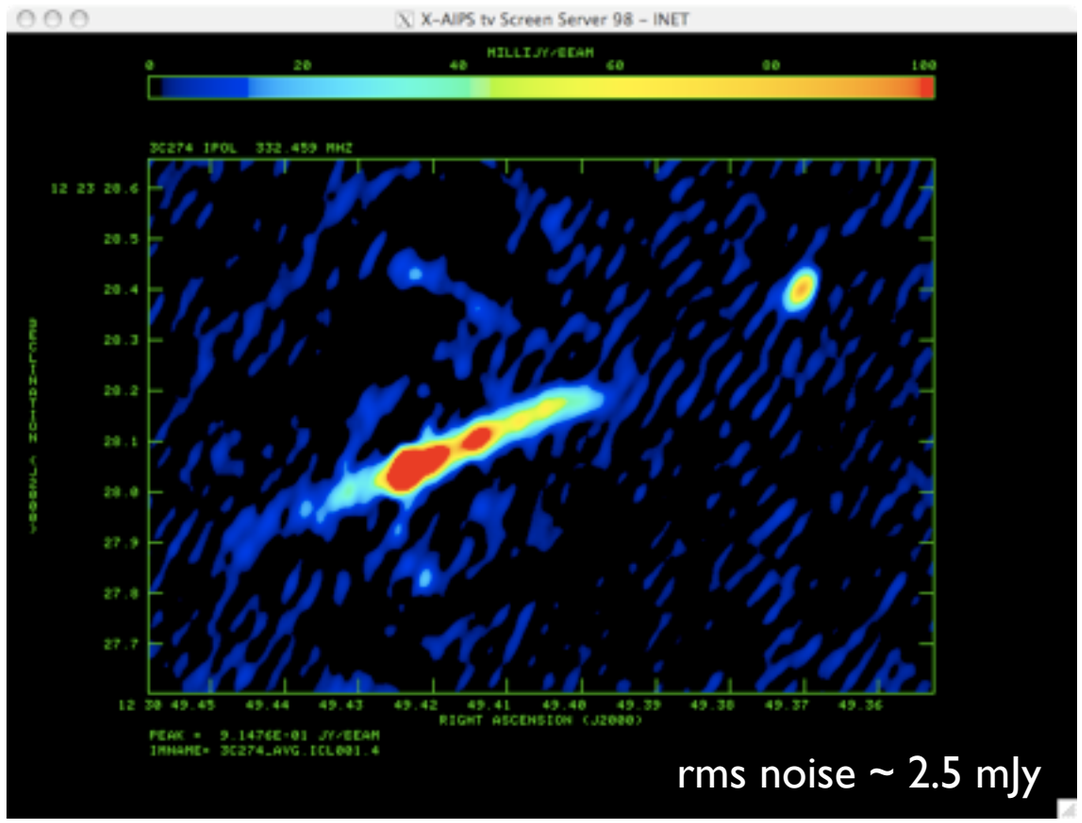

rms noise ~ 2.5 mJy

Time to try both amplitude and phase corrections at the same time - next slide:

Aside: all CLEANing presented here was done automatically without windows being set around the emission - usually one would set windows but I wanted to see how self-cal/CLEAN would work without "human guidance".

Plot of the amplitude telescope gain corrections using last map as a model:

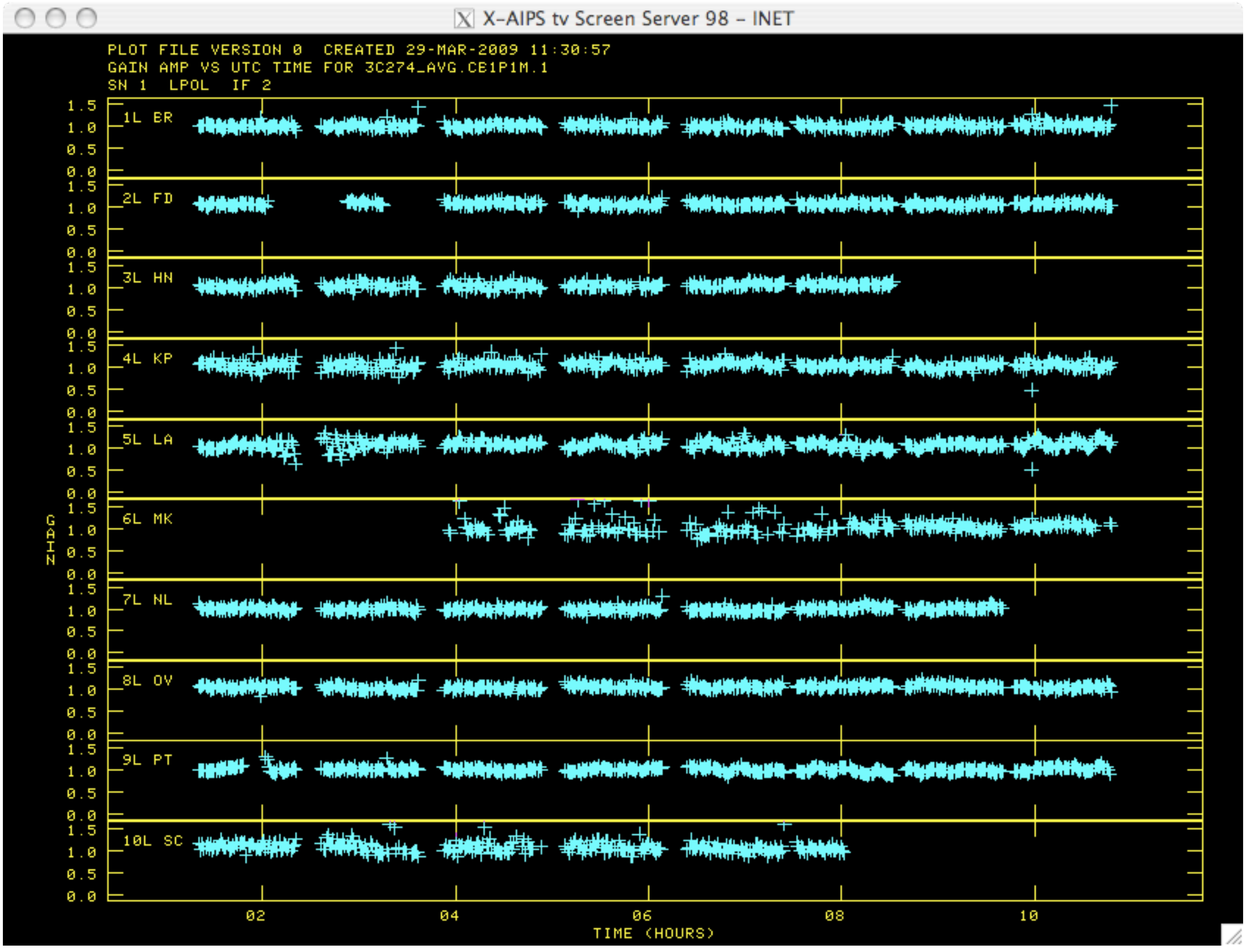

Image of the first map (phase only corrections), second map (another round of phase corrections), third map (amplitude and phase corrections):

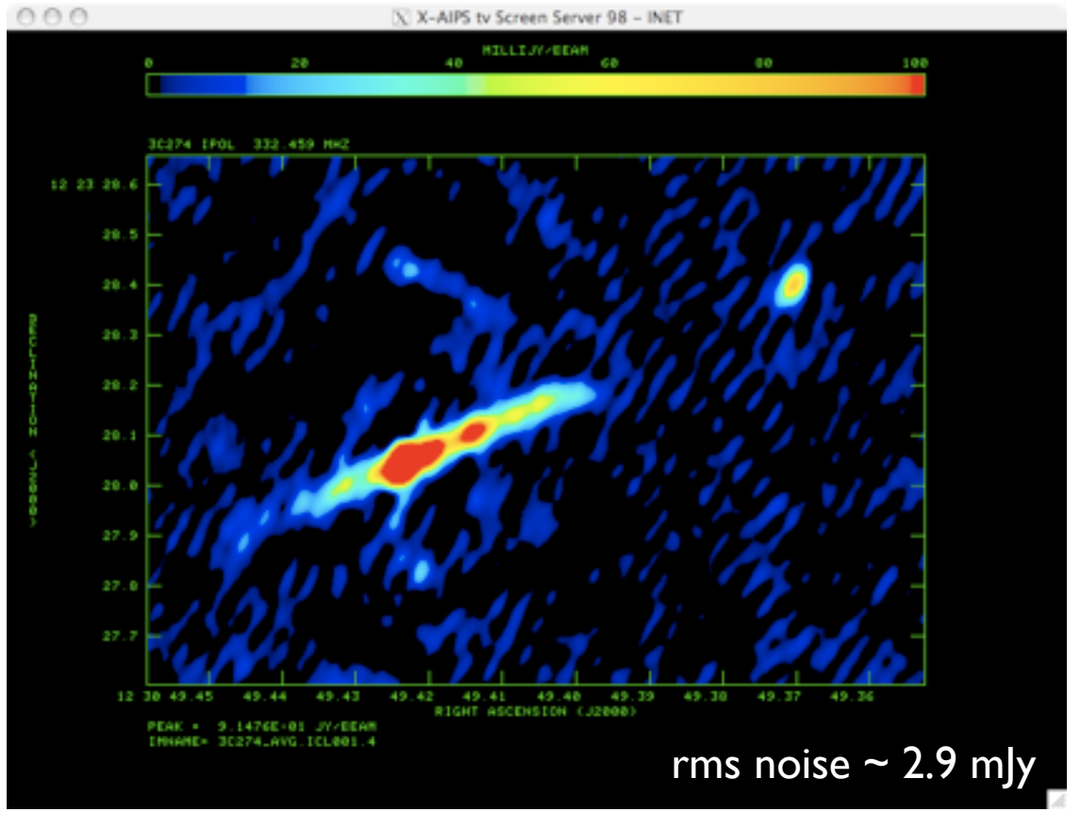

rms noise ~ 2.9 mJy

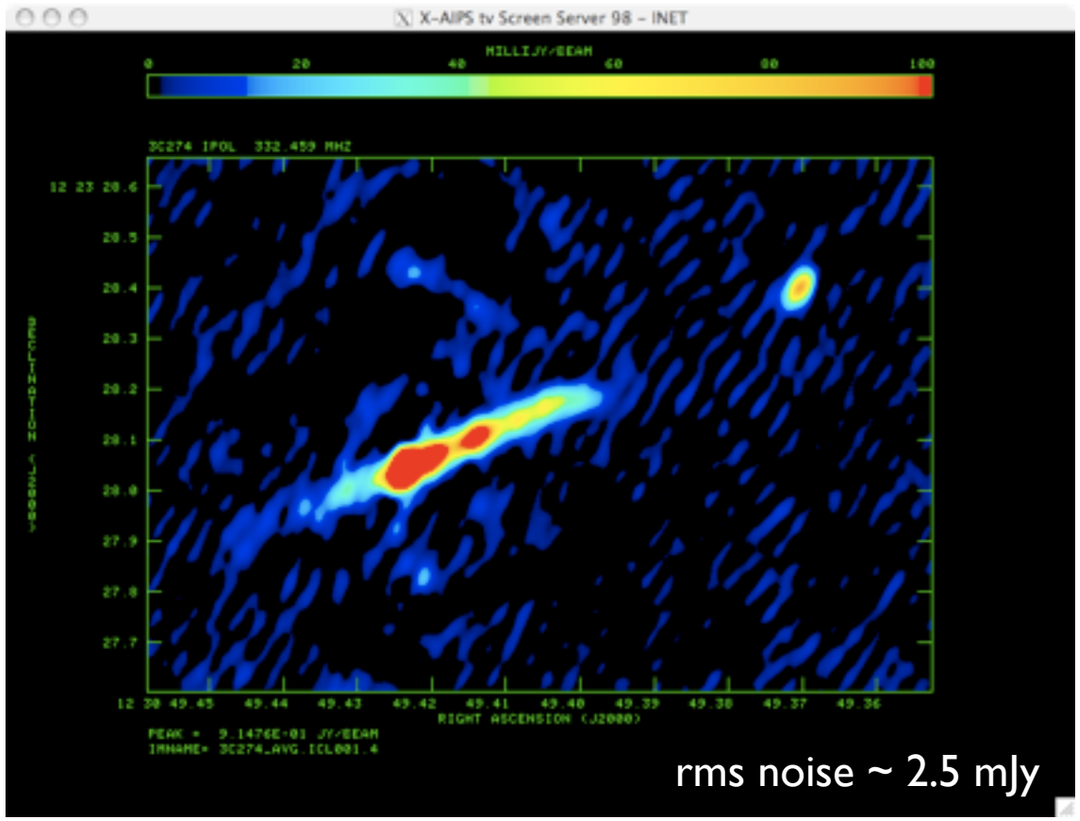

rms noise ~ 2.5 mJy

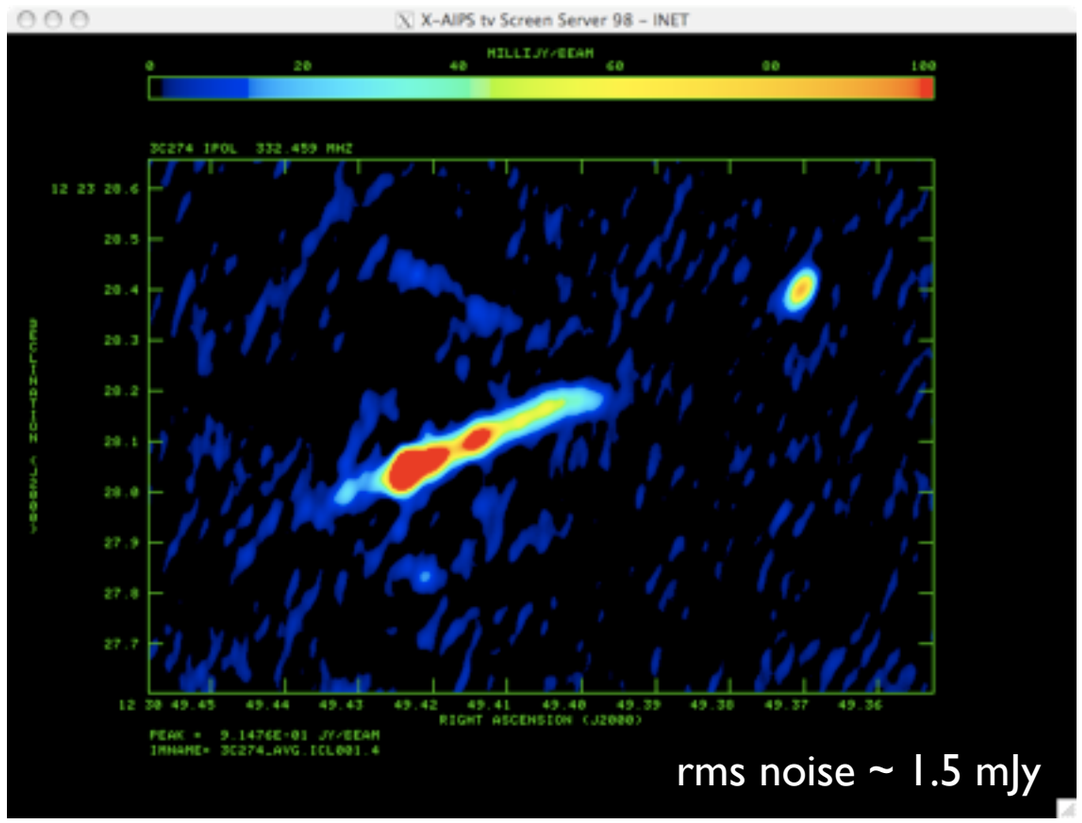

rms noise ~ 1.5 mJy

Application of the first round of amplitude telescope gain corrections leads to a significant improvement in the image (left).

Between map 1 and map 3, the r.m.s. noise level has halved.

Image of the first, second, third, fourth map..... - note reduction in rms noise levels

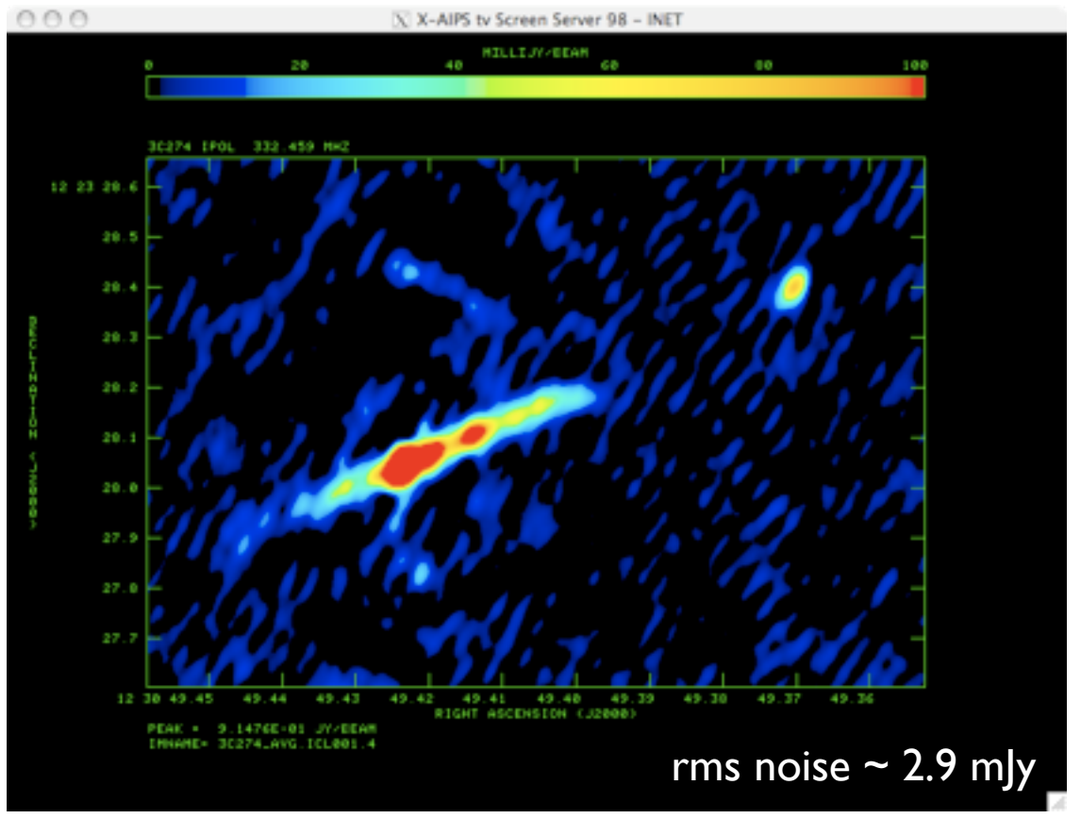

rms noise ~ 2.9 mJy

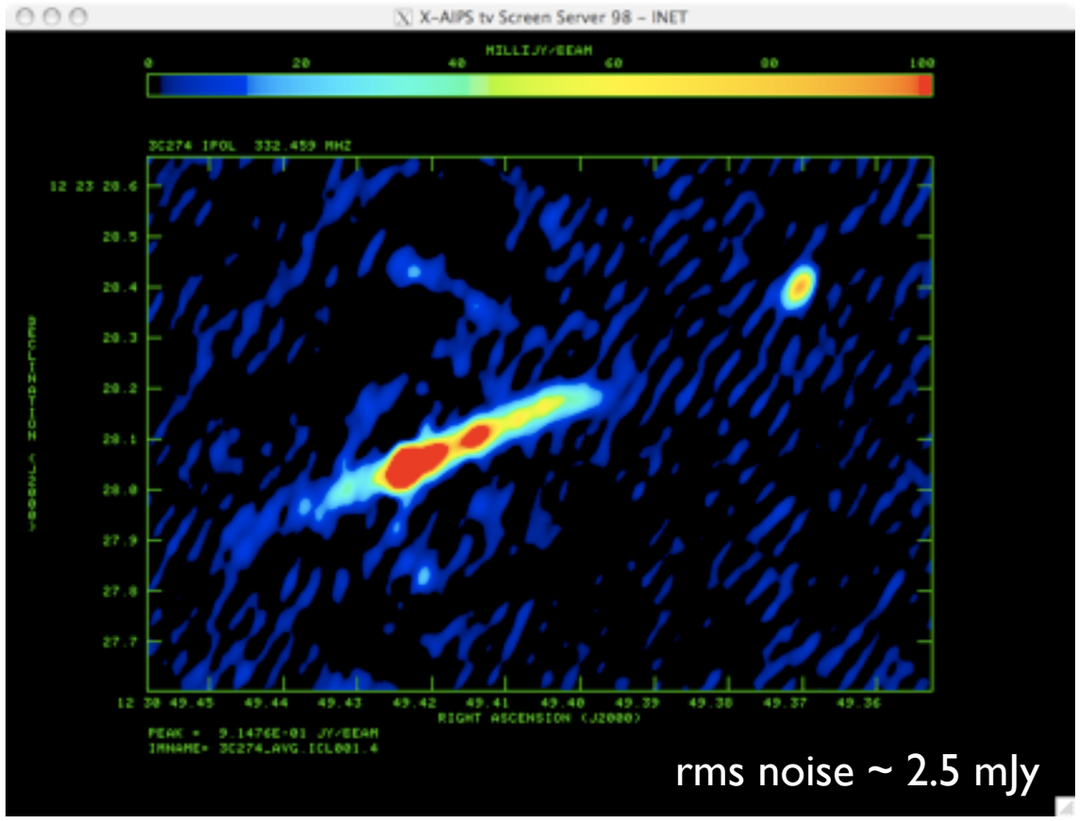

rms noise ~ 2.5 mJy

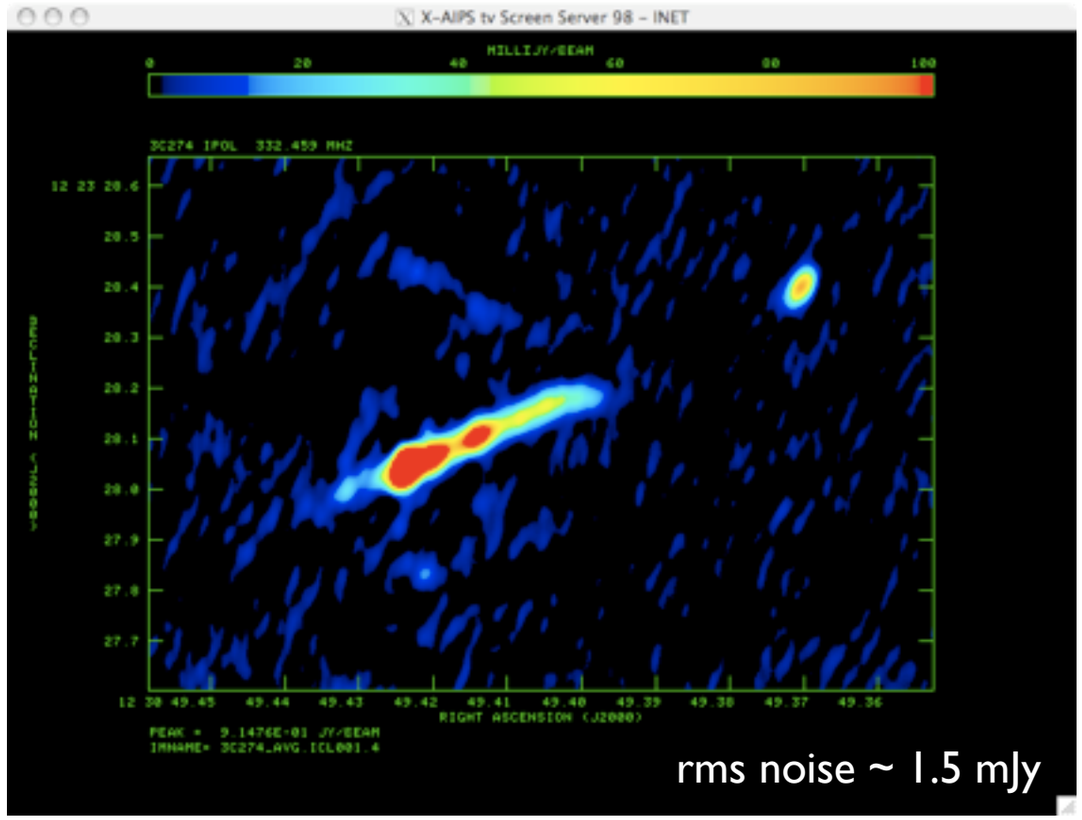

rms noise ~ 1.5 mJy

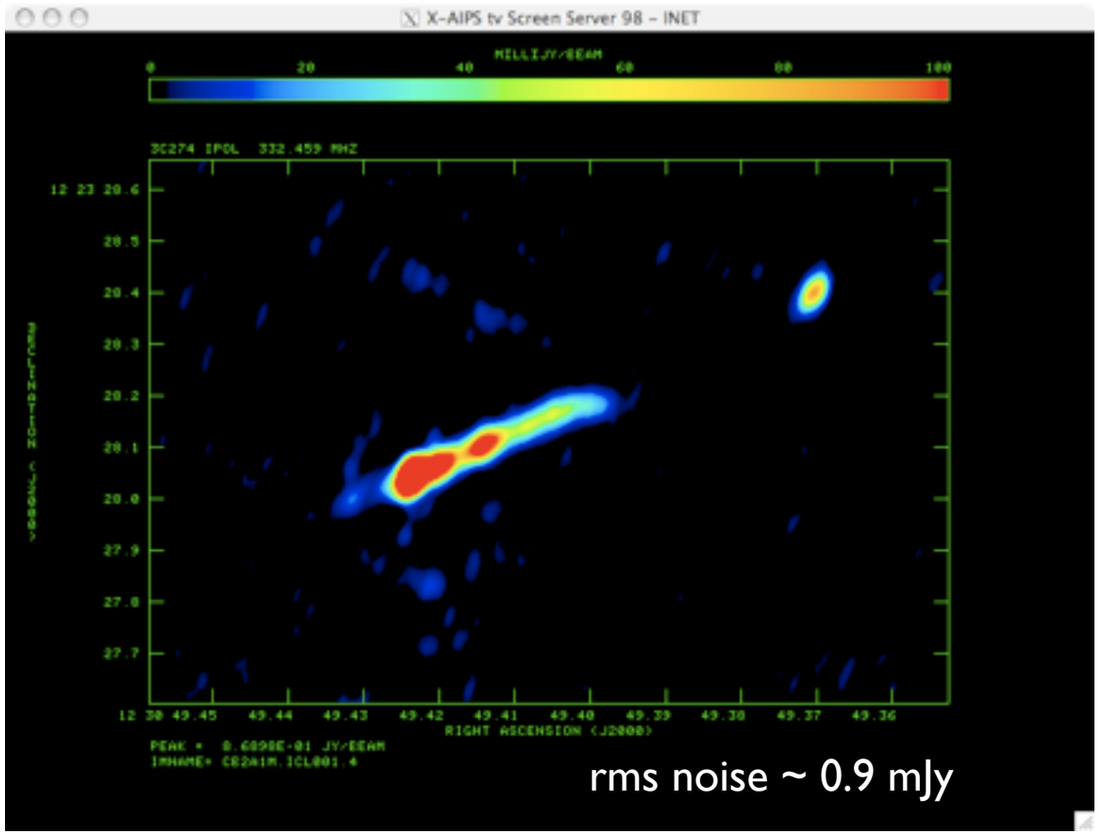

rms noise ~ 0.9 mJy

Plot of the data used to produce map 4 but with the source model (purple line) superimposed on the amplitude visibilities (baselines to telescope Pie Town, PT, only shown):

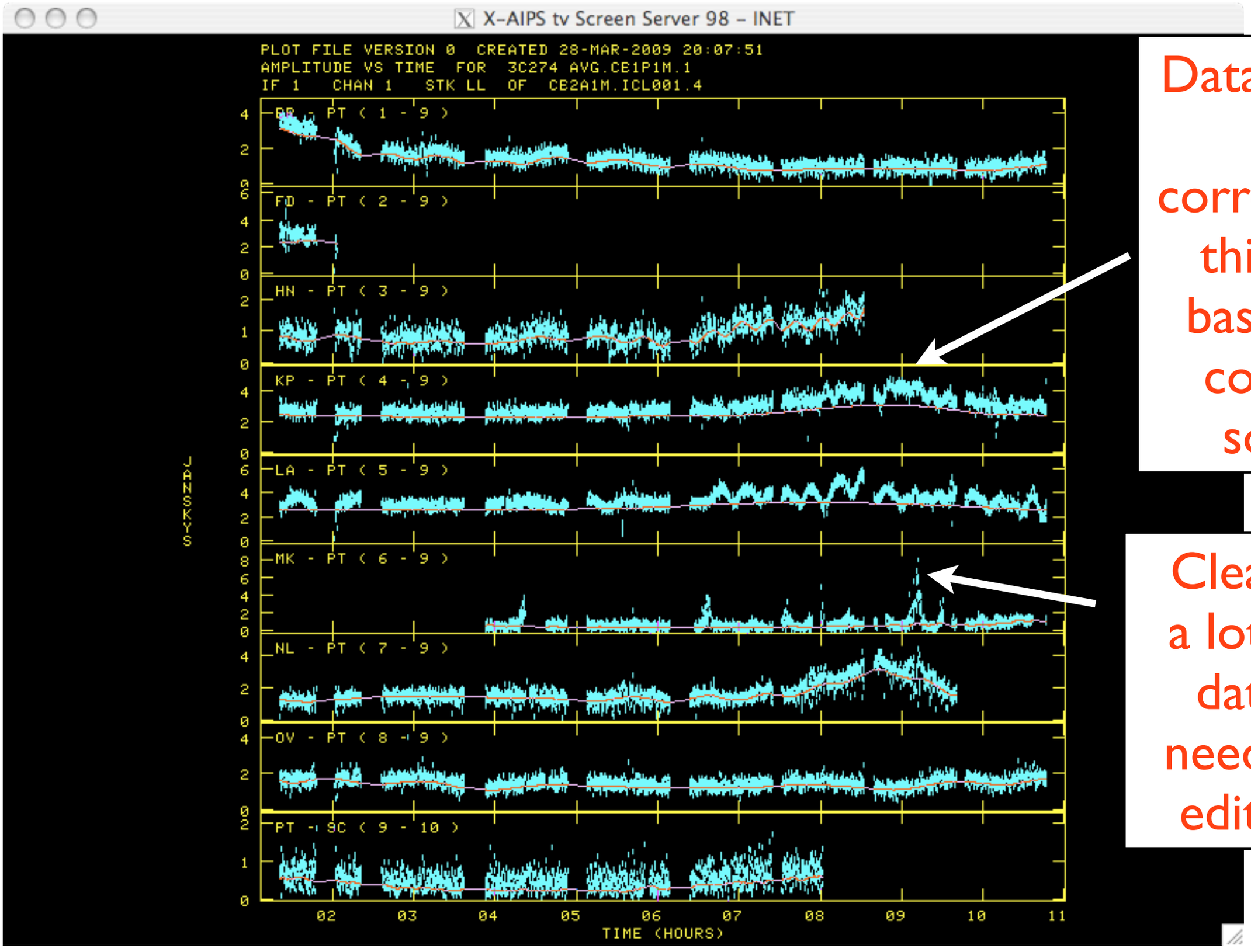

Data don't fit - RFI correlated on this short baseline or confusing source?

Clearly still a lot of bad data that needs to be edited out

Plot of the data used to produce map 4 with the source model superimposed on the phase visibilities (baselines to telescope Pie Town, PT, only shown):

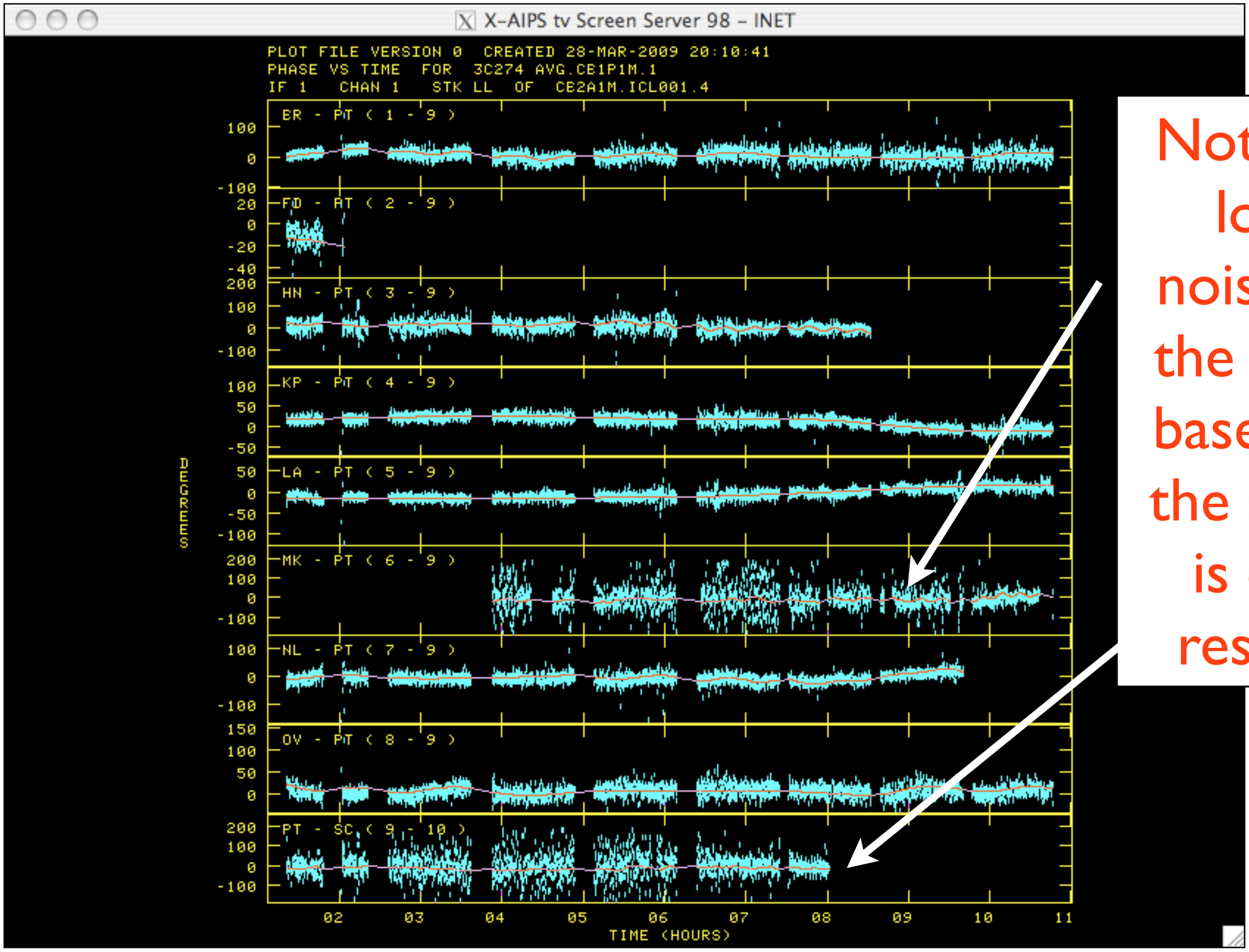

Note data looks noisier on the longer baselines - the source is quite resolved

A plot of the uv-data (amplitude) vs baseline length:

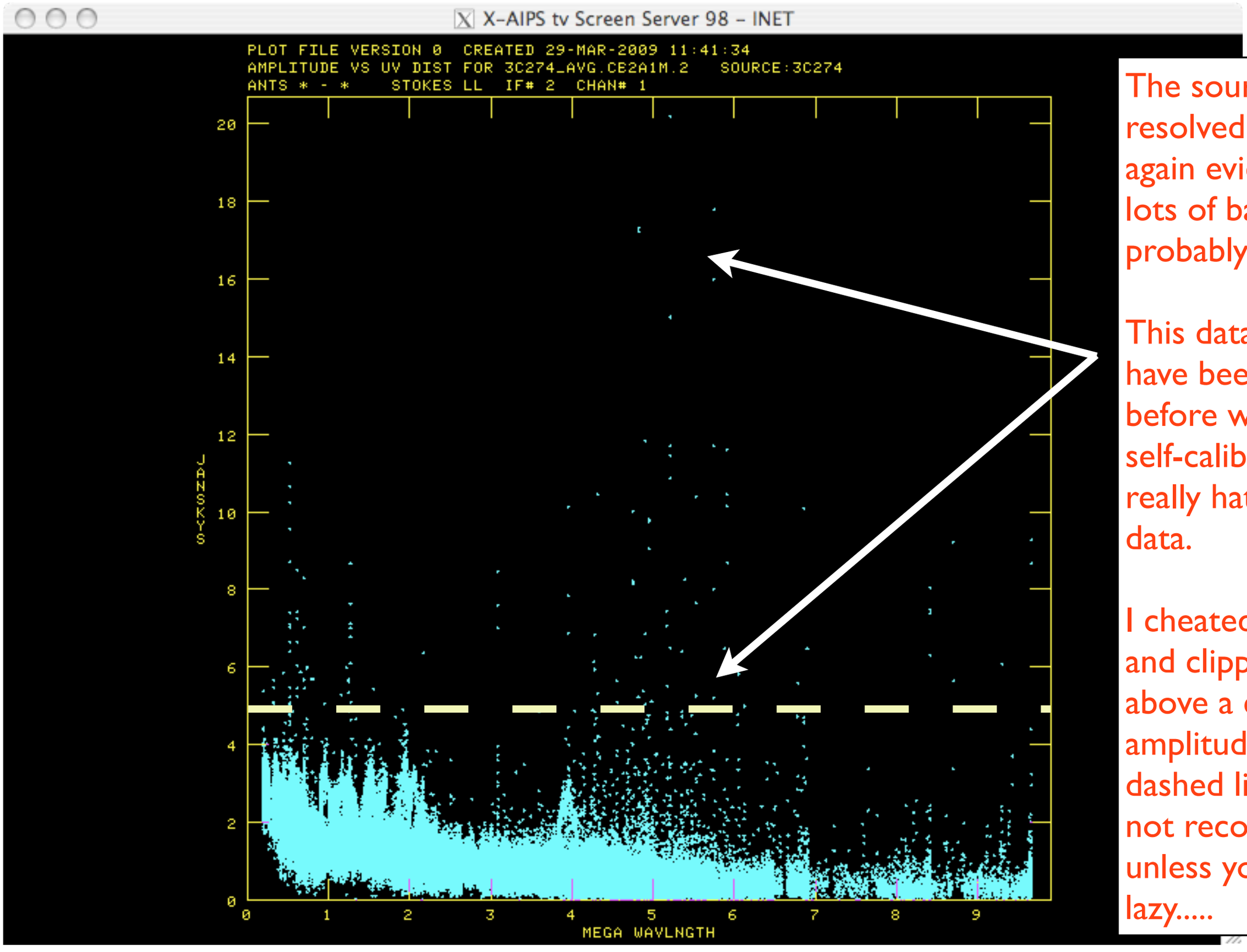

The source is quite resolved but there is again evidence for lots of bad data - probably RFI.

This data set should have been edited before we tried any self-calibration - but I really hate editing data.

I cheated at this point and clipped the data above a certain amplitude (see dashed line) - really not recommended unless you are very lazy.....

The new map after clipping out some of the bad data:

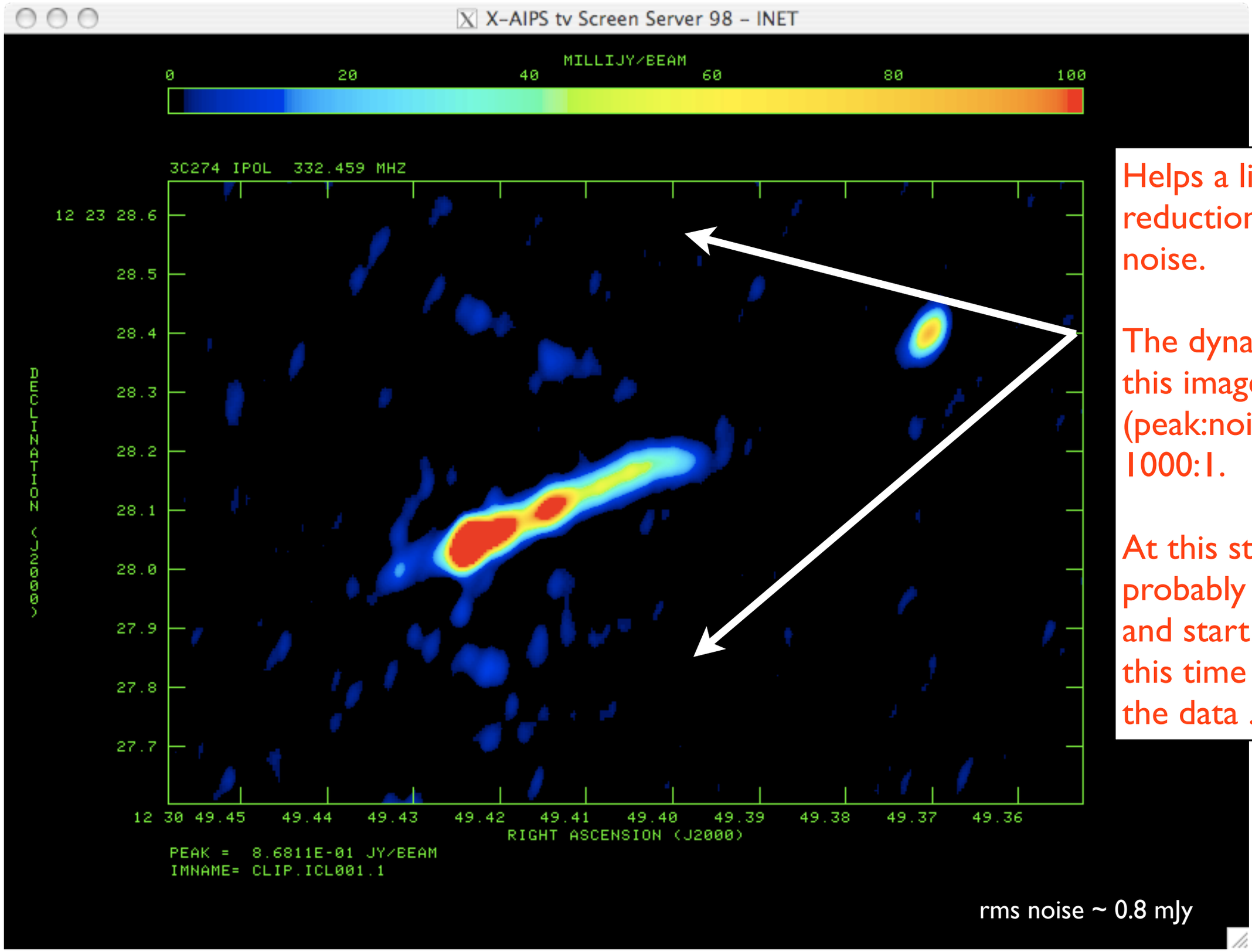

Helps a little - small reduction in rms noise.

The dynamic range of this image (peak:noise) is only ~ 1000:1.

At this stage its probably time to stop and start again - but this time carefully edit the data .

3C274 - HST

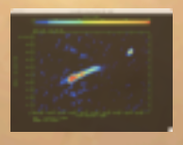

VLBI has v. high resolution!

Phase referencing

Self-calibration requires the target source to be detected (SNR > 1) within the coherece time, on the majority of baselines for reliable telescope corrections and target image to be generated.

We saw in Lecture 2, (eqn) that the sensitivity of a single dish is given by:

$$\Delta T = \frac{T_{tot}}{\sqrt{(2d\nu\tau)}}$$

Similarly, for a single interferometer baseline:

$$\Delta S_{ij} = (SEFD_i\, SEFD_j/(2\Delta\nu\Delta t))^{1/2} \quad \text{(Jy)} \quad [13]$$

e.g. for the VLBA SEFD = 300 Jy and $\Delta\nu$ ~ 128 MHz. For a coherence time, Δt, of say 2 minutes at 5 GHz, ΔS_{ij} ~ 1.7 mJy. A 7-sigma detection ==> that the source should have an unresolved flux density of ~ 10 mJy.

Many of the most interesting sources have flux densities that are fainter than 10mJy.

The technique of Phase Referencing is used to detect these sources:

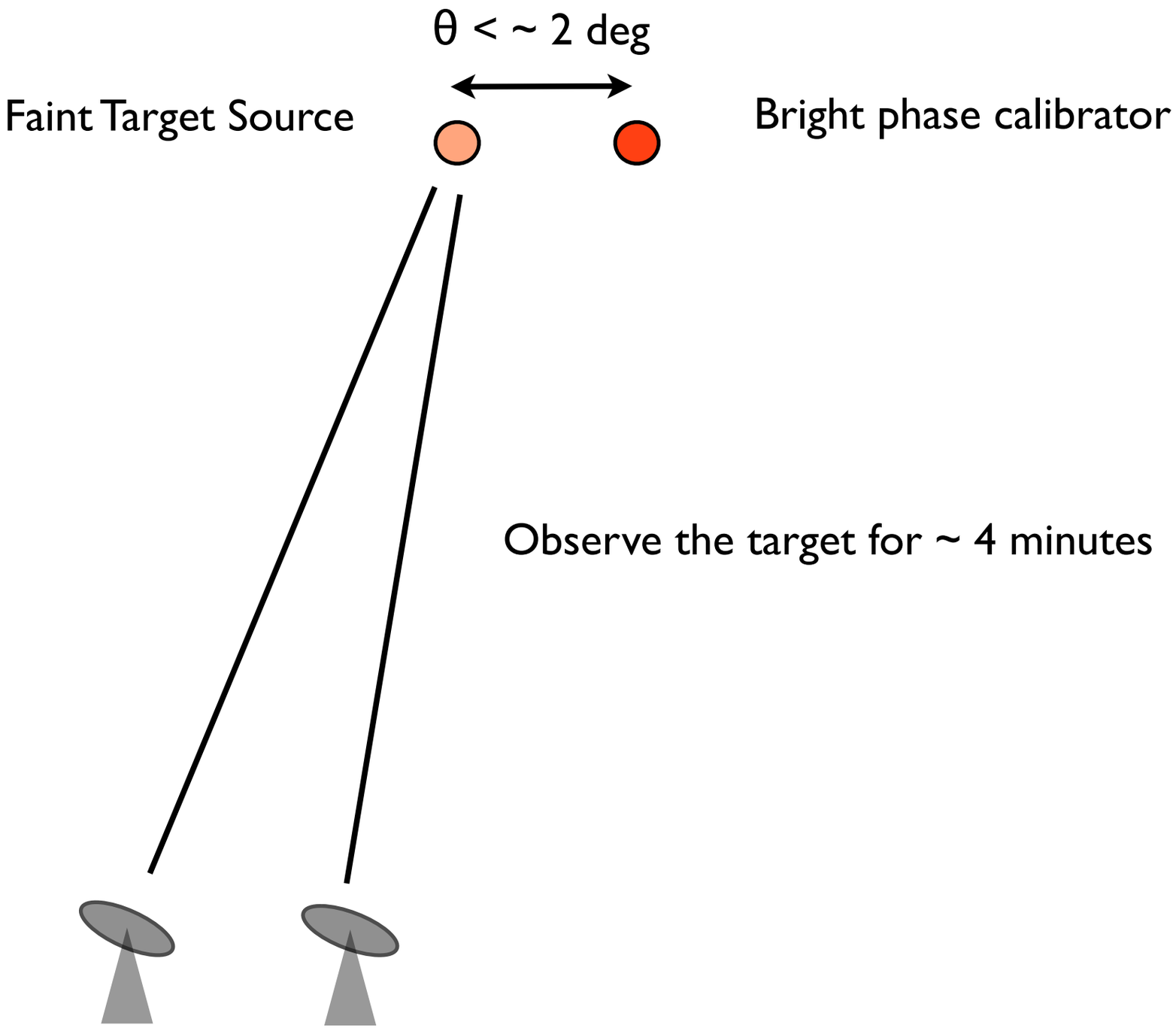

Observe the target for ~ 4 minutes

Faint Target Source

Bright phase calibrator

Then switch to the brighter phase calibrator for ~ 1.5 minutes

Faint Target Source

Bright phase calibrator

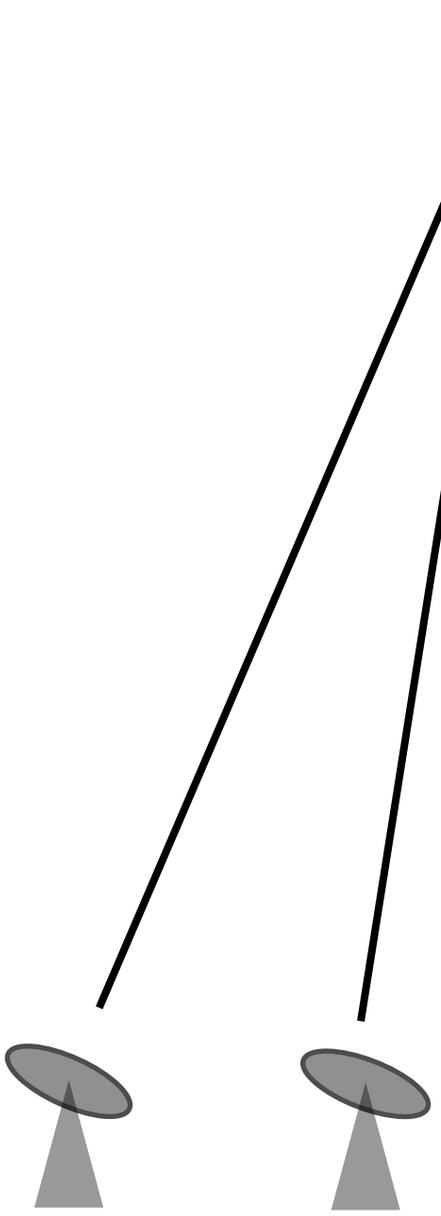

Then switch back to the target for
~ 4 minutes

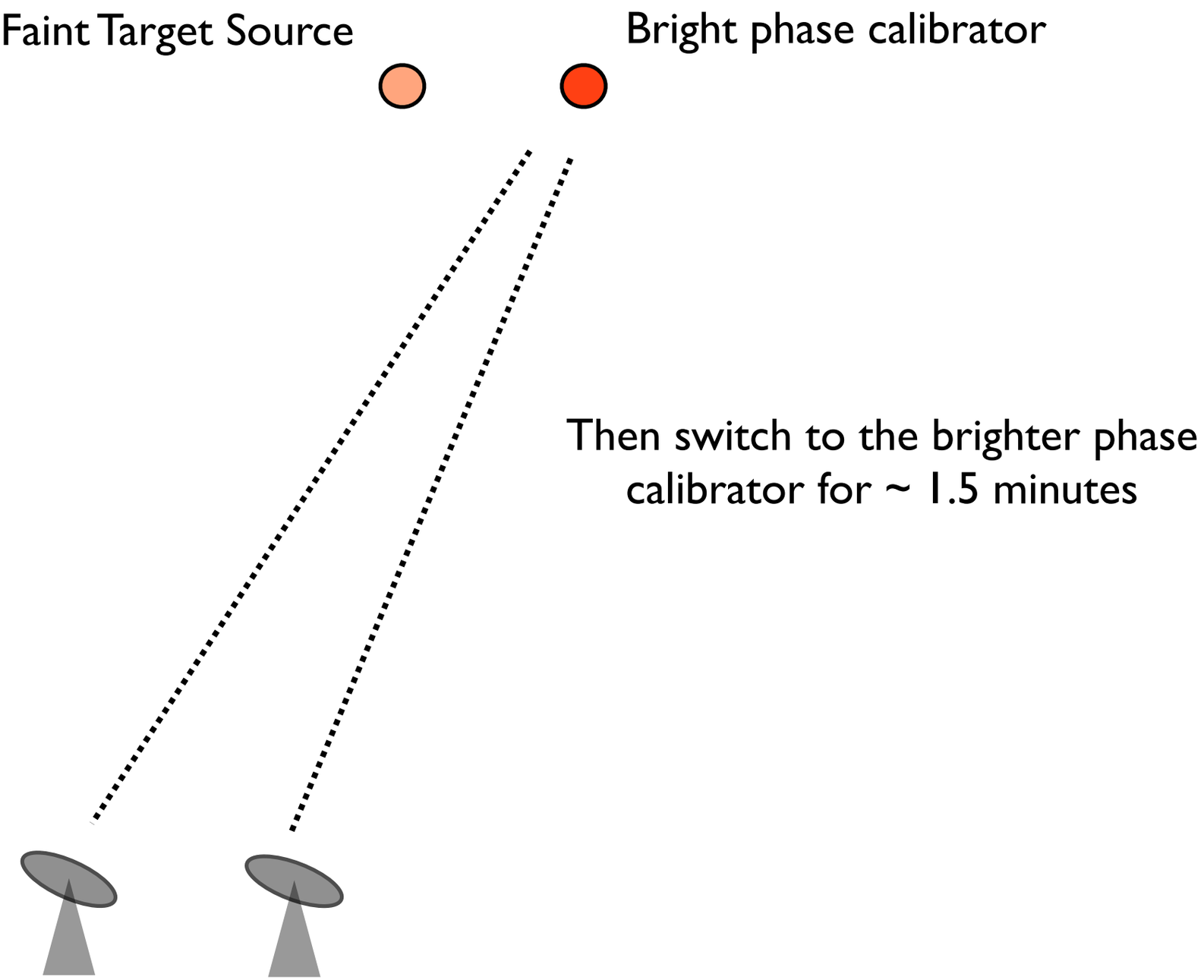

The telescope corrections determined for the bright calibrator are applied to the target source data. Phase reference observations specify a “cycle time” (=time on target + time on calibrator). Cycle times ~ 8 mins are common at cm wavelengths, but at much higher frequencies cycle times of 0.5 mins are sometime successfully employed. For short cycle times, the telescopes must be fast movers.

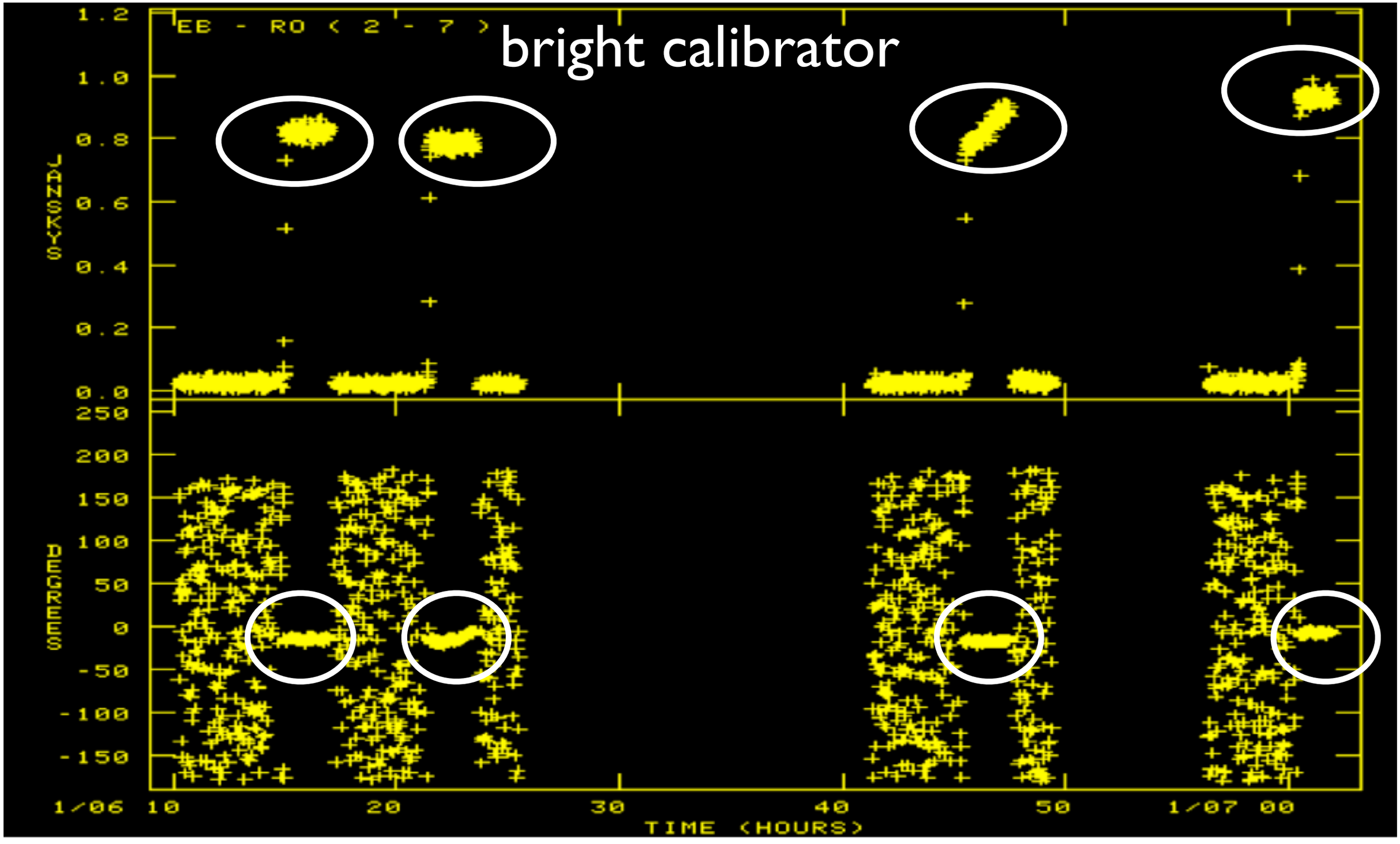
EB - RO < 2 - 7 >
bright calibrator
JANSKYS
1.2
1.0
0.8
0.6
0.4
0.2
0.0
250
200
150
100
50
0
-50
-100
-150
DEGREES
1/06
10
20
30
40
50
1/07
00
TIME (HOURS)

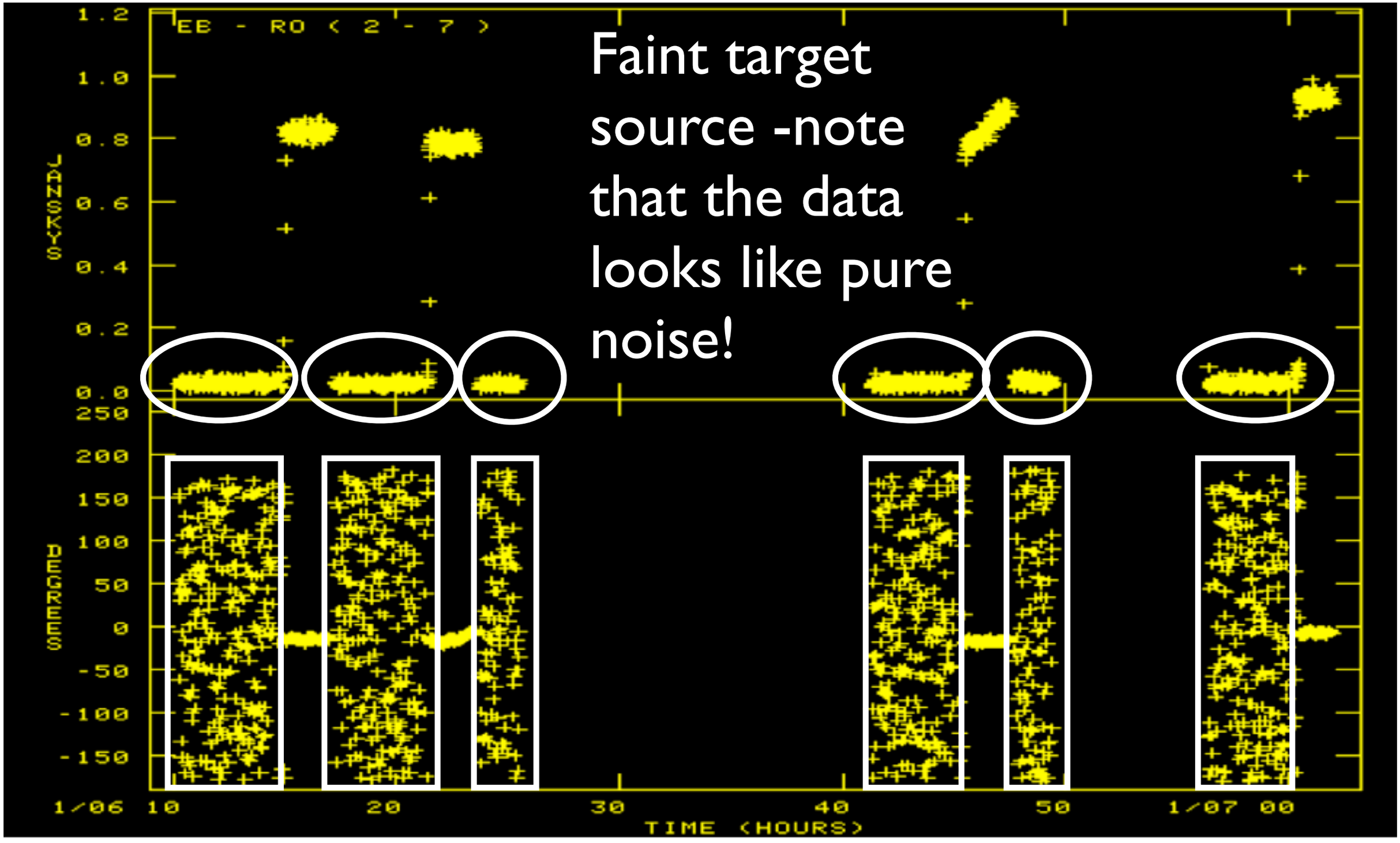
EB - RO < 2 - 7 >
Faint target source -note that the data looks like pure noise!
JANSKYS
1.2
1.0
0.8
0.6
0.4
0.2
0.0
250
200
150
100
50
0
-50
-100
-150
DEGREES
1/06
10
20
30
40
50
1/07
00
TIME (HOURS)

So the idea is to take the telescope corrections (amplitude and phase) determined from self-calibrating the bright calibrator, and apply them to the faint target. The basic assumption is that for sources located in roughly the same region of sky, corrections for one source, also apply to the other.

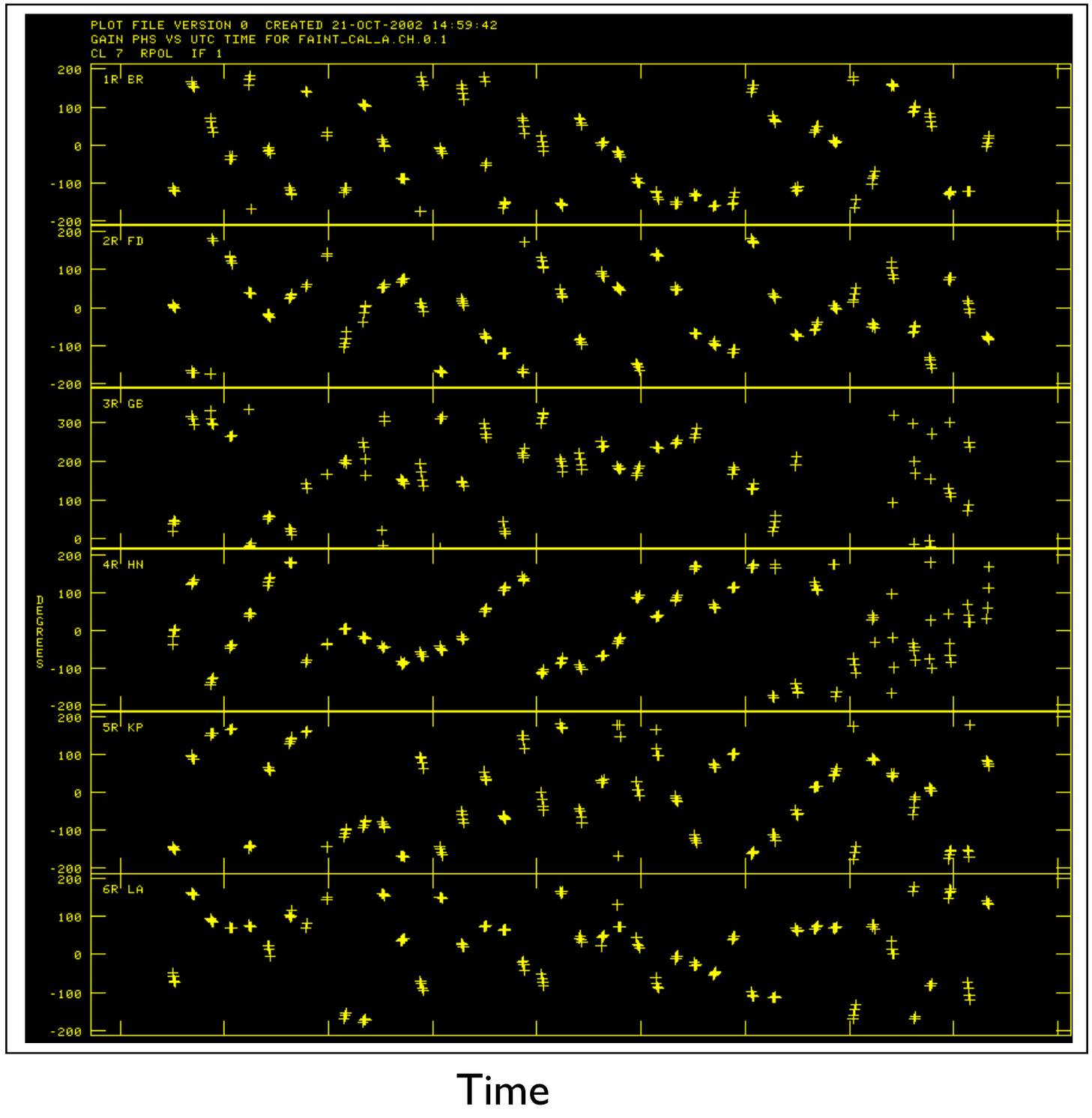

ϕ

Left: phase corrections determined from the calibrator.

The telescope corrections are interpolated into the periods where the faint target was being observed:

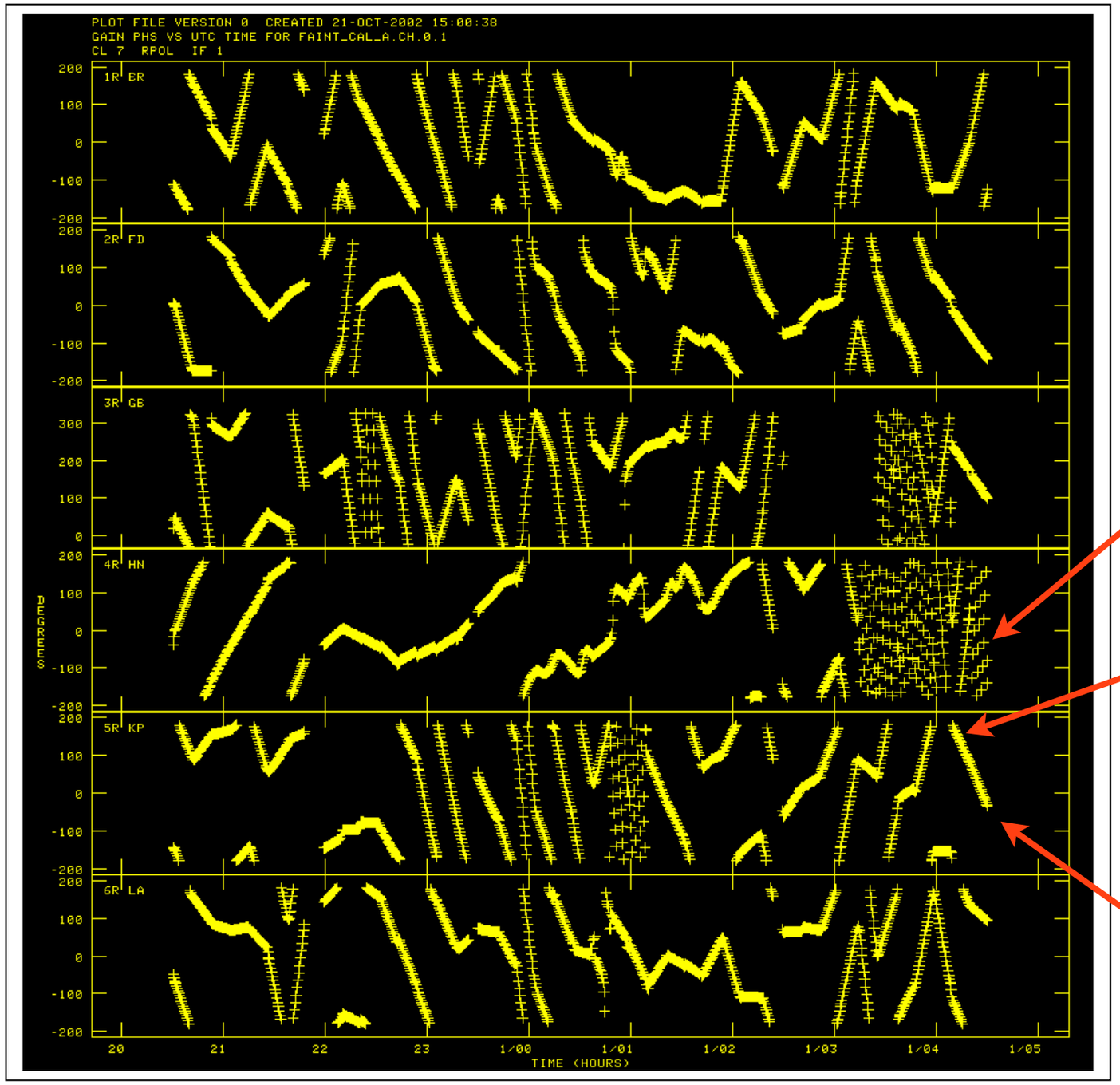

ϕ

Time

Left: phase corrections (including interpolated values).

Note that there are some periods where it is difficult to follow the phase.

But for most times the interpolation looks reasonable.

Aside: You can also estimate the coherence time of the data e.g. ~ 200 degrees in 20 mins, => coherence time of ~ 5 mins.

The technique of phase referencing permits the coherence time of the target data to be extended across the entire observation (many hours). This means that the sensitivity of the observations continue to scale as $(\Delta t)^{1/2}$.

For an interferometer array of N identical telescopes, the noise on a single baseline (see eqn[13]) is:

$$\Delta S_{ij} = SEFD/(2\Delta\nu\Delta t)^{1/2}$$

Image sensitivity is the standard deviation of N(N-1)/2 samples, each with a standard deviation ΔS_{ij}. So the r.m.s. noise measured in the image, ΔI is just:

$$\Delta I = \Delta S_{ij}/(N(N-1)/2)^{1/2} = SEFD/(N(N-1)\Delta\nu\Delta t)^{1/2} \quad [14]$$

where Δt is now the time spent by the telescope "on-source". Assuming no losses, then for the VLBA, N=10, Δt = 8hr and taking values as before => $\Delta I \sim 25$ microJy. In practice various losses must be taken into account (e.g. electronic losses, digitisation etc) => $\Delta I \sim 40$ microJy.

In principle, phase-reference observations with the VLBA can detect sources as faint as $5\Delta I \sim 200$ microJy. More sensitive arrays like the EVN can reach even fainter limits.

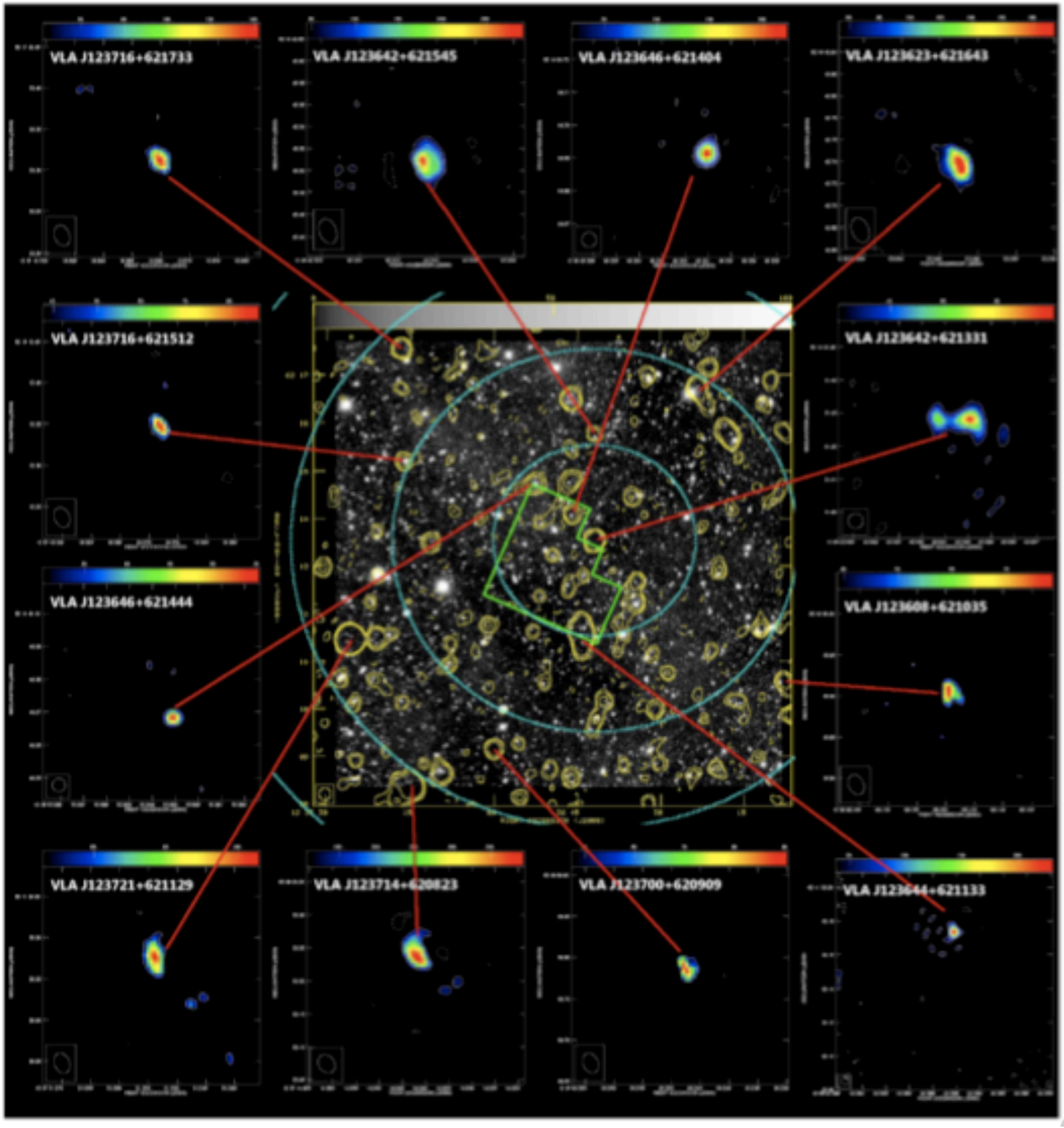

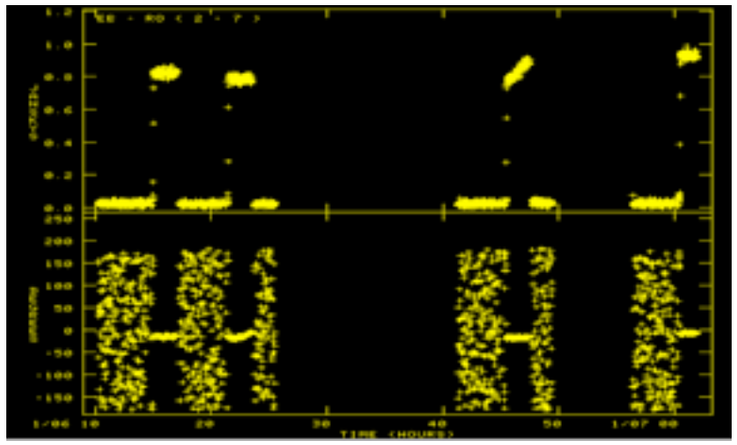

Phase reference works well in practice.

The noisy VLBI data presented above, produced detections of faint sub-mJy radio sources in the Hubble Deep Field (left).

These images reach noise levels of 7 microJy using a global VLBI array.

Wide-field Imaging & Survey Speed

Wide-field imaging of the full primary beam requires the use of special techniques.

The first problem is that in Lecture 4, eqn[12]) we showed that:

$$V(u,v,w) = \int_{-\infty}^{+\infty}\int_{-\infty}^{+\infty} A(x,y)I(x,y)\exp(i2\pi(ux+vy+w(1-x^2-y^2)^{1/2})\frac{dxdy}{(1-x^2-y^2)^{1/2}}$$

For non-coplanar arrays w=0. But for 2-D arrays eqn[12] is only strictly valid PROVIDED a small region of sky is to be imaged, i.e. that $1/2(x^2+y^2)w << 1$.

If this is not the case, we introduce a phase error into the data, $\Delta\phi$.

From [12] we can see that the error would be of order:

$$\Delta\phi = 2\pi(1/2(x^2+y^2)w = \pi(x^2+y^2)w$$

The maximum value w can ever have is the max baseline length:

$$\Delta\phi = \pi(x^2+y^2)B_{max}/\lambda$$

$$= \pi\theta^2 B_{max}/\lambda$$

$$= \pi\theta^2 / \theta_{beam} \qquad [15]$$

e.g. for the VLA (A-array) at 20cm, an error of 0.1 radians corresponds to sources located 1.3 arcmins from the phase centre.

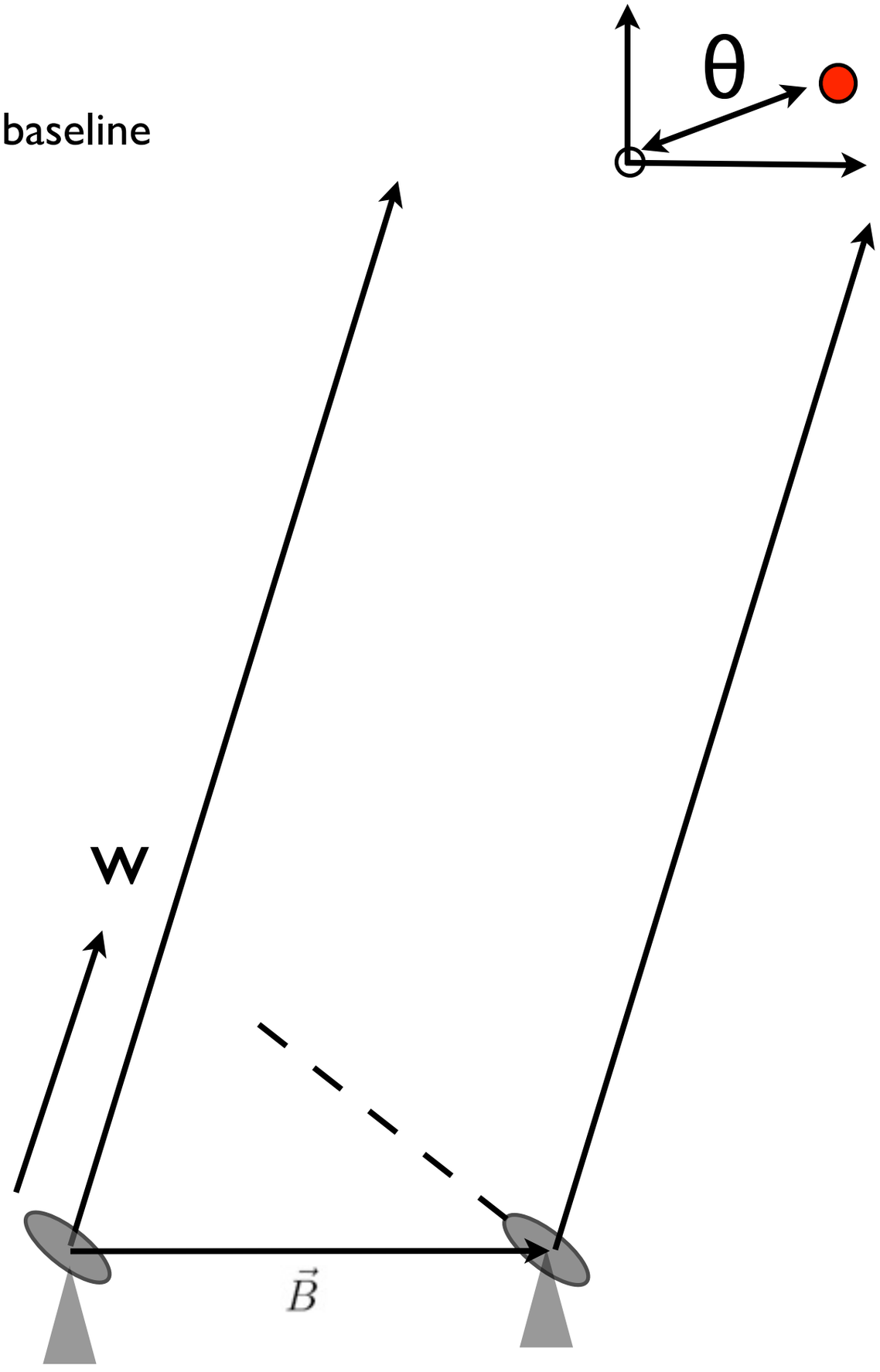

A practical solution is to split the field of view up into many 2-D patches - each with an appropriate $e^{i2\pi w}$ correction factor (see right).

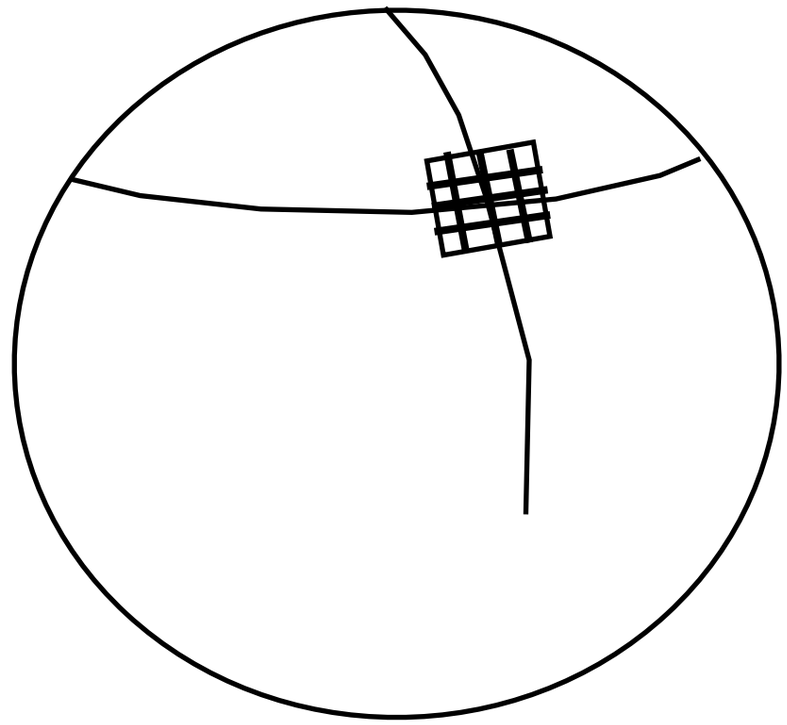

Other important effects that limit the field of view of an interferoemter array include: *bandwidth smearing* and *time averaging*.

Bandwidth smearing:

During correlation, the delay is correct for only one particular point on the sky - usually the phase centre (where the target is located).

For all other source positions there will be an error introduced by applying a delay that is strictly only true for the phase centre & a particular frequency:

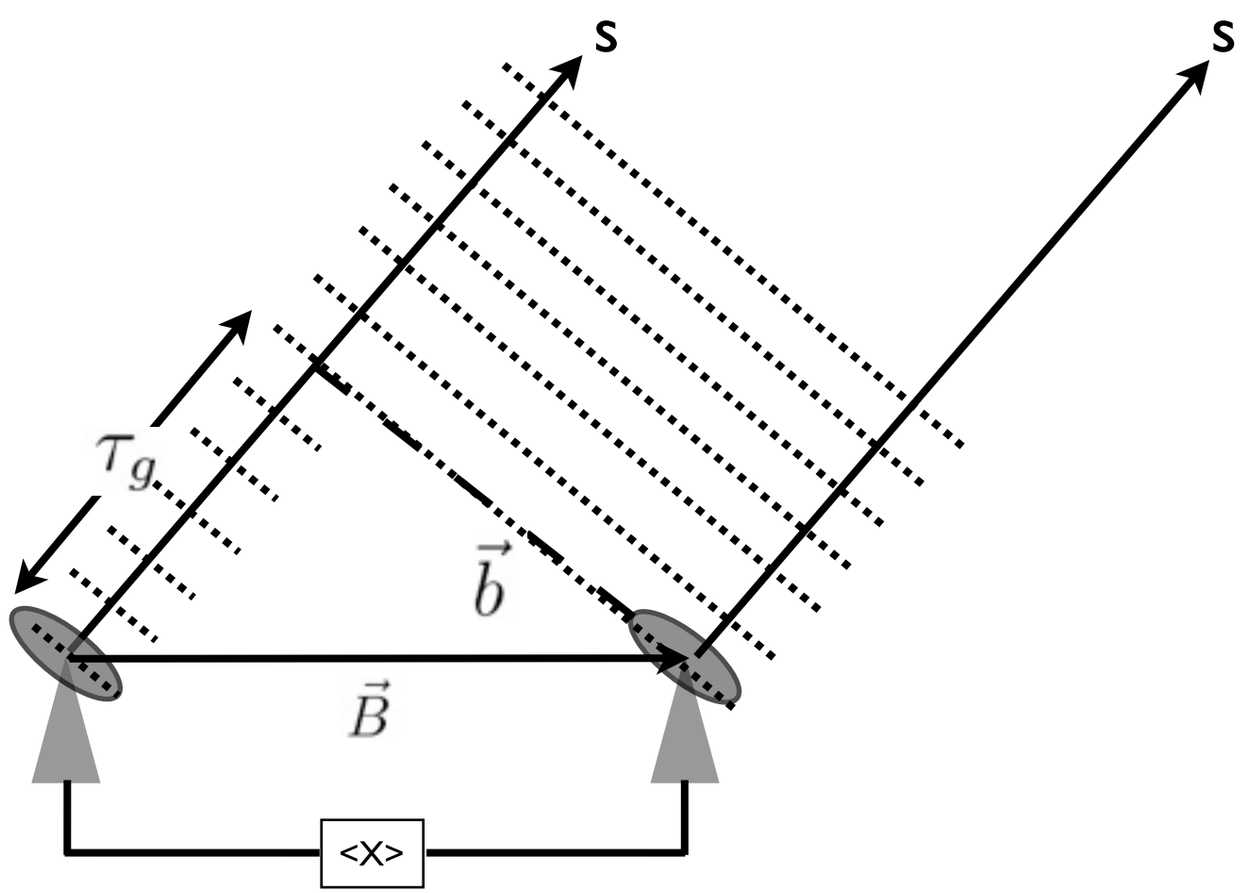

From eqn[4] lecture 4,

$$\Phi = 2\pi\nu\tau_g$$

and

$$d\Phi = 2\pi\nu\, d\tau_g = (2\pi\nu/c)B\cos(\theta)\, d\theta$$

for the worse possible case i.e. longest possible projected baseline:

$$d\Phi = 2\pi\nu\, d\tau_g = (2\pi\nu/c)B\, d\theta$$

Another complicating factor is that interferometers observe a range of frequncies simultaneously, $\Delta\nu$:

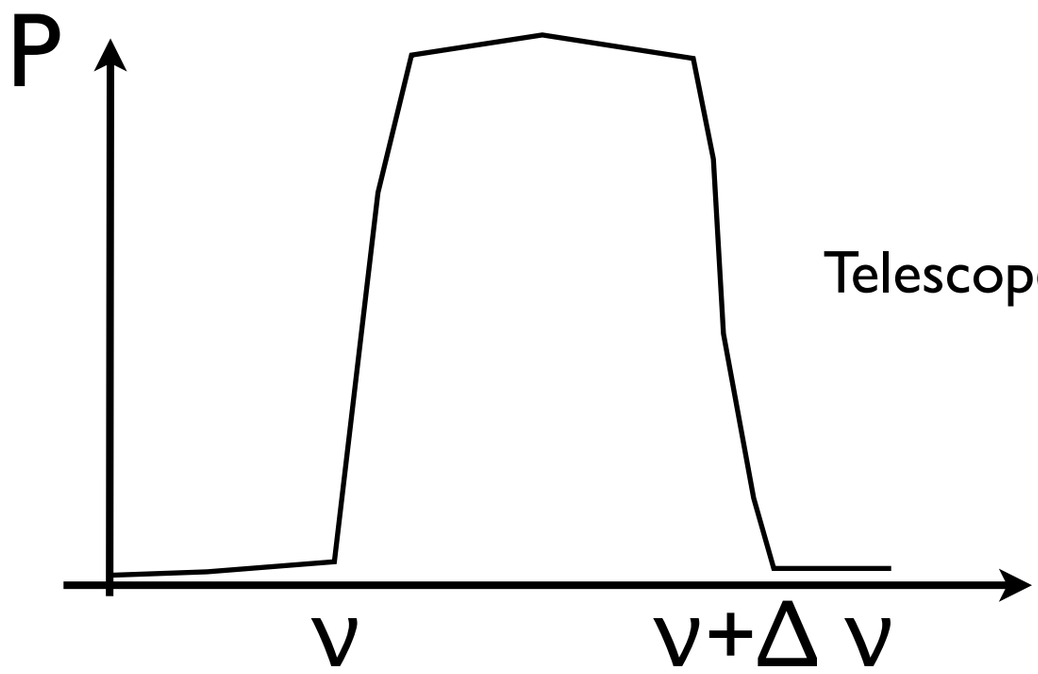

Telescope passband of bandwidth $\Delta\ \nu$

$$d\Phi_\nu - d\Phi_{\nu+\Delta\nu} = 2\pi B/c\ (\nu+\Delta\nu - \nu)\ d\theta = 2\pi B/c\ \Delta\nu\ d\theta$$

$$= 2\pi B/(\nu\lambda)\ \Delta\nu\ d\theta = 2\pi\ (\Delta\nu/\nu)\ d\theta/\theta_{beam} \qquad [16]$$

The term $\Delta\nu/\nu$ is called the fractional bandwidth.

In the worst possible case $d\Phi_\nu - d\Phi_{\nu+\Delta\nu} = 2\pi$ and we have complete de-correlation across the band.

Graphically:

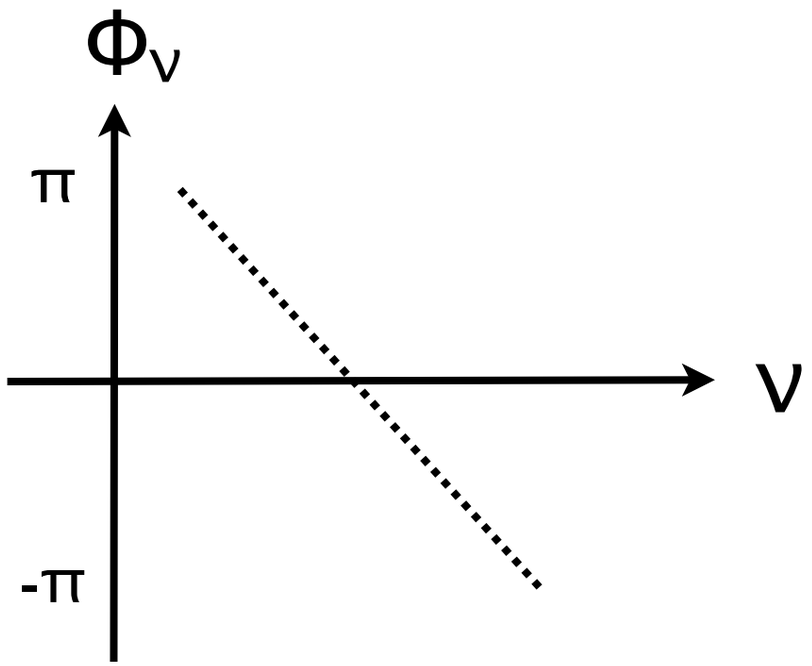

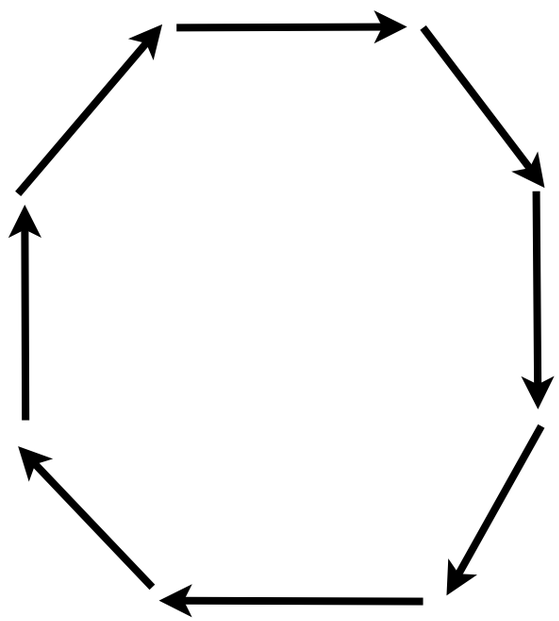

= 0
ie. complete
decorrelation

In order to avoid complete decorrelation:

$$(\Delta\nu/\nu) << \theta_{beam}/d\theta$$

For θ_{beam} ~ 1 arcsecond (VLA 20cm, A-array), $d\theta$ ~ 15 arcmin

$$\Rightarrow \Delta\nu/\nu << 0.001$$

For ν = *1400 MHz*, $\Rightarrow \Delta\nu << 1$ *MHz*.

Correlators must generate a frequency spectrum with very high resolution in order to map out large fields of view:

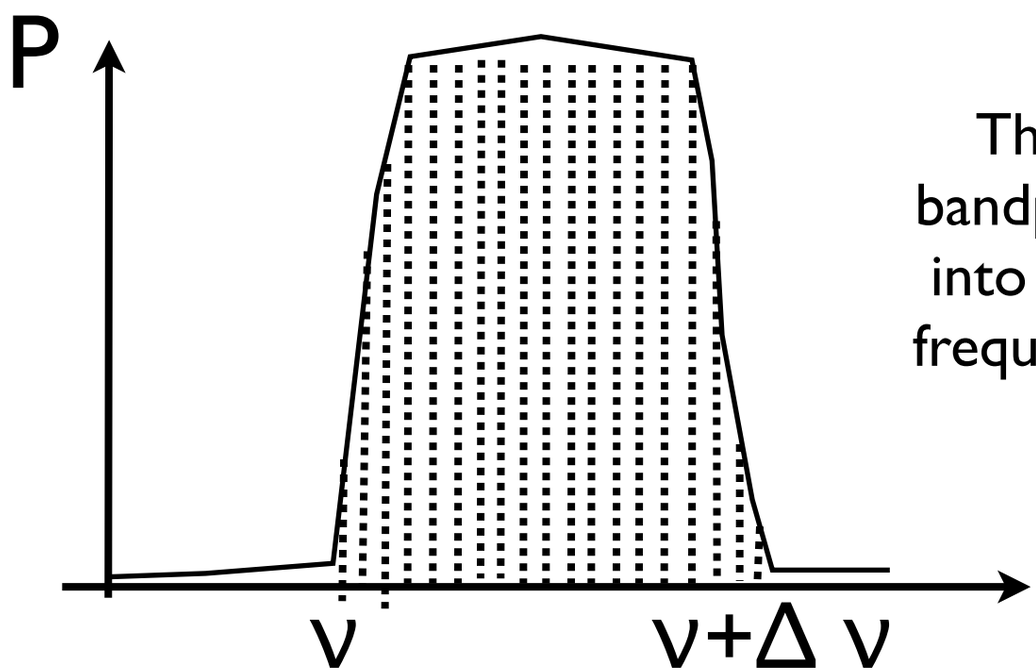

The telescope bandpass is split up into many narrow frequency channels.

Its possible to rigorously show (see TMS and SIRA book) that the relative amplitude of the peak response to a point source as a function of distance from the phase centre is given by the following function:

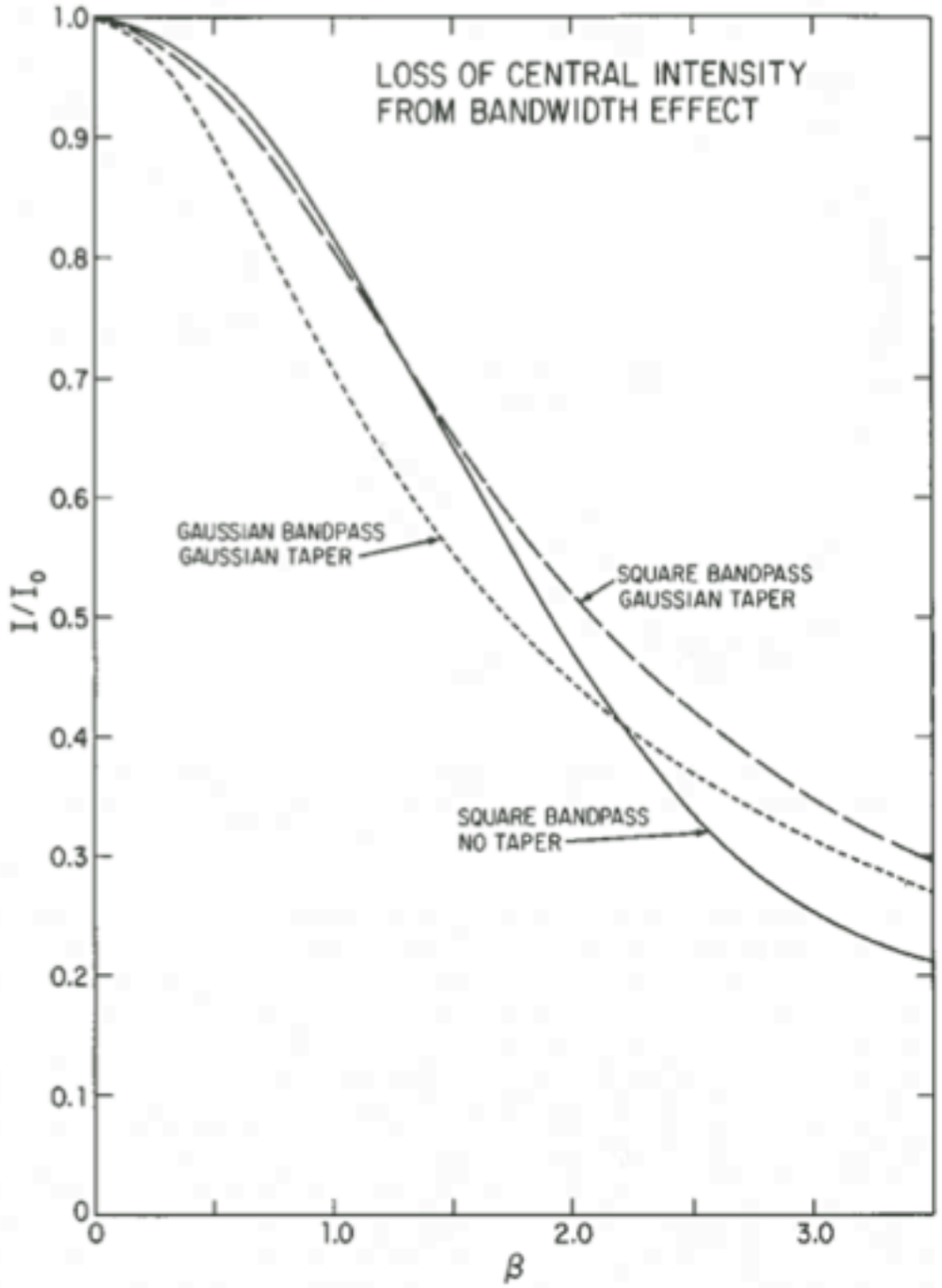

Figure 18–1. The reduction in peak response to a point source, I/I_0, for each of the band shape and taper combinations discussed in Sections 1.2 through 1.4, plotted as a function of the dimensionless parameter β.

$$\beta = (\Delta\nu/\nu)\, d\theta/\theta_{beam} \quad [17]$$

So, for a reduction of < ~10% due to bandwidth smearing, $\beta \sim 0.7$ (see figure left).

For the global VLBI array, observing at 1660MHz, $\theta_{beam} \sim 3$ milliarcsecond, for a field of view, $d\theta \sim 1$ arcsec $\Delta\nu/\nu \sim 0.0015$.

Observing at 1660 MHz this requires $\Delta\nu < 2.4$ MHz.

For continuum expts with a total bandwidth of say 256 MHz, that implies that there must be ~ 100 independent spectral channels.

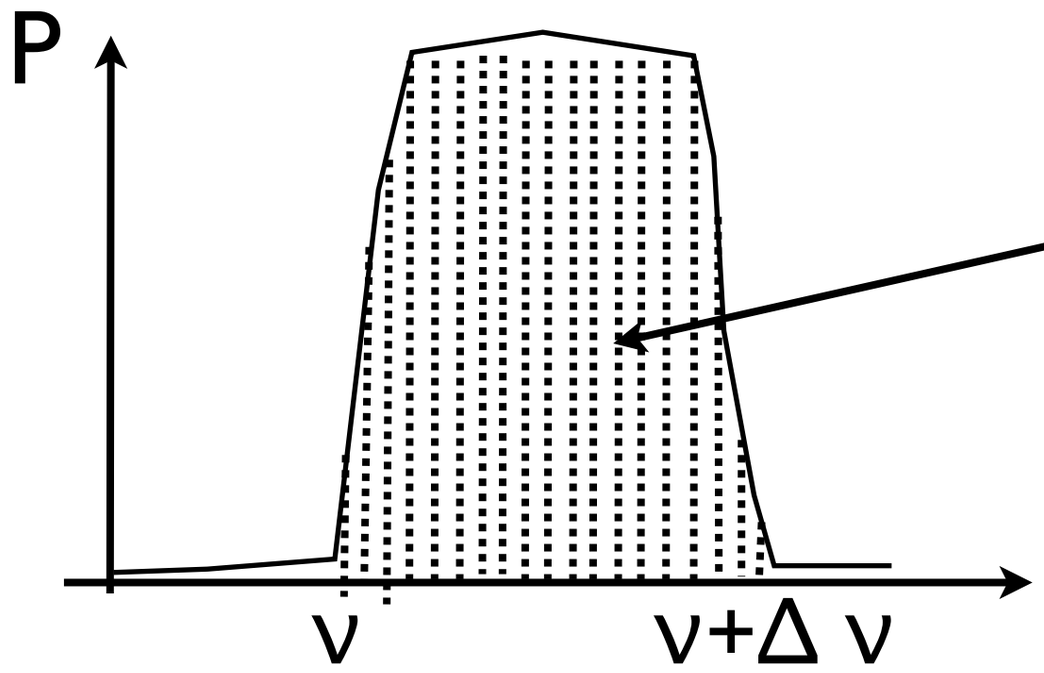

For the Global VLBI array the data must be correlated so that ~100 frequency channels span the 256 MHz band.

To better understand bandwidth smearing its instructive to take a look at what's happening in the u-v plane. Consider a single baseline (for clarity):

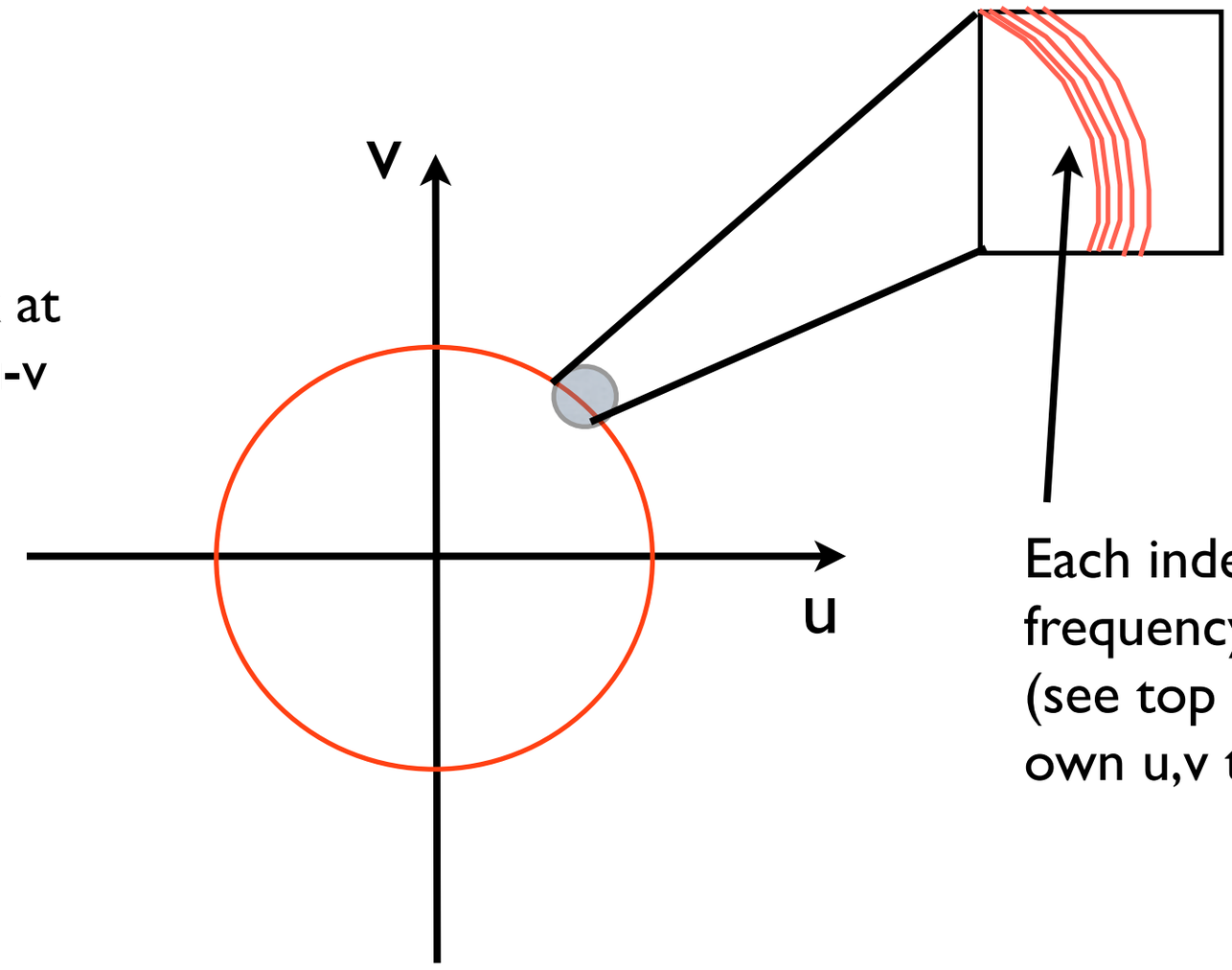

Each independent frequency channel (see top left) has its own u,v tracks.

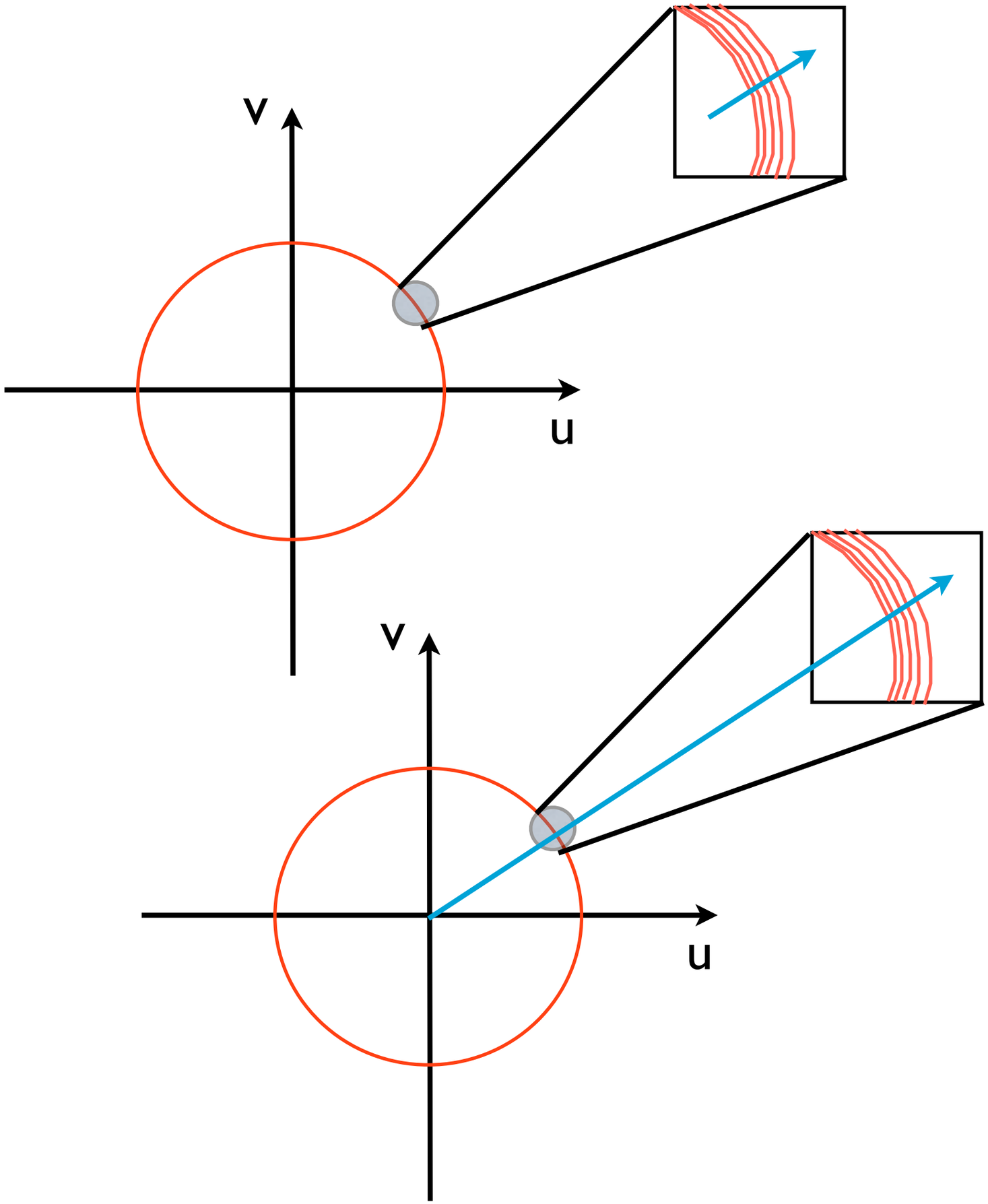

if we average across these narrow channels (see blue arrow above) to produce a single channel; in the image plane this leads to radial smearing of radio sources at the edge of the map (see blue arrow below).

Right: a bandwidth smeared image of a source lying at the edge of the primary beam of MERLIN antennas - courtesy Tom Muxlow.

The source is smeared in the radial direction - towards the phase centre of the map (see red arrow) which lies tens of arcminutes away.

To avoid bandwidth smearing, wide-field continuum interferometry observations are correlated so that many thousands of independent spectral channels are produced (like a spectral line data set). This leads to very LARGE data sets which are difficult to handle and process.

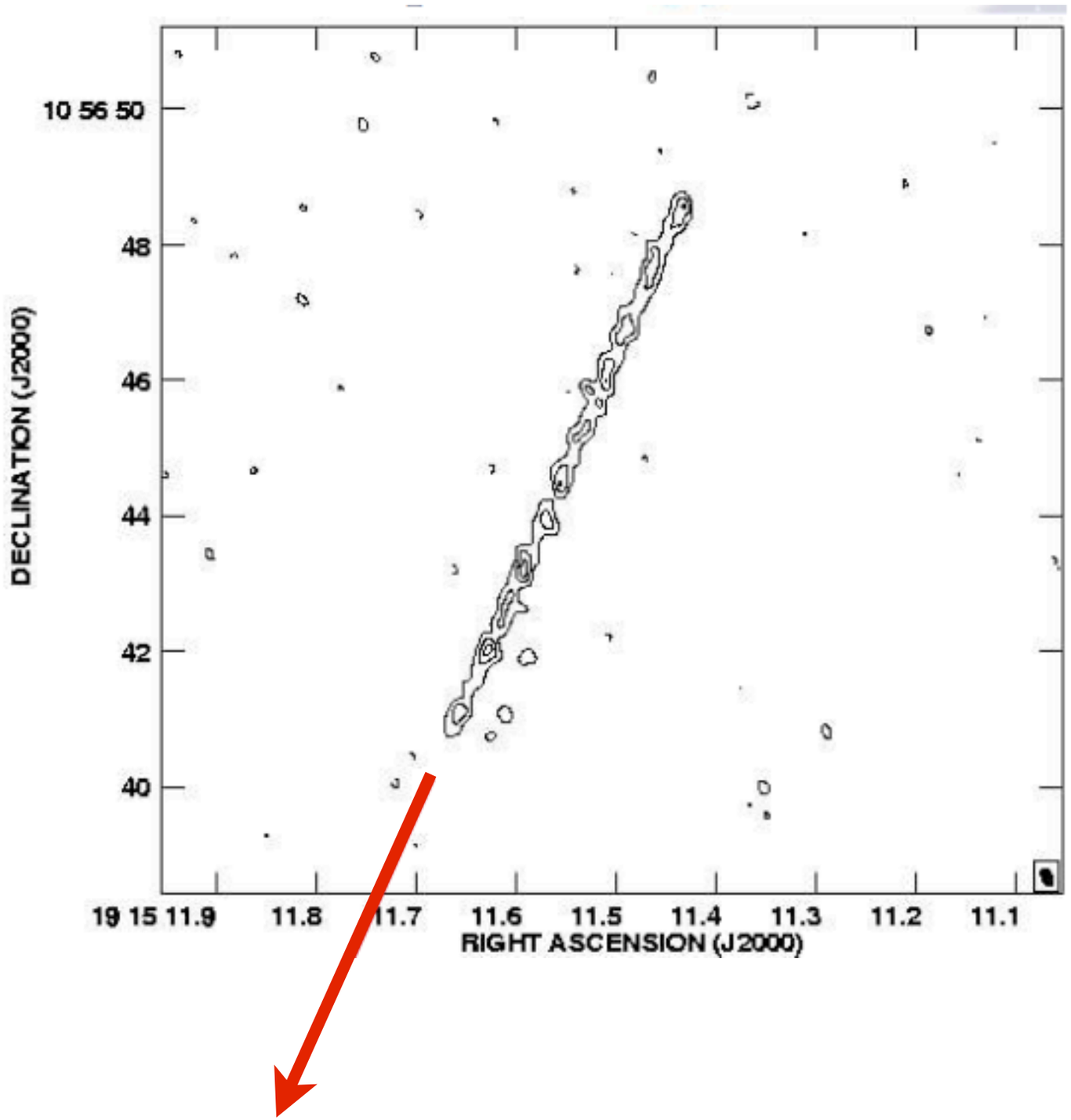

Towards the phase centre, many tens of arcminutes away.

Notes:

(i) the effect of bandwidth smearing scales as θ_{beam} (see eqn 17) i.e. it scales as baseline length. Bandwidth smearing is a big problem for VLBI arrays when the observer desires to image a large field of view.

(ii) for bandwidth smearing the integrated flux density measured in the map is preserved but the surface brightness is reduced:

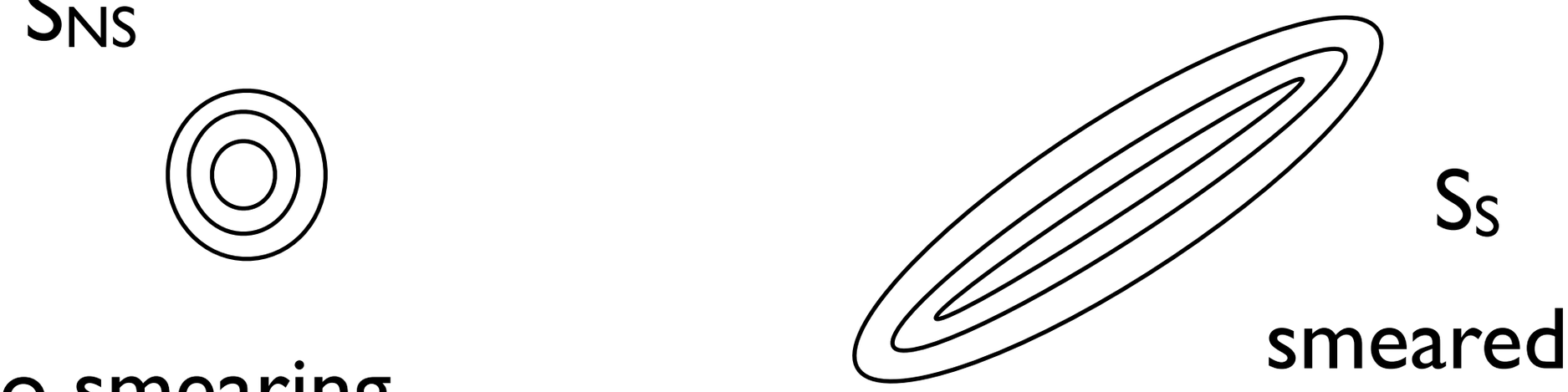

In the smeared image the peak flux density in the map is very much reduced i.e. the surface brightness of the smeared image << the non-smeared image. However, the area of the smeared image is much larger. The two effects compensate for each other so that the measured integrated flux density of the 2 images is the same ($S_{NS} = S_S$).

Notes:

(iii) Note that for a given *fixed* array/observing bandwidth smearing is independent of the observing frequency:

$$(\Delta\nu/\nu)\ d\theta/\theta_{beam} = (\Delta\nu/\nu)\ d\theta/(\lambda/B) = \Delta\nu\ d\theta\ B/c$$

This means that if a spectral channel of width 1 MHz produces no significant smearing for MERLIN at 1.6 GHz, the same is true for all other MERLIN observing frequncies.

Time averaging

Typically correlators accumulate the correlation function for a given baseline for period of a few seconds e.g. at the WSRT the integration time (sometime also called the accumulation period) is ~ 10 seconds. For VLBI arrays its usually shorter (a few seconds).

The effects of using long correlator integration times when imaging a wide-field of view is best understood by looking at data in the uv-plane. Using integration times that are too long, leads to sources at the edge of the field being smeared and distorted.

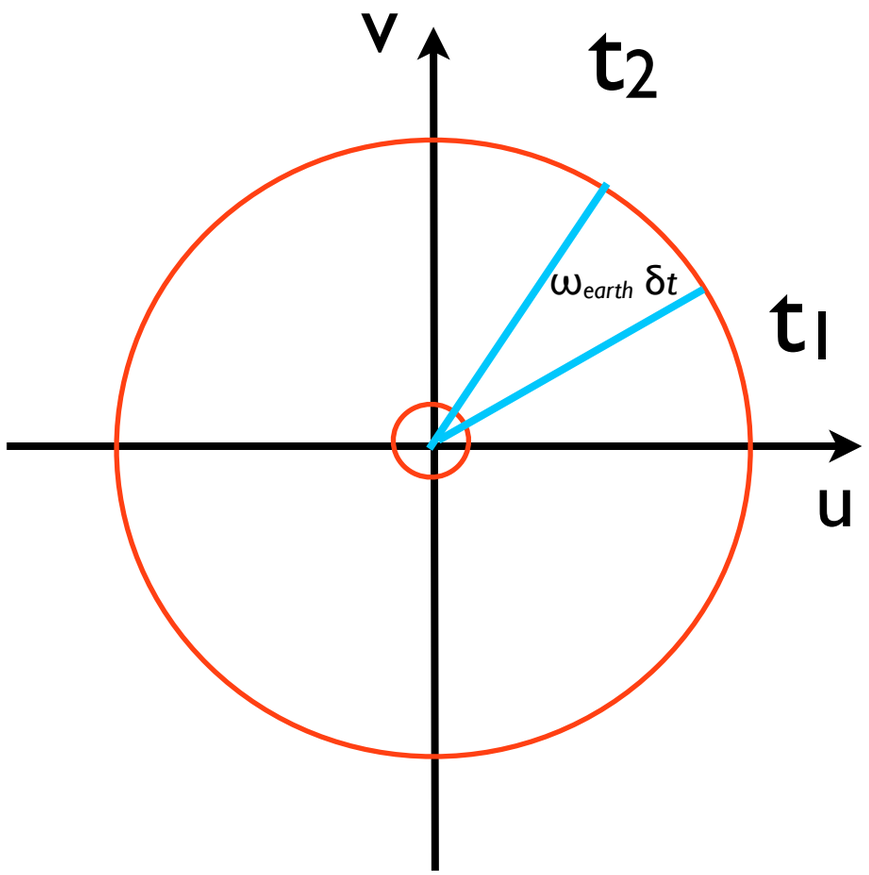

In an integration time of δt (t_1 - t_2), the baseline rotates through an angle:

$$\omega_{earth}\ \delta t$$

where ω_{earth} is the angular rotation rate of the Earth. [Note this is only exactly true for a source at declination 90 degrees]

As can be seen from the figure above, in the image plane the effect of time smearing scales with baseline length:

$$\omega_{earth}\ \delta t\ (u^2+v^2)^{1/2} \sim \omega_{earth}\ \delta t\ B/\lambda$$

e.g. an integration time of a 10 seconds may not lead to much smearing on a short baseline (see figure above), but for a long baseline the effect is significant.

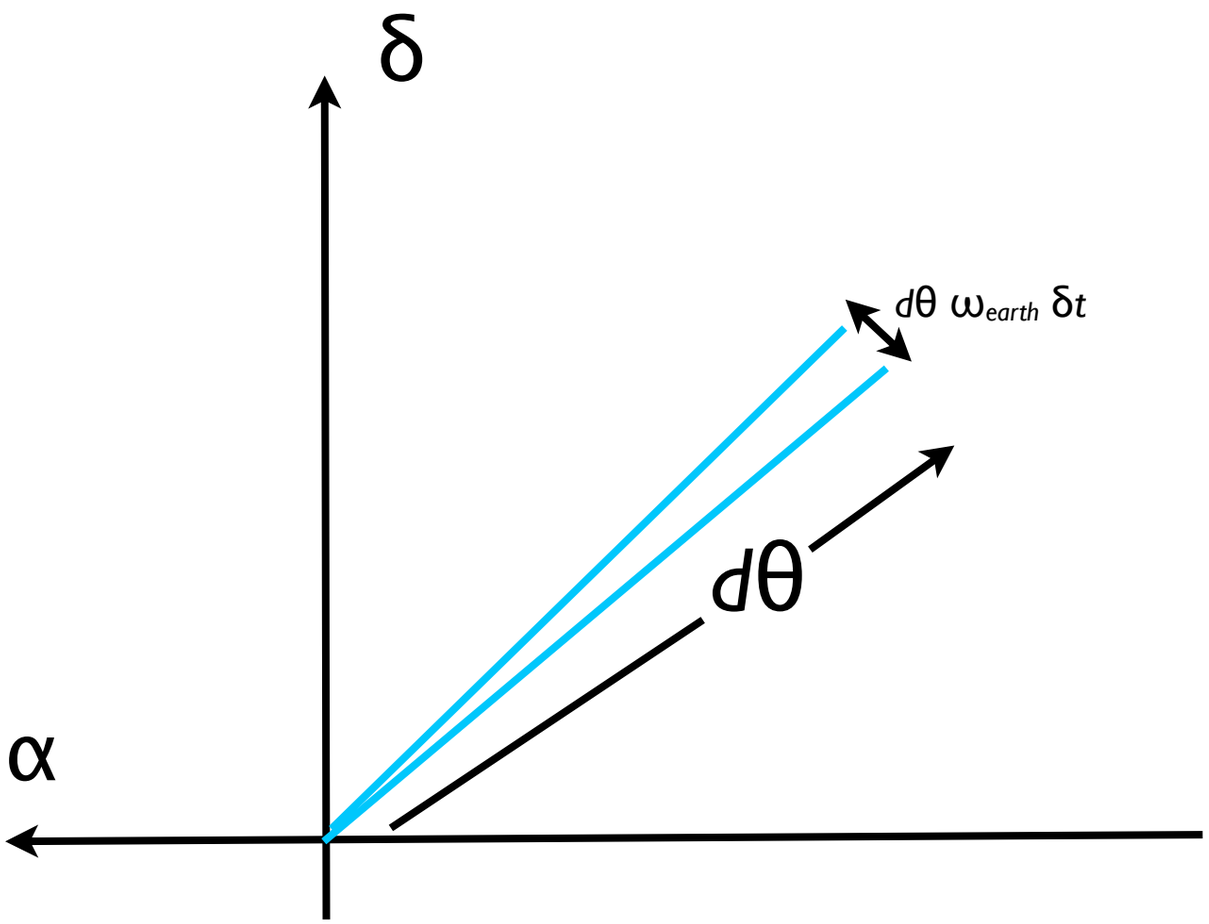

Just like bandwidth smearing the effect of time averaging scales with the desired field of view $d\theta$.

A reasonable rule of thumb (see above) is that the (small angle) rotation that occurs during the integration time in the image plane, should be much less than the synthesised beam i.e.

$$d\theta\ \omega_{earth}\ \delta t\ << \theta_{beam}\ \ or\ \ \delta t\ << (\theta_{beam}/d\theta)/\omega_{earth}$$

For the global VLBI array, observing at 1660MHz, $\theta_{beam} \sim 3$ milliarcsecond, for a field of view, $d\theta \sim 1$ arcsec => $\delta t << 42$ *seconds*.

A more rigorous treatment (see TMS and SIRA) demonstrates that the bandwidth smearing term $(\Delta\nu/\nu)\ d\theta/\theta_{beam}$ is complementary to the time smearing function $\delta t\ \omega_{earth}\ d\theta/\theta_{beam}$

Thus for more accuracy we can employ the dimensionless parameter β.

$$\delta t\ \omega_{earth}\ d\theta/\theta_{beam} = \beta \qquad [19]$$

If we take β=0.7 (i.e. we are prepared to see a 10% reduction in the response of a source due to time smearing), and if we consider the previous example e.g. a global VLBI array, observing at 1660 MHz, $\theta_{beam} \sim 3$ milliarcsecond, for a field of view, $d\theta \sim 1$ arcsec => $\delta t \sim 30$ *seconds*.

Note (see first figure in this discussion) that the time averaging effects depend not only on baseline length but also frequency:

$$\delta t\ \omega_{earth}\ d\theta/\theta_{beam} = \delta t\ \omega_{earth}\ d\theta\ B\ \nu/c$$

Note that an integration time of a 10 seconds may not lead to much smearing on a short baseline (see figure above), but for a long baseline the effect is significant. Or 10 seconds may be fine at a low observing frequency for a given baseline but too large for a much higher frequency.

The integration time used by the correlator must assume the worst case (e.g the longest baseline of the array). After correlation a baseline length dependent averaging of the data can take place (helps to reduce the data volume - a little).

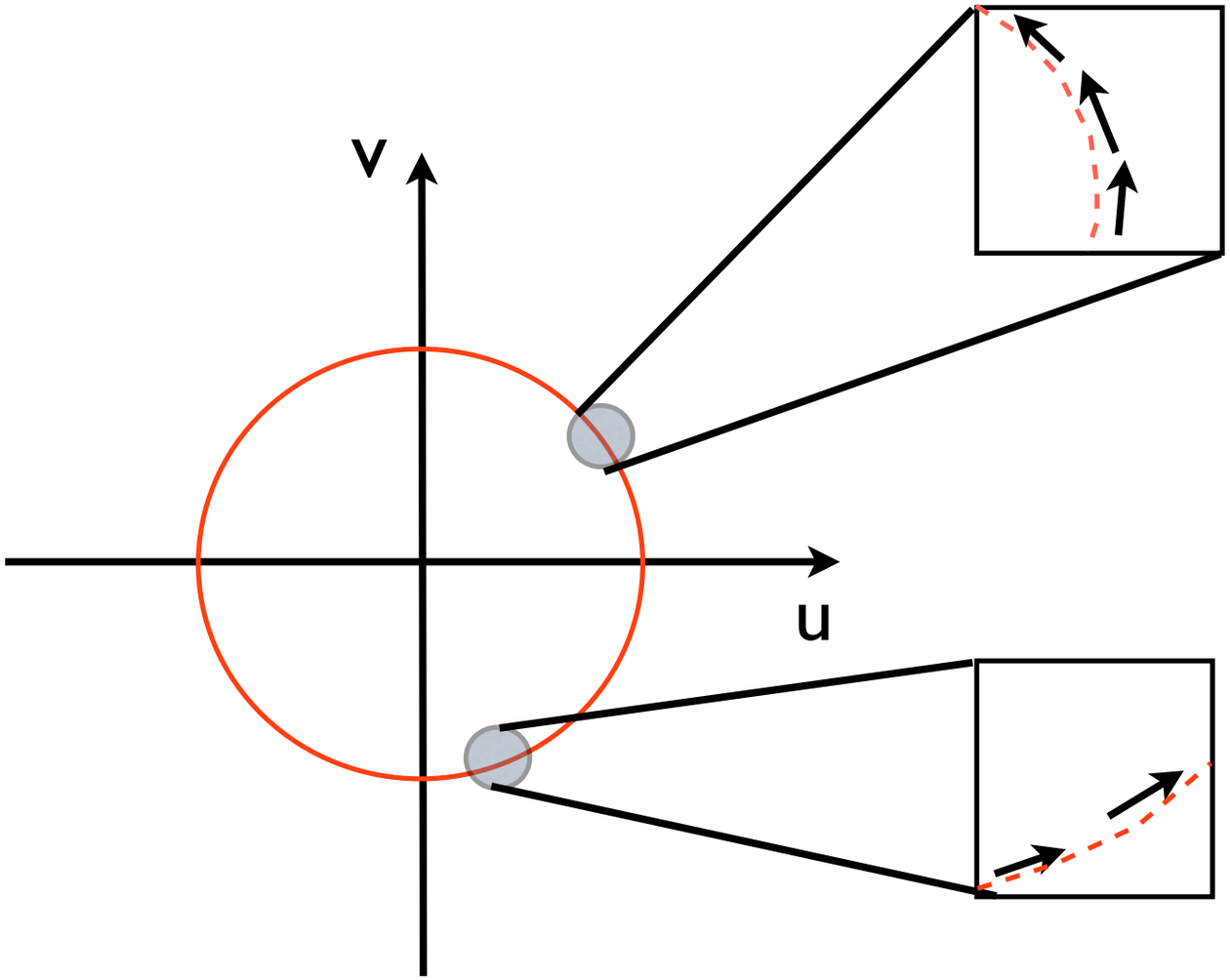

Averaging the data (left) leads to azimuthal smearing around the uv-ellipses.

Time averaging leads to more complex smearing of the source in the image plane than the radial smearing associated with bandwidth smearing (see above). The smearing depends on the uv-coverage. When the uv-coverage is very fore-shortened i.e. one dimensional (e.g. in the case of the WSRT observing a low declination source), then you can expect time smearing to produce azimuthal smearing: in the image plane.

For a given array, time averaging is usually the main limitation to the field of view at HIGH frequencies. At low frequencies bandwidth smearing tends to be a bigger problem than time averaging.

An example of time smearing (again courtesy Tom Muxlow) is shown right.

This should be a point source but is clearly very distorted by time smearing. There is no obvious relation to the direction of the field centre (red arrow).

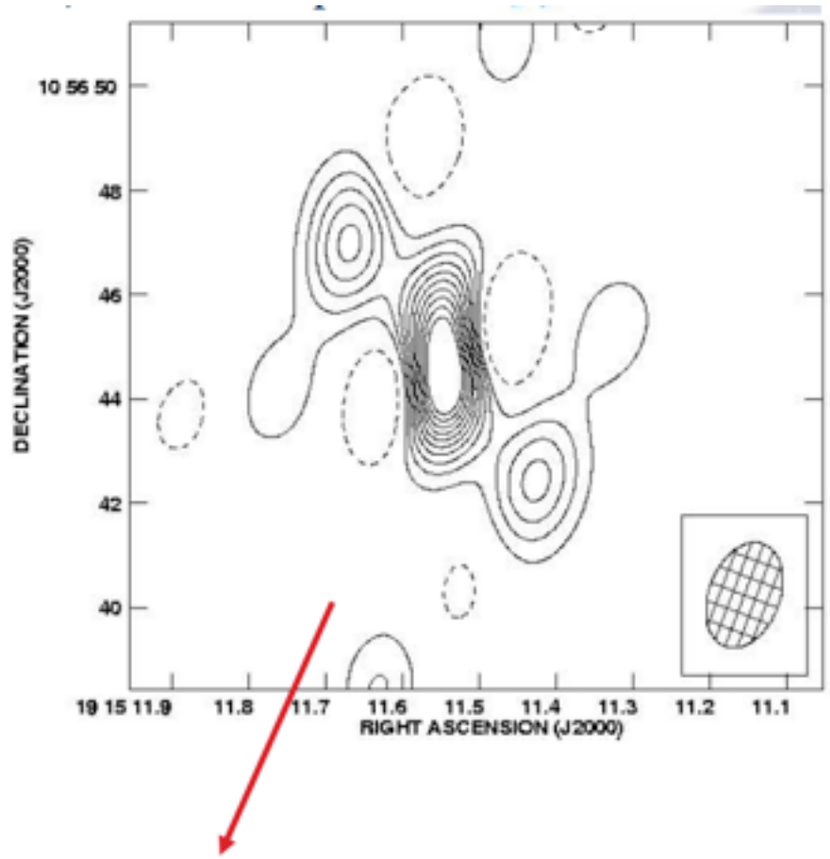

Notes:

(i) Unlike bandwidth smearing, time averaging is dependent on frequency (an integration time thats good for one frequency will not be good enough for another (higher) frequency).

(ii) Time averaging is dependent on baseline length - remember the practical data set ? On long baselines the visibility function changes more rapidly than on short baselines (for a given sky model).

(iii) Unlike bandwidth smearing, time averaging does not preserve the total flux density.

(iv) finally, the effects of bandwidth smearing and time averaging are additive (cumulative). If you employ an integration time that leads to a fall off in the response of 10% at the edge of the desired field of view, and you also employ a spectral resolution that also falls off to 10% at the edge of the field of view, then when you make the map you will see a 20% reduction in the response of a source at the edge of the field of view.

Finally another way of thinking about the effects of averaging data is that by averaging the data you mis-label the data as a function of time and frequency.

As a result, in interferometry, averaging the data always leads to information loss.

The practical effect is that the recovery of the true brightness distribution of off-axis sources (i.e. sources that are not located at the centre of the field) is severely compromised.

Note also that the process of averaging "freezes in" bad data. Once averaged in time and frequency there is no way to correct errors that occur on time (or frequency) scales that are less that the average time (or averaged-up bandwidth).

==> DON'T AVERAGE THE DATA UNLESS YOU HAVE TO

(or at least understand that the FoV is heavily reduced after averaging).

Primary beam attenuation

The shape of the antenna power pattern represents the ultimate restriction on the observers field of view.

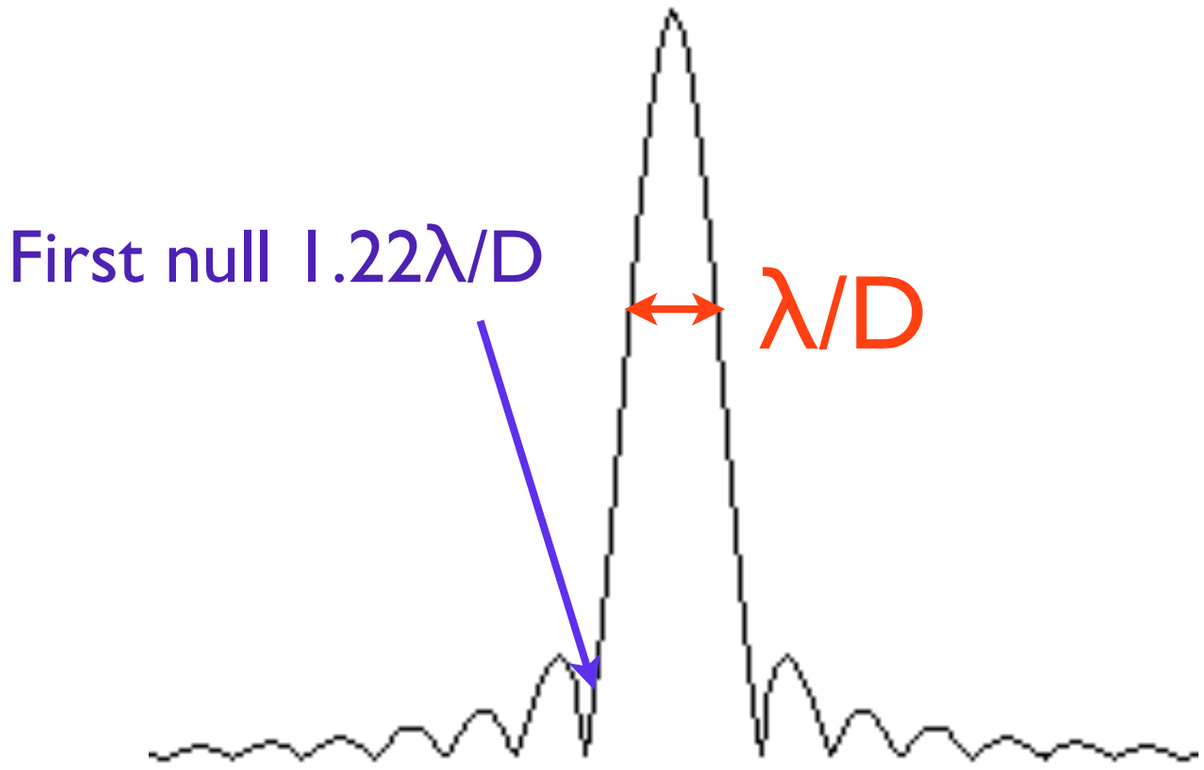

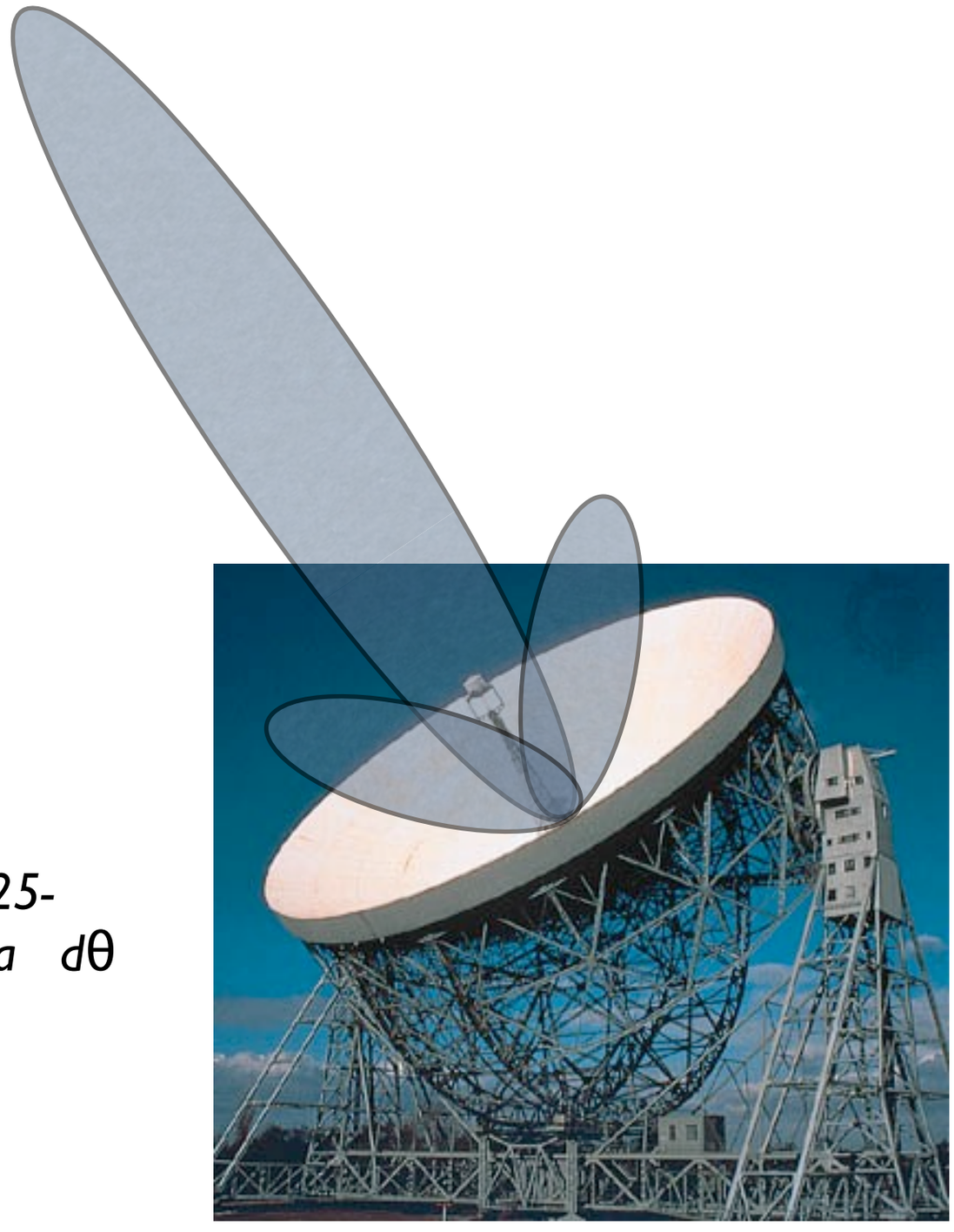

e.g. at 18cm, Lovell telescope, *dθ ~ 8 arcmin; for a 25-metre antenna dθ ~ 25 arcmin; for a 6 metre antenna dθ ~ 1.8 deg.*

The change in the response of the primary beam of antennas in an array can be corrected for, if the shape of the primary beam is well measured and if the array is made up of antennas of the same type/size (not always the case e.g. MERLIN, Global VLBI). This is called making a primary beam correction. If this is not applied, the flux densities you measure at the edge of the fields will be less than the true flux density.

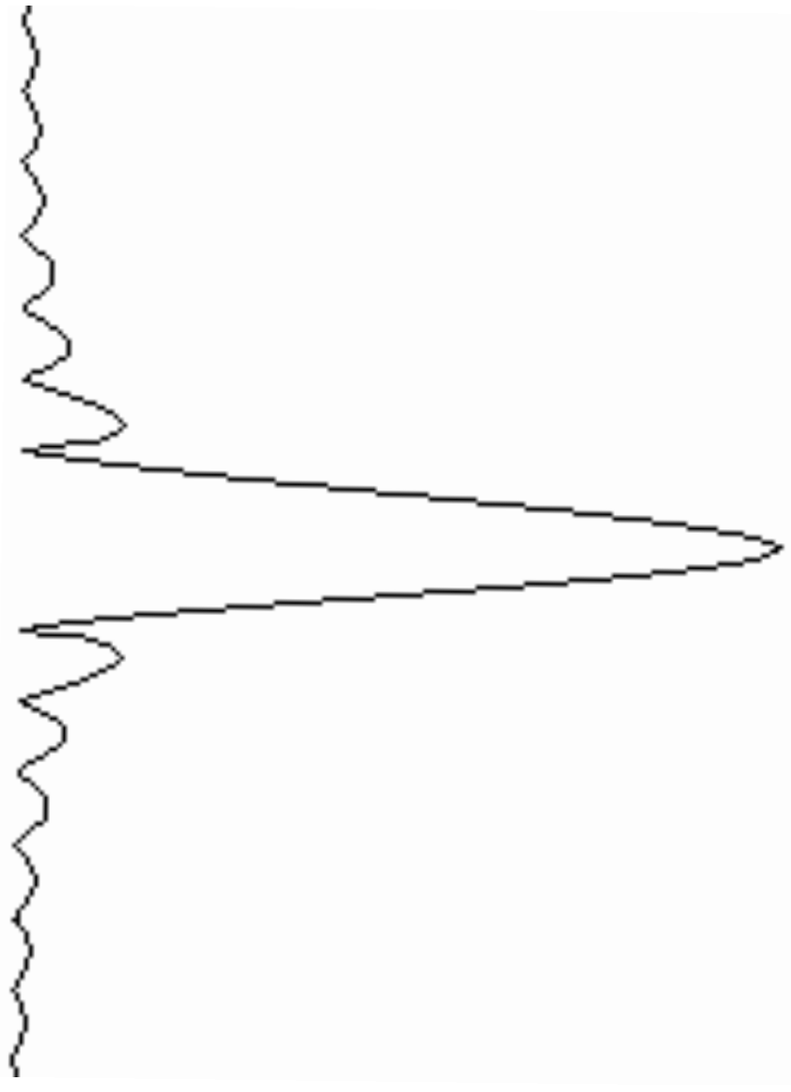

In VLBI sometimes arrays like WSRT and VLA are phased-up to look like a single large telescope.

The primary beam is then very small (λ/B rather than λ/D). For example, for the WSRT the FoV is reduced to only 10 arcseconds when the phased array is used as an element of the EVN.

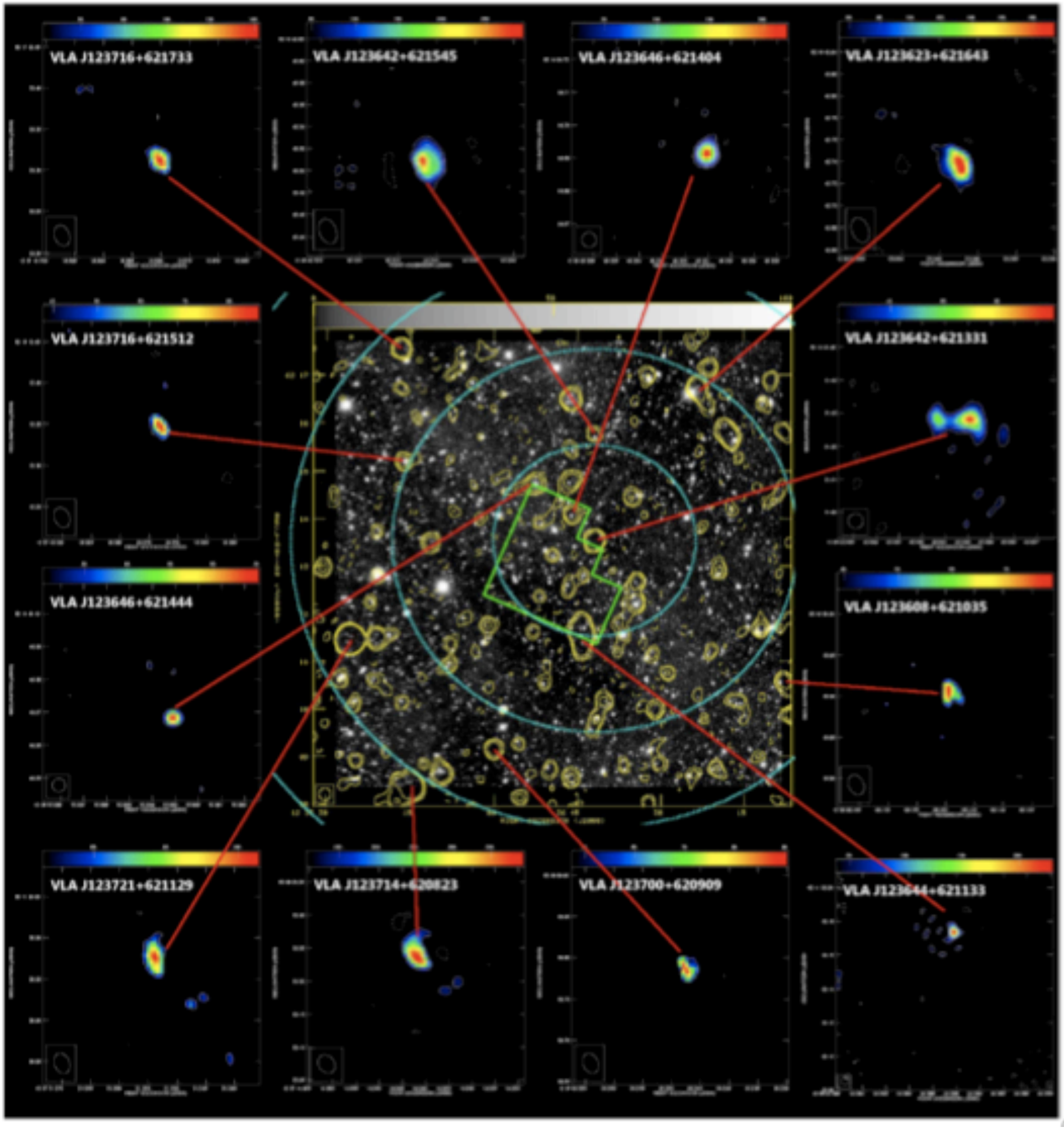

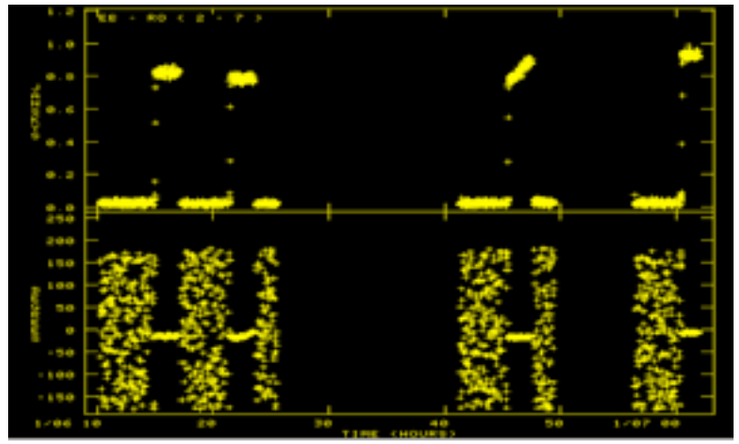

The data I showed earlier was a wide-field VLBI data set. The integration time was 0.25 seconds and the data were stored as 1024 channels each 32 kHz in width.

Even so, for sources at the edge of the field about 2/3 of the data must be thrown away because of smearing effects.

The size of the data set is ~ 1 Terabyte.

Survey - figures of merit (FoM)

Wide-field imaging is clearly important for the efficiency of large radio surveys.

The figure of merit of a radio telescope as a survey instrument is given as the number of square degrees per second it can image down to a given sensitivity limit.

Recall (eqn 14)

$$\Delta I = SEFD/(N(N-1)\Delta\nu\Delta t)^{1/2}$$

then the time Δt to reach a given sensitivity limit (for point sources) ΔI is

$$\Delta t = SEFD/(N(N-1)\Delta\nu\ \Delta I^2) \sim SEFD^2/(N^2\Delta\nu\ \Delta I^2)$$

The number of square degrees per second that can be surveyed to a sensitivity limit (ΔI) is then given by:

$$SS = F\ \Delta\nu\ (N\Delta I/SEFD)^2 \qquad [20]$$

where F is the field of view (in square degrees).

This leads to some interesting results e.g. imagine we wish to conduct a survey down to 1 mJy. let's see how the following telescopes compare in terms of survey FoM:

VLA@1400 MHz (SEFD= 300 Jy, N=27, $\Delta\nu$=50MHz). One beam has a field of view of 0.2 sq deg

$$\Rightarrow SS_{VLA} = F\,\Delta\nu\,(N\Delta I/SEFD)^2 \sim 0.08$$

WSRT@1400 MHz (SEFD= 300 Jy, N=14, $\Delta\nu$=160MHz). One beam also has a field of view of 0.2 sq deg:

$$\Rightarrow SS_{WSRT} \sim 0.07$$

WSRT-APERTIF@1400 MHz (SEFD= 400 Jy, N=14, $\Delta\nu$=300MHz). One beam also has a field of view of 0.2 sq deg but there are 25 independent beams:

$$\Rightarrow SS_{WSRT\text{-}APERTIF} \sim 1.8$$

EVLA@5000 MHz (SEFD= 300 Jy, N=27, $\Delta\nu$=2000MHz). One beam has a field of view of 0.02 sq deg

$$\Rightarrow SS_{EVLA} \sim 0.3 \qquad **$$

More about imaging

Data weighting: An important aspect we have not yet covered is data weighting. Every visibility has an amplitude and a phase, but in addition it also has a weight W(u,v):

$$I^D(x,y) = \int\int W(u,v)V(u,v)e^{-i2\pi(ux+vy)}dudv$$

The data can be weighted in many different ways:

Natural weighting - here we use the statistical weights: $W_i \sim 1/\sigma_i^2$ - each i^{th} visibility is weighted by the inverse of the variance squared. This kind of weighting optimises the r.m.s. noise in the final image and therefore maximises the chance of detecting faint point sources. For detection experiments - this is usually the weighting form to use.

Note that in arrays with telescopes of very different sensitivities (e.g. VLBI arrays) the effects of natural weighting need to be considered with care. Right: 300-metre Arecibo and a 25-metre VLBA telescope to scale!

VLBA

. e.g. consider a global VLBI array including Arecibo (SEFD ~ 3 Jy telescope) and the ten telescopes of the VLBA (each 300 Jy telescopes). From eqn[13] baselines that include Arecibo will have a weight which is 10 times larger than VLBA-VLBA baselines:

$W_{ARECIBO\text{-}VLBA} = 1/(3.300)^{1/2}$ $W_{VLBA\text{-}VLBA} = 1/(300.300)^{1/2}$

$W_{ARECIBO\text{-}VLBA}/W_{VLBA\text{-}VLBA} \sim 10.$

This means the baselines that include Arecibo will dominate any image that is produced using natural weighting. Natural weighting maximises the detection threshold for point sources (important for detection observations of faint sources) but it will not produce a good image of a source that is well detected on all baselines! Indeed, the 45 baselines of the VLBA will not contribute very much to the final image with this kind of weighting scheme.

Pure uniform weighting - in this case all the data have the same weights (unity) - no matter what. This produces a well behaved "nice" dirty beam (e.g. lower side lobes than natural weighting since the latter does not make full use of all u-v points) but the noise in the map is higher.

Uniform weighting - in this case the statistical weights (used in natural weighting) are modified.

$$W_i = W_i / \sum W_i$$

here the summation is restricted to some finite region of the u-v plane. The effect is to weight-up areas of the uv-plane where the natural weights are low.

Inverse density weighting - here the weights are replaced by the local density of u-v data points:

$$W_i = W_i / \rho$$

- this weights up regions of the u-v plane where data are sparse (e.g. on the longest baselines). The result is that the longest baselines are weighted up, the synthesised beam becomes smaller but the r.m.s. noise usually increases significantly.

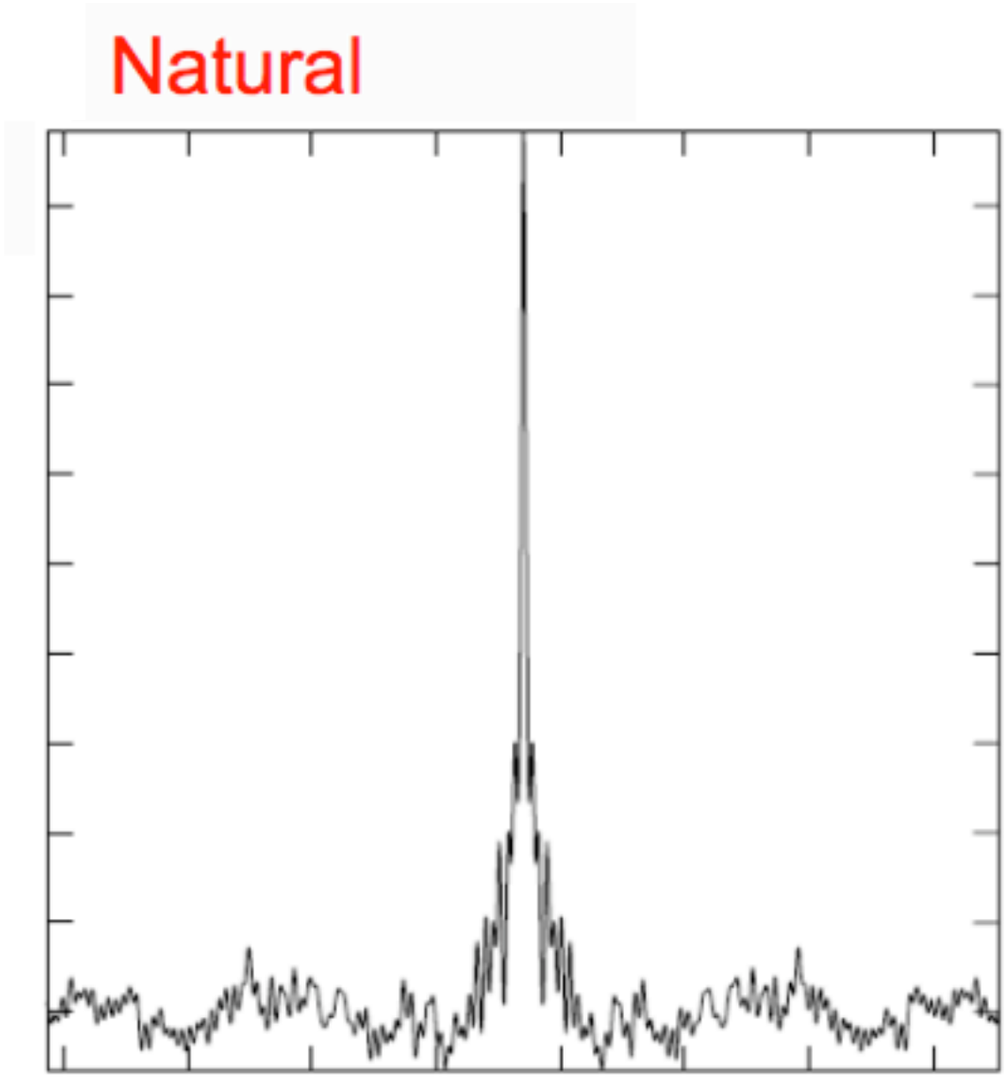

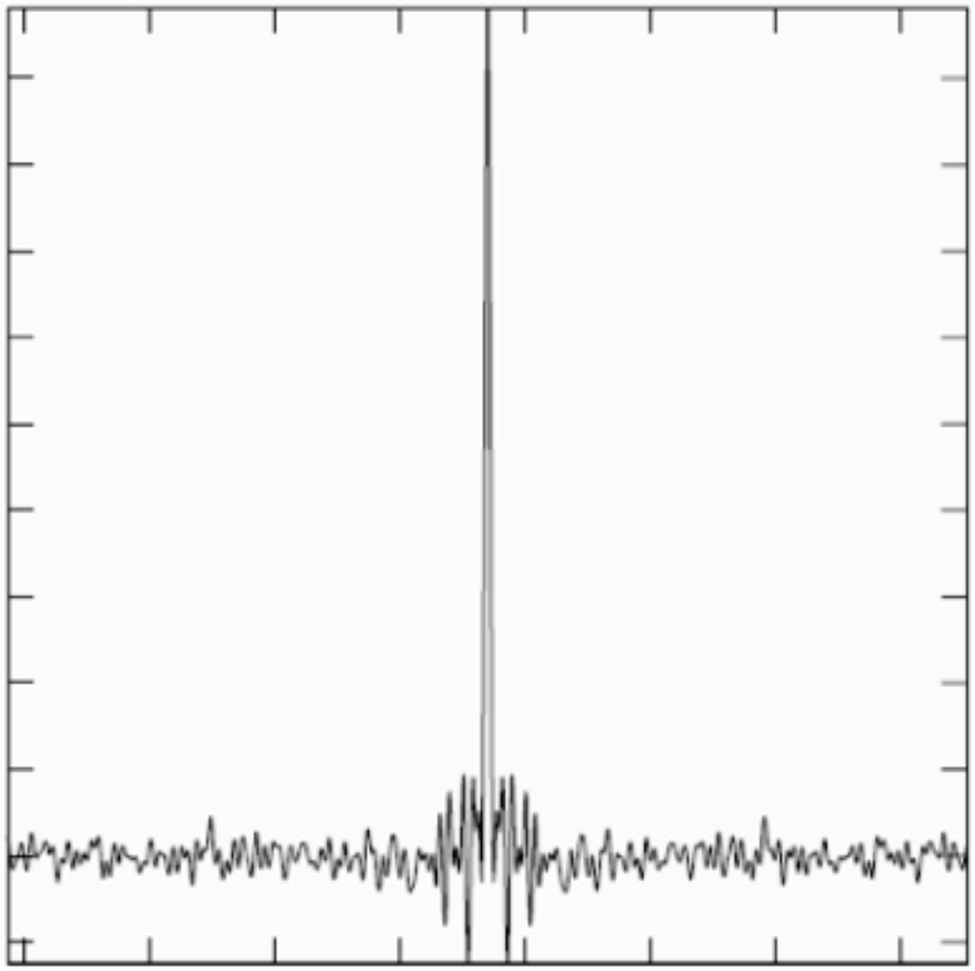

Dirty beams for Natural and Uniform weighting - courtesy Simon Garrington

Robust weighting - the weights are modified according to the Robust parameter. R = +5 produces something v.close to natural weighting, R= -5 produces near pure uniform weighting and R=+4.... to .....-4 provides a weighting scheme that lies between these two extremes. This gives a fine degree of control for astronomer in terns of data weighting. Robust weighting is widely used (Briggs PhD thesis1995).

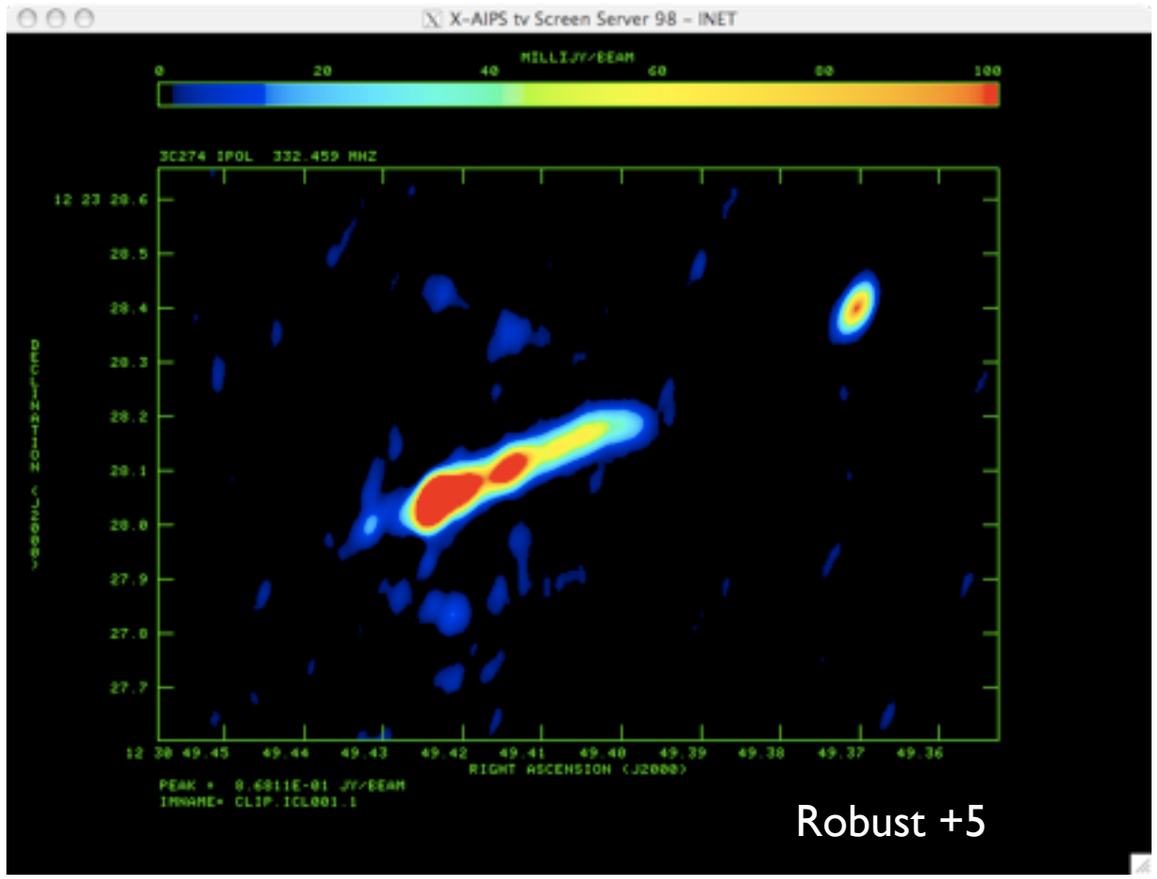

Robust +5

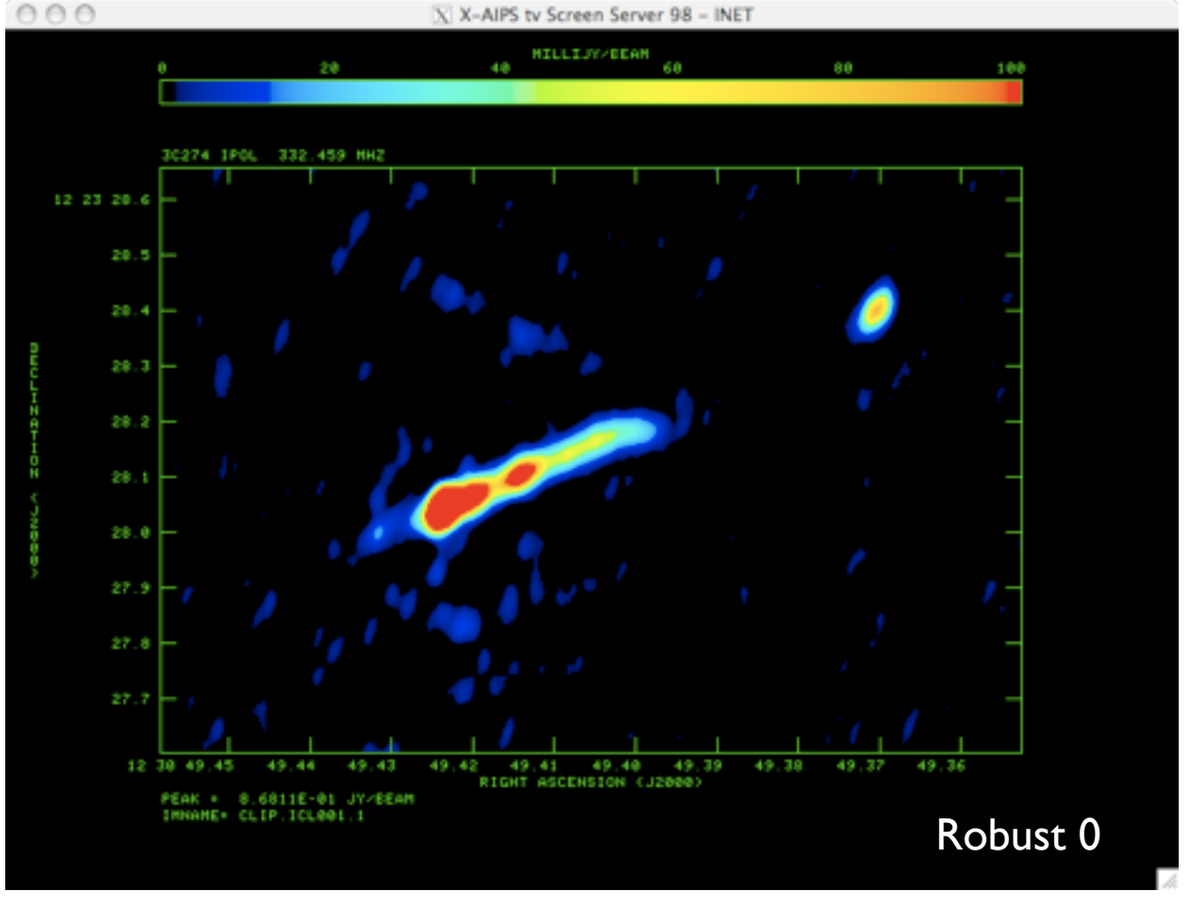

Robust 0

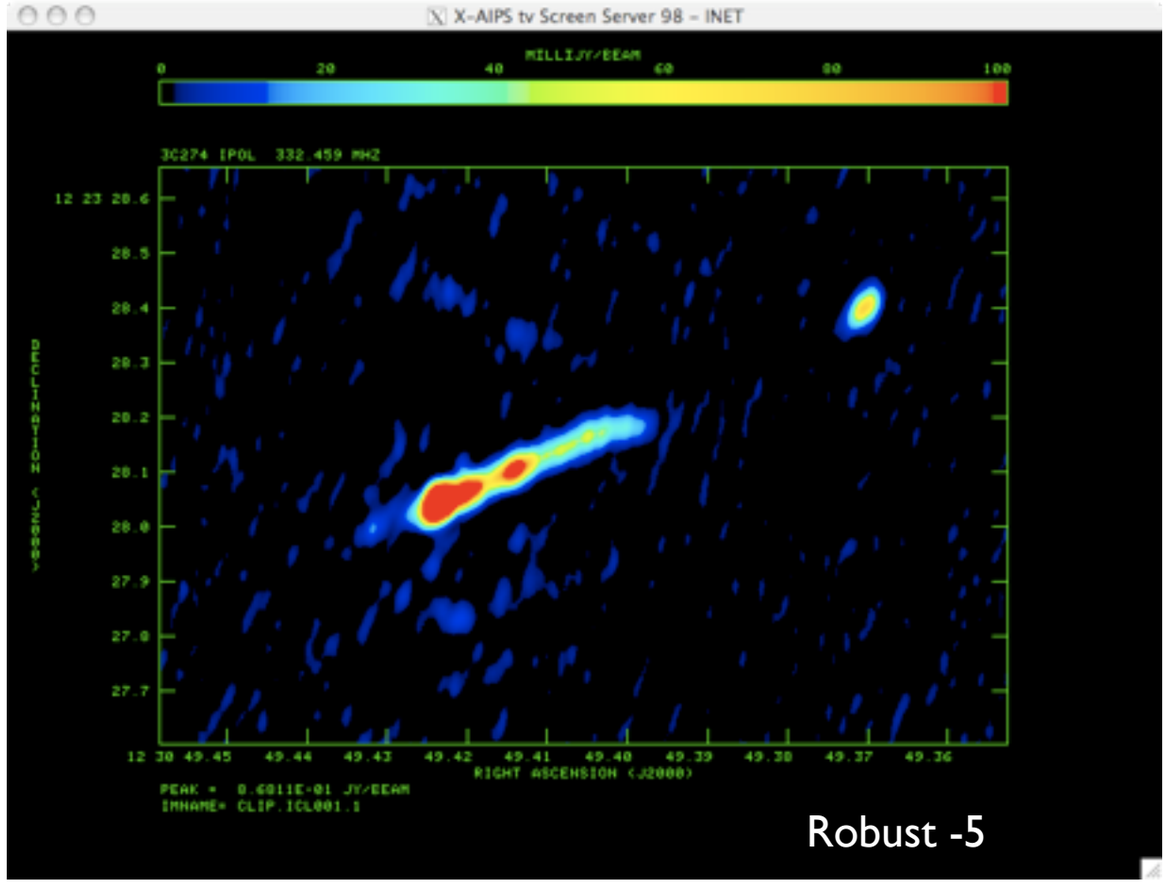

Robust -5

More on Deconvolution

Most maps in the literature are produced via the CLEAN algorithm (or some variant of it). For most observations CLEAN does very well.

However, for very extended sources, the fact that CLEAN uses delta functions to represent the source leads to artefacts in the image. CLEAN tends to break up extended emission into lumps, and occasionally introduces ripples corresponding to unsampled Fourier components in the uv-plane.

CLEAN has difficulty properly represented extended sources like this (a Supernova remnant) via delta functions.

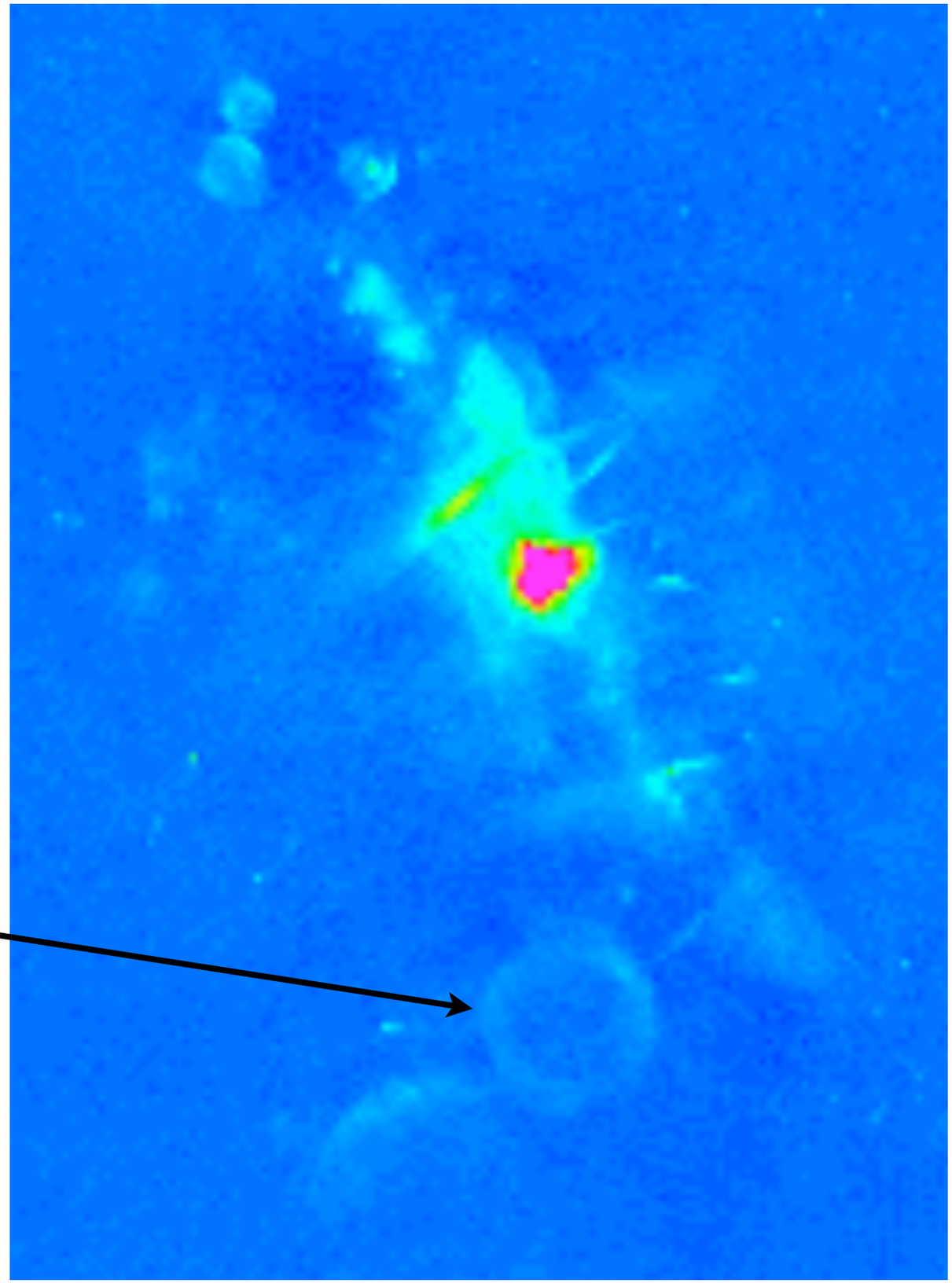

In the past other algorithms were used e.g. the Maximum Entropy Method (MEM). This algorithm tries to find the lowest contrast or smoothest positive image which fits the original data within the noise - it does not deal well with really compact features in the image however.

Multi-scale CLEAN algorithms attempt to recognize that the emission in the sky usually comes on a variety of scale sizes; it decomposes the image into Gaussians of the specified scale sizes. This means it does not spend huge amounts of time CLEANing large extended sources pretending that they are really collections of delta functions.

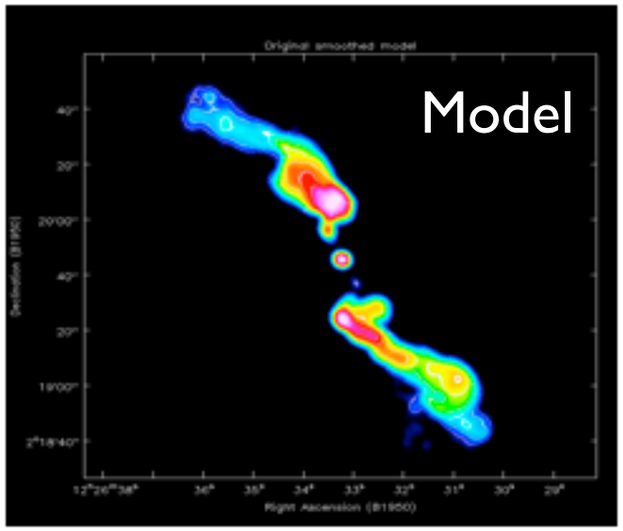

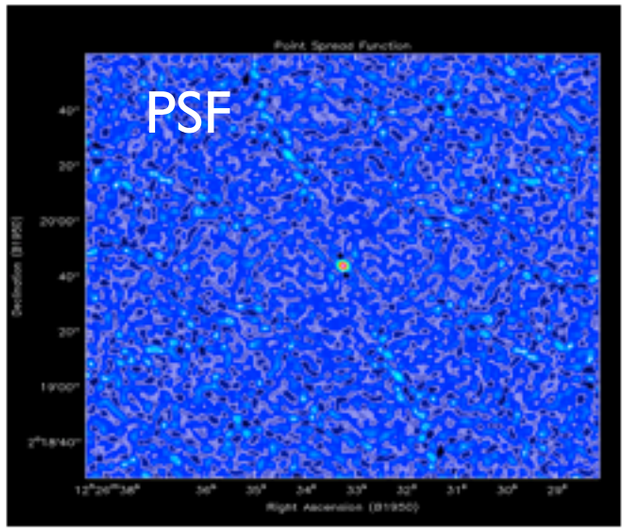

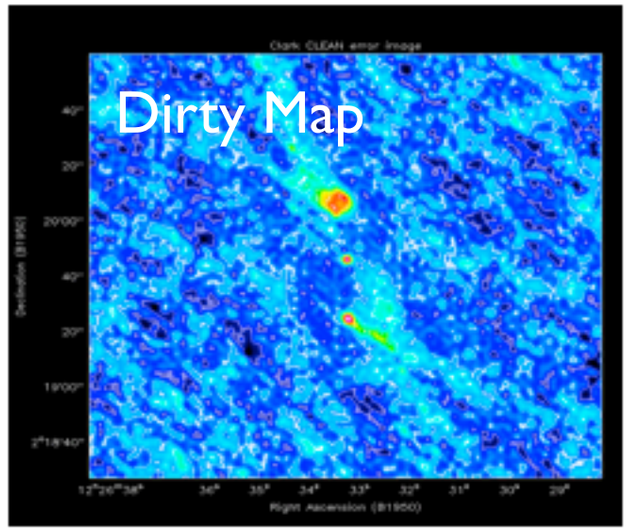

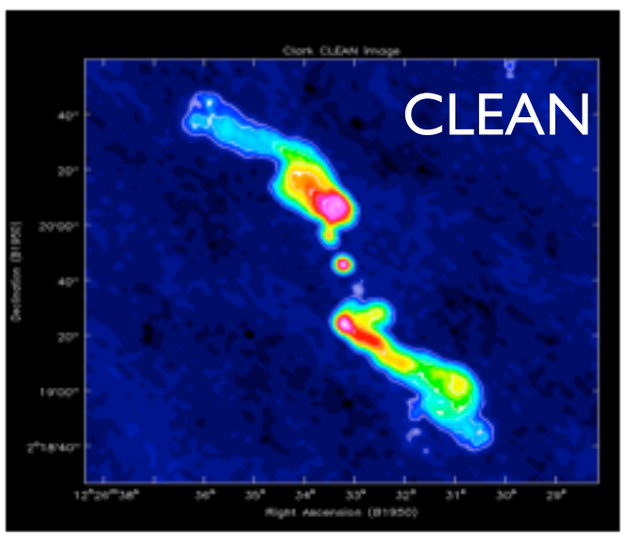

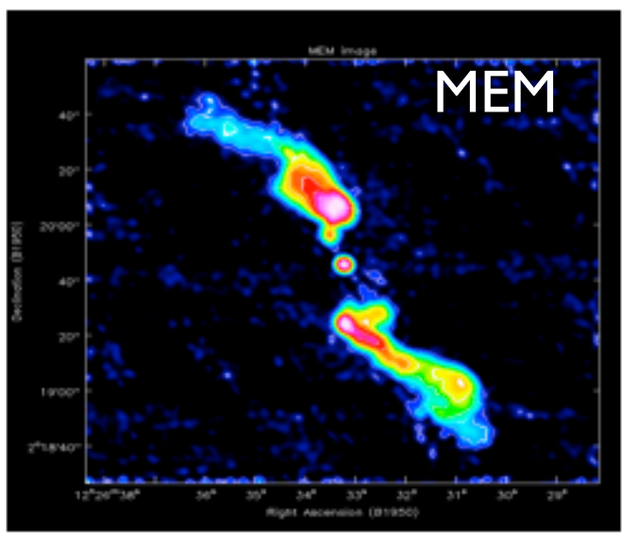

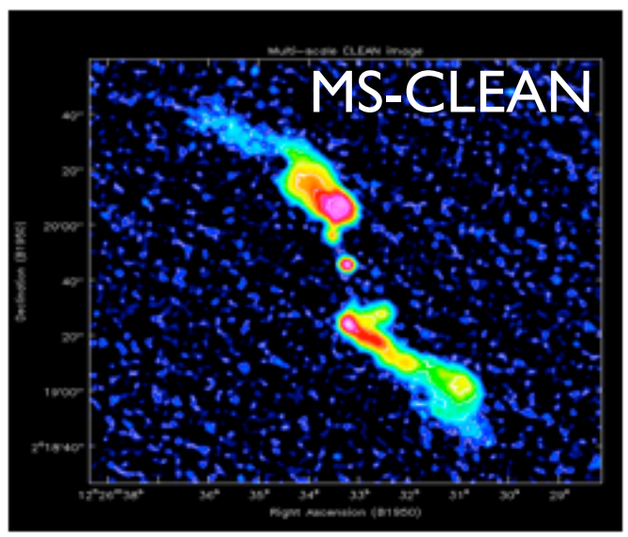

Image courtesy
Wim Brouw
- take your pick!

Irrespective of which algorithm you use, the spatial structure of an object can only be mapped on scales which are sampled by the projected baselines, or which can be estimated by interpolation between baselines.

The shortest *projected* baseline B_{min} determines the largest-scale structure which is not filtered out of the synthesis image.

The largest-scale structure θ_{max} (not to be confused with the field of view!) which can be detected is roughly given by

$$\theta_{max} < \sim \lambda/(2B_{min})$$

High Dynamic Range Imaging

At low frequencies (e.g. 1.4 GHz) there are always bright sources in the field of view of interferometers like the VLA, WSRT and MERLIN. Sometime it can be difficult to achieve the noise level you would expect from thermal noise calculations (i.e. the noise level we would expect from eqn[14]). In this case, the image is said to be "Dynamic range limited".

The dynamic range (DR) of an image is defined as:

$$DR = \frac{\text{peak flux density in map}}{\text{off-source r.m.s. noise level}}$$

DRs of 10000:1 can be fairly easily achieved. However, for deep field studies this may not be enough.

e.g. if an image is Dynamic range limited at 10000:1 and the brightest source in the field is 1 Jy, this implies that the r.m.s. noise level in the map will be limited to 1/100000 = 100 microJy. But the sensitivity of the array is much better than this and many deep surveys wish to reach microJy noise levels.

Errors that limit the dynamic range of an image include

(i) non-closing errors due to baseline (not antenna) based errors (e.g. small changes in telescope passbands on short time scale or errors in the correlator etc.)
(ii) telescope pointing errors,
(iii) non-isoplanatic effects.

Baseline based corrections can be applied to data to remove the effects of non-closing errors. The other errors are more difficult to correct for.

Pointing errors are problematic because the effect is not unifrom over the full field of view:

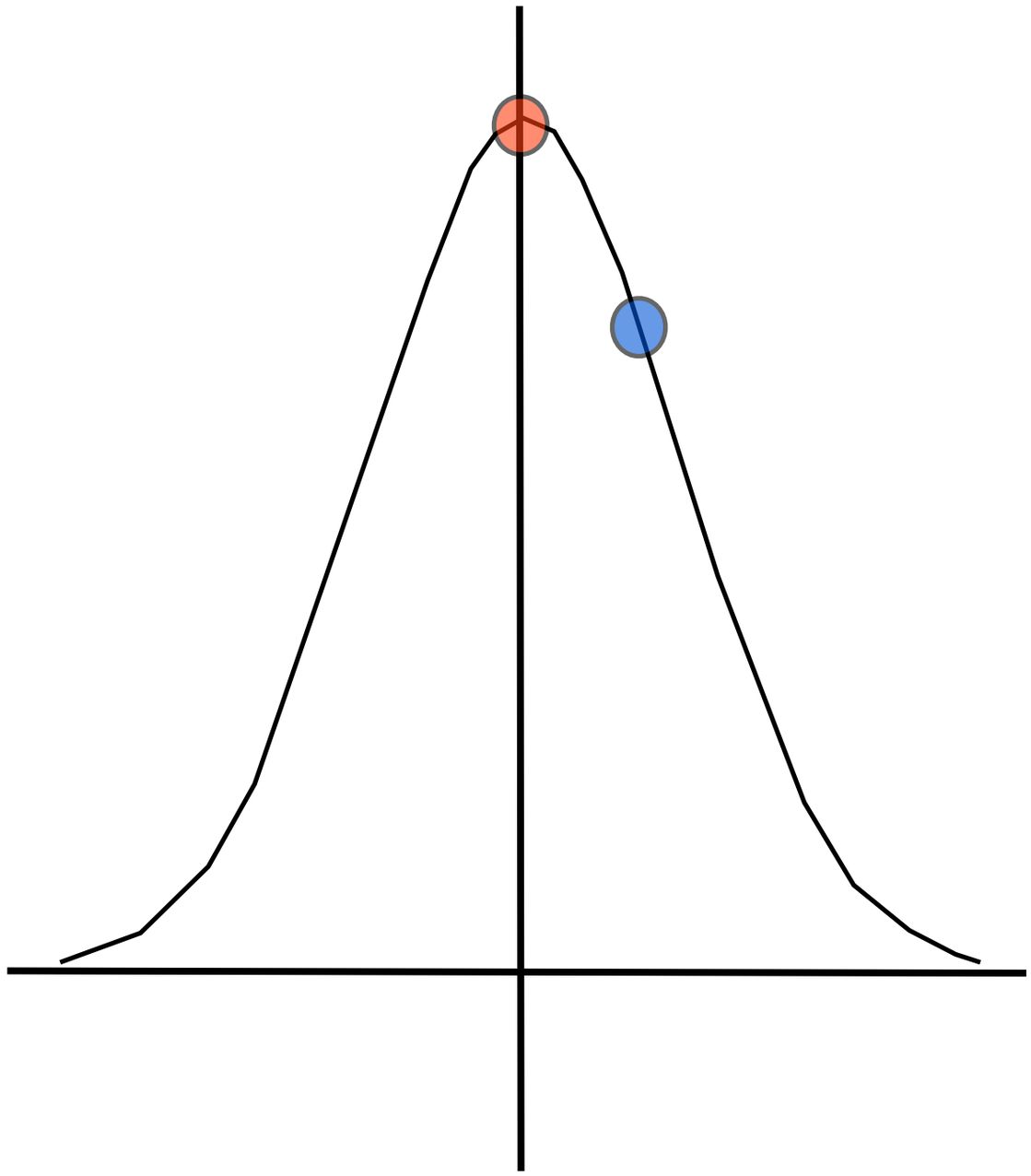

left:

cartoon representing no pointing errors - red source is at the field centre. But there are other sources in the field (e.g. the blue source).

What happens if we introduce a pointing error ?

Now we introduce a pointing error:

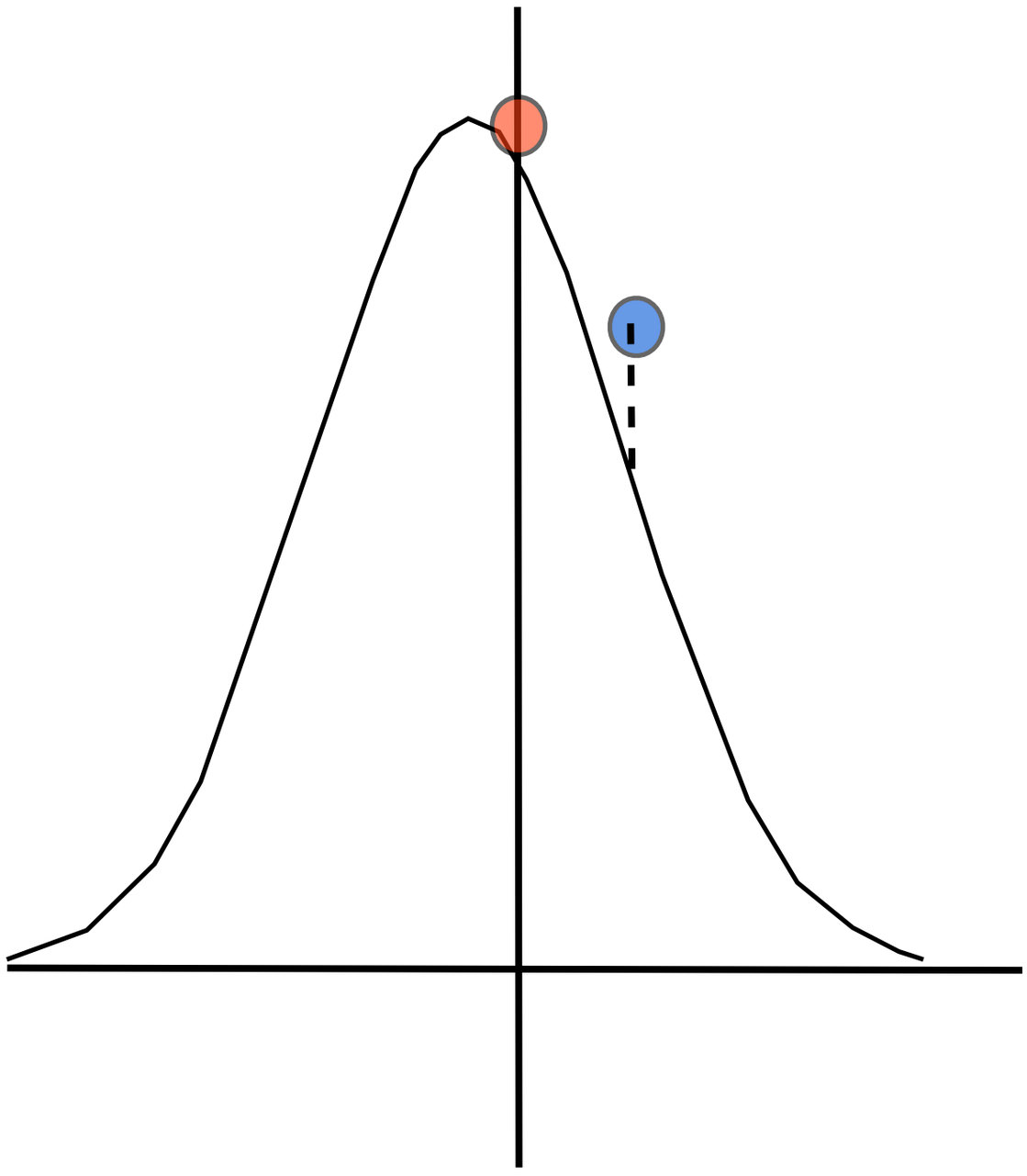

The red source sees a small reduction in the response of the telescope at its position.

However, sources at the edge of the beam (where the response of the beam is changing quickly) see a large reduction of the telescope response at their position.

This is difficult for self-cal to cope with - in its simplest form it assumes that a single telescope-based amplitude correction is a good description of the calibration problem.

What tends to happen in practice is that the self-cal corrections (solutions) are usually biased towards the position of the brightest source in the field.

There are other cases in which the amplitude and phase corrections vary across the field of view i.e. they are not only a function of time but also position (see eqn[7]):

$$g_i(t) \Longrightarrow g_i(t,\theta)$$

Radio astronomers talk about the "isoplanatic patch" - this is the angular size of a patch of sky for which the phase errors due to troposphere and/or ionopshere are highly correlated and can be considered to be identically the same.

We usually hope for this simple case (i.e. the one that current self-cal algorithms can cope with) where the field of view we wish to image is smaller than the isoplanatic patch.

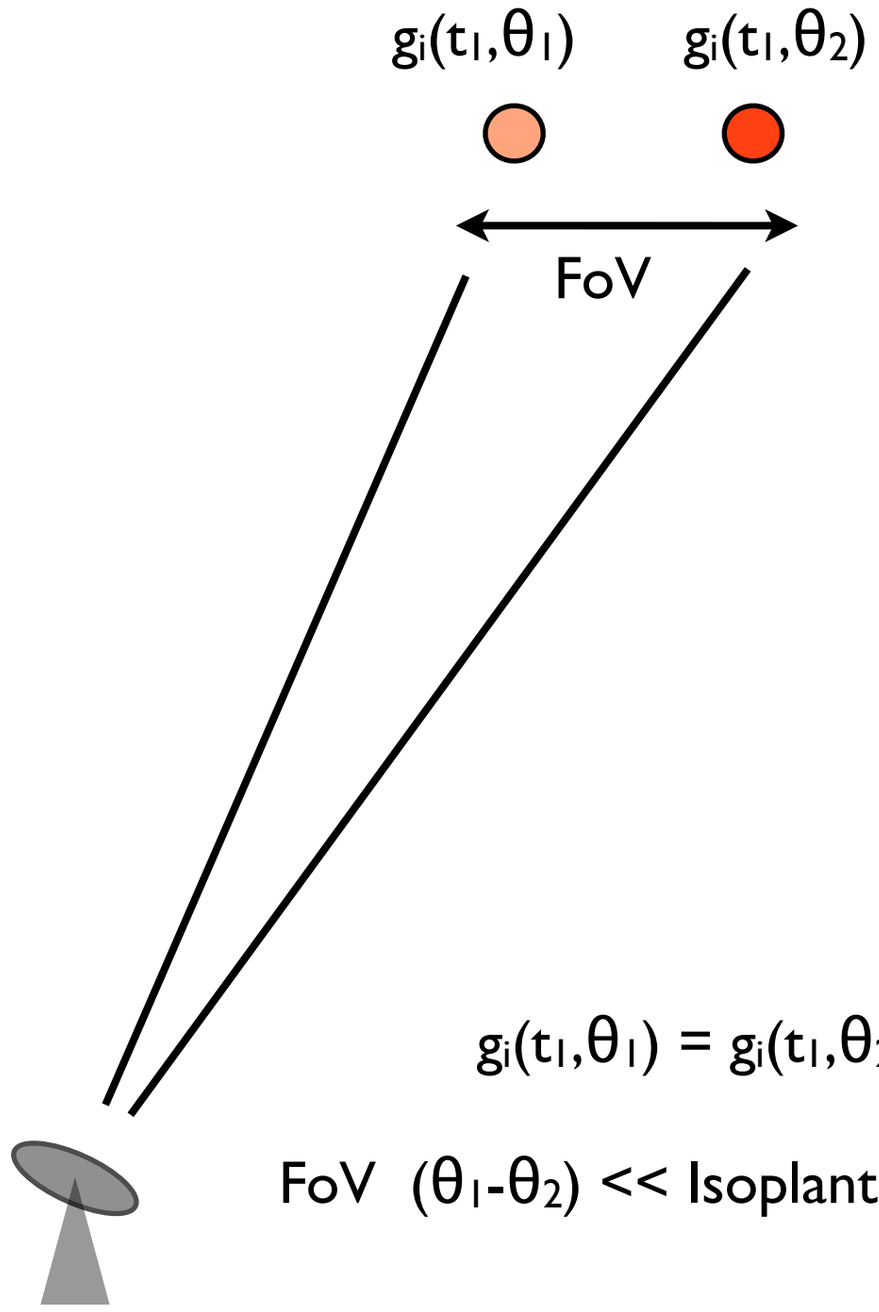

$g_i(t_1,\theta_1) = g_i(t_1,\theta_2)$

FoV $(\theta_1-\theta_2)$ << Isoplantatic patch

**

The case we wish to avoid:

$$g_i(t_1,\theta_1) \neq g_i(t_1,\theta_2)$$

FoV $(\theta_1-\theta_2)$ >> Isoplantatic patch

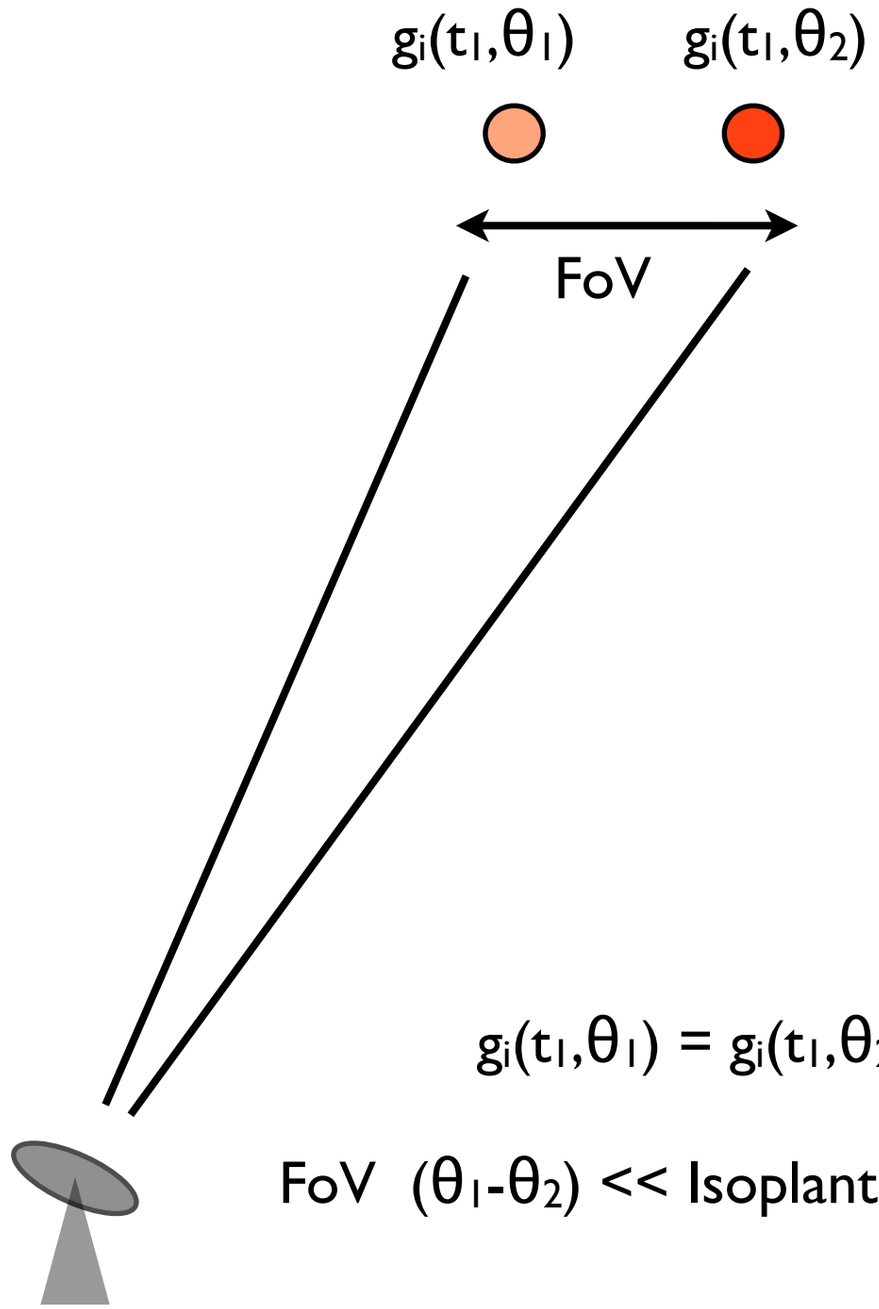

$$g_i(t_1,\theta_1) = g_i(t_1,\theta_2)$$

FoV $(\theta_1-\theta_2)$ << Isoplantatic patch

**

Reality is different: non-isoplanicity is a problem at low frequency (< few hundred MHz):

Field of view (telescope primary beam) is larger;

Ionosphere is far away (100's of km c.f. the troposphere);

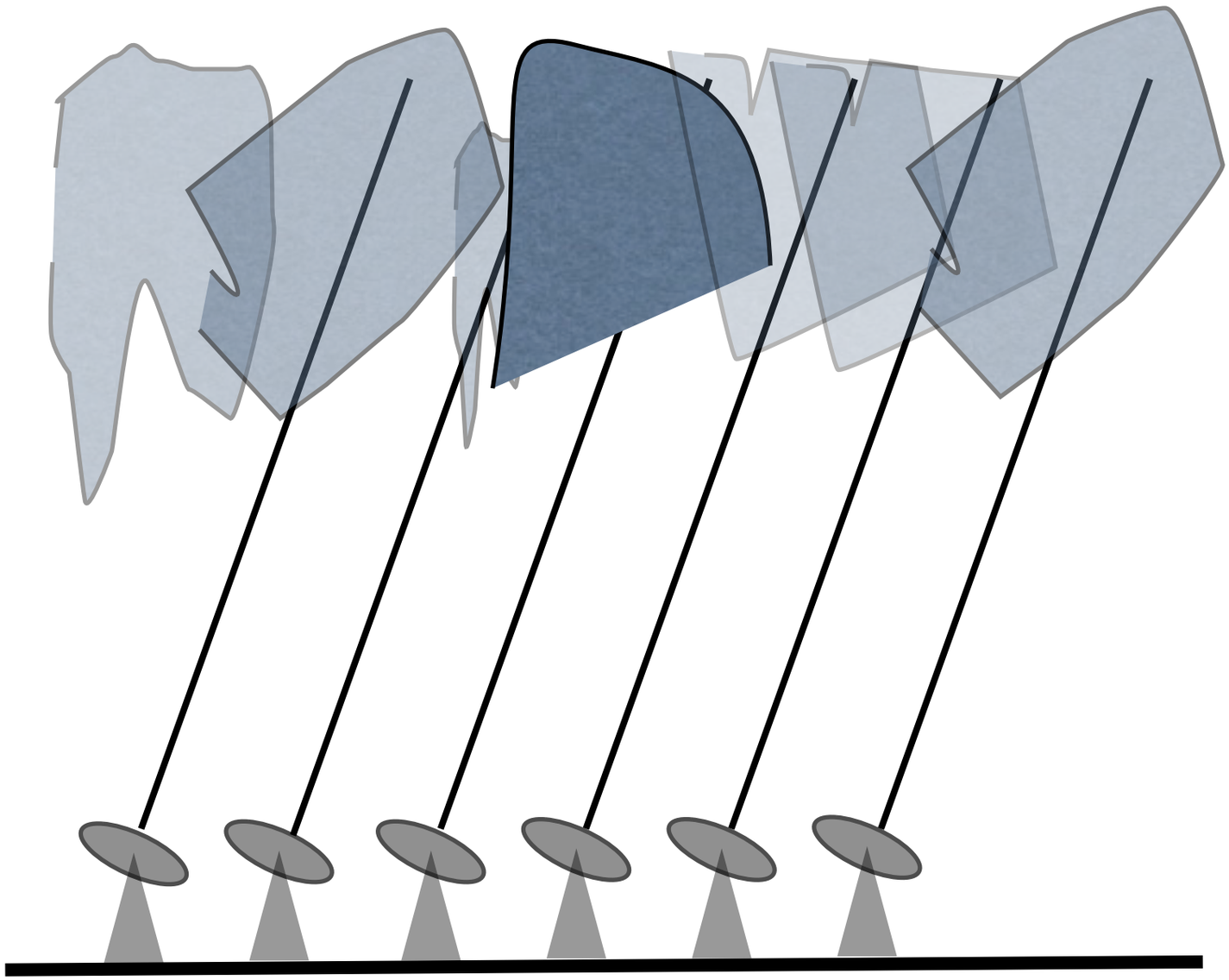

left: Isoplanatic patch size is < ~10 km;

Beam covers more than one patch typically;

Different patch over each antenna - even for relatively short baseline arrays.

Even at higher frequencies small errors (due to non-isoplanicity) or pointing errors may limit the dynamic range of very deep, high dynamic range images.

Currently a lot of work is going into developing new self-calibration algorithms for LOFAR and other low frequency telescope. These new algorithms attempt to solve for the telescope errors across the field of view in a consistent way. This should work (fingers crossed!) provided there are enough bright sources to adequately sample the field (this is work in progress!)

Pathological case (right): M82 and M81 - seperated by ~ 40 arcminutes - errors in the M82 field ripple into M81 field (N.B. this image has been self-cal'd and CLEANed! Observing frequency is 1.4 GHz, dynamic range is limited to 50:1 ! - image courtesy, Tom Oosterloo.

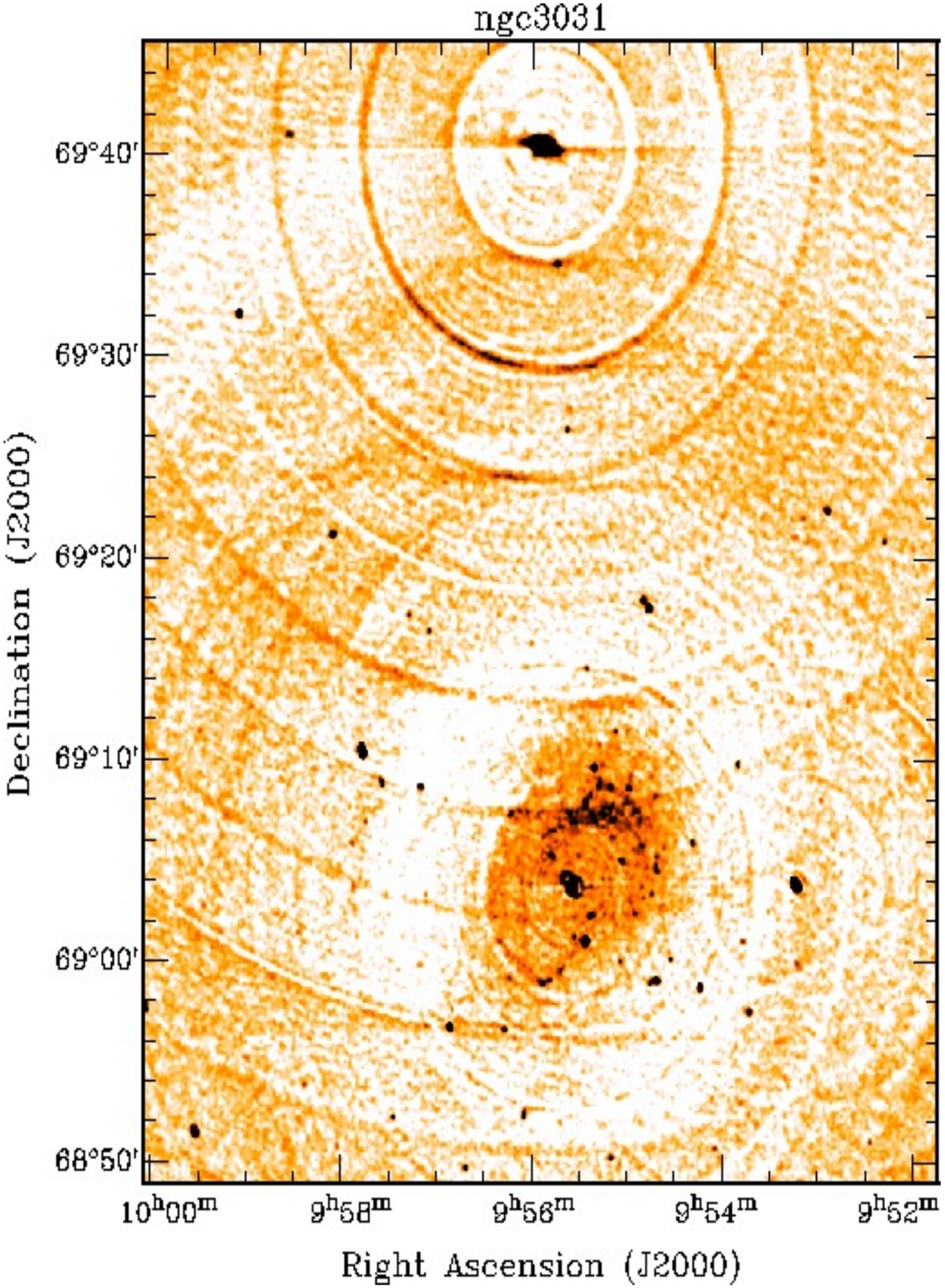

So even at higher frequencies small errors (due to non-isoplanicity) or pointing errors may limit the dynamic range of very deep, high dynamic range images.

A technique that is being used to correct for pointing errors (and other non-isoplanatic effects) is called "peeling" (google Tom Oosterloo).

The basic recipe is as follows:

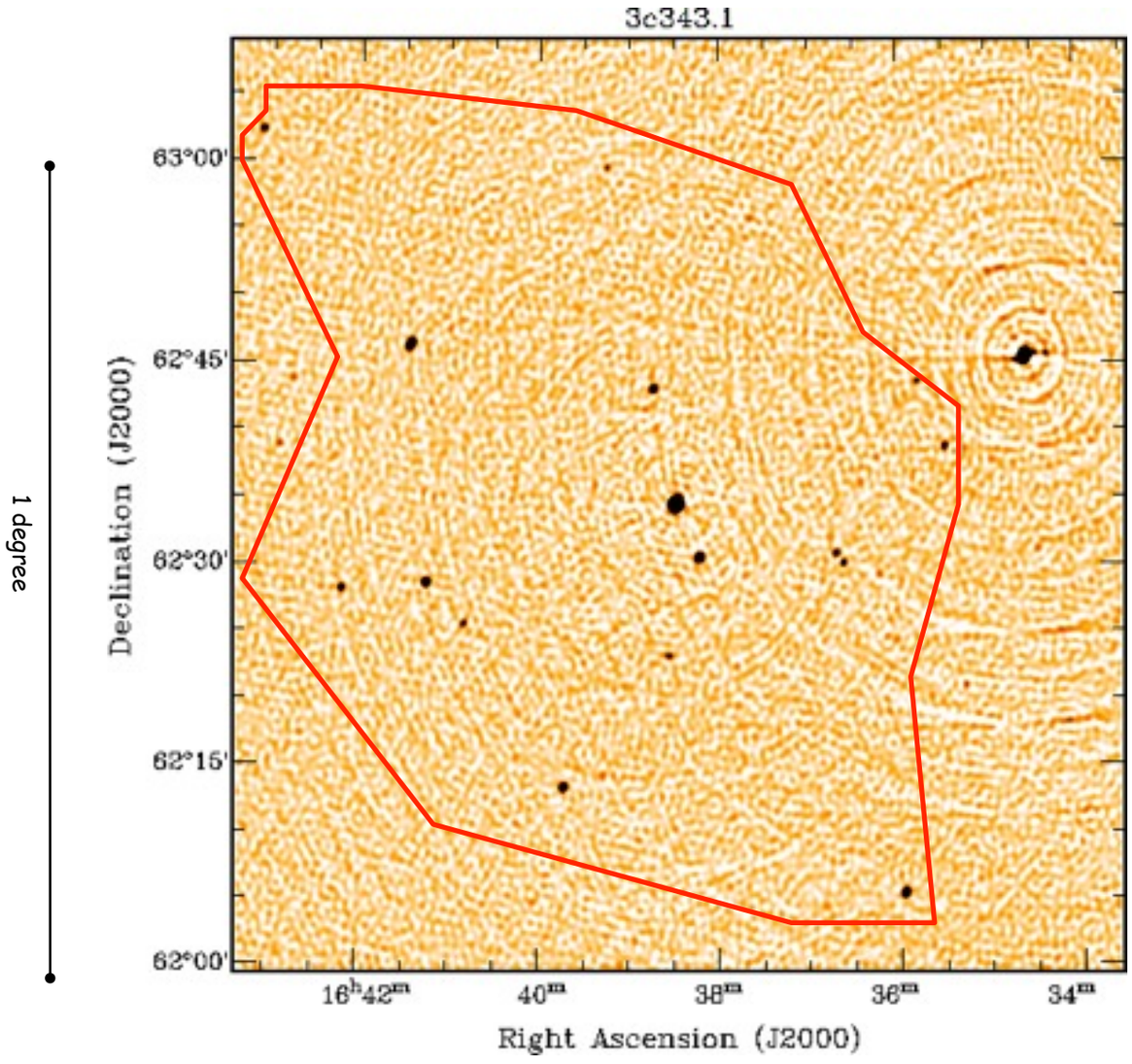

Self-cal full field

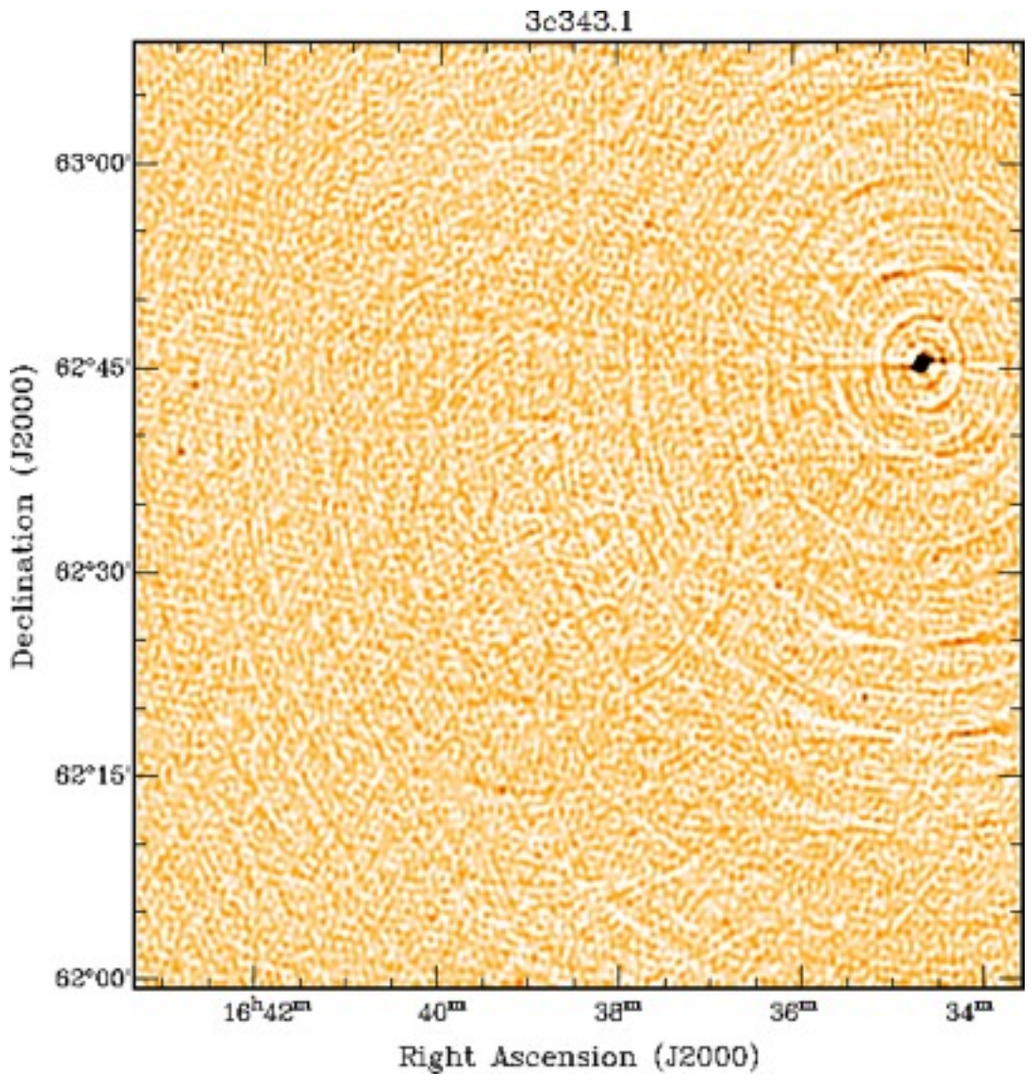

Subtract "central" sources - only one off-axis source is left

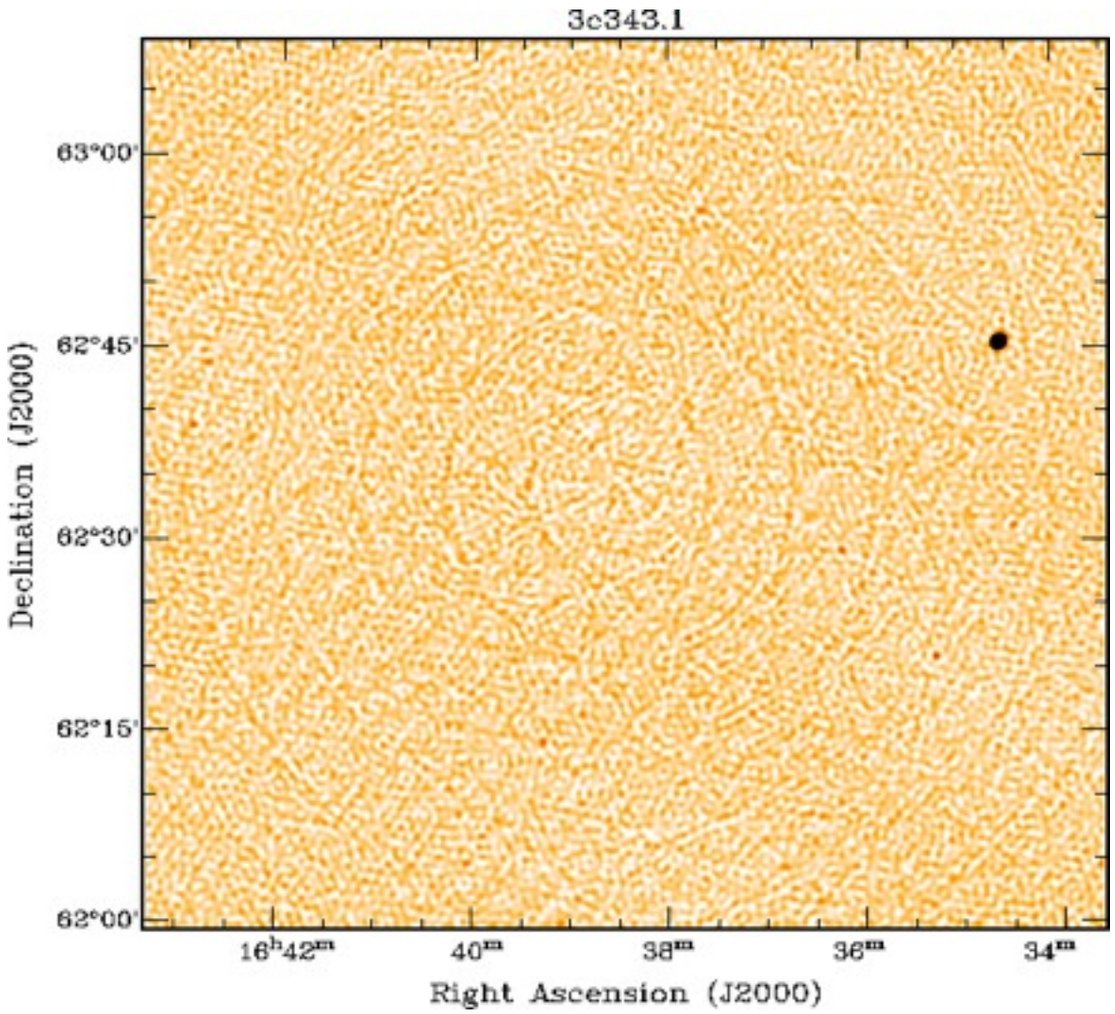

Self-cal on off-axis source, apply corrections and make image.

N.B. that errors previously associated with off-axis source have disappeared.

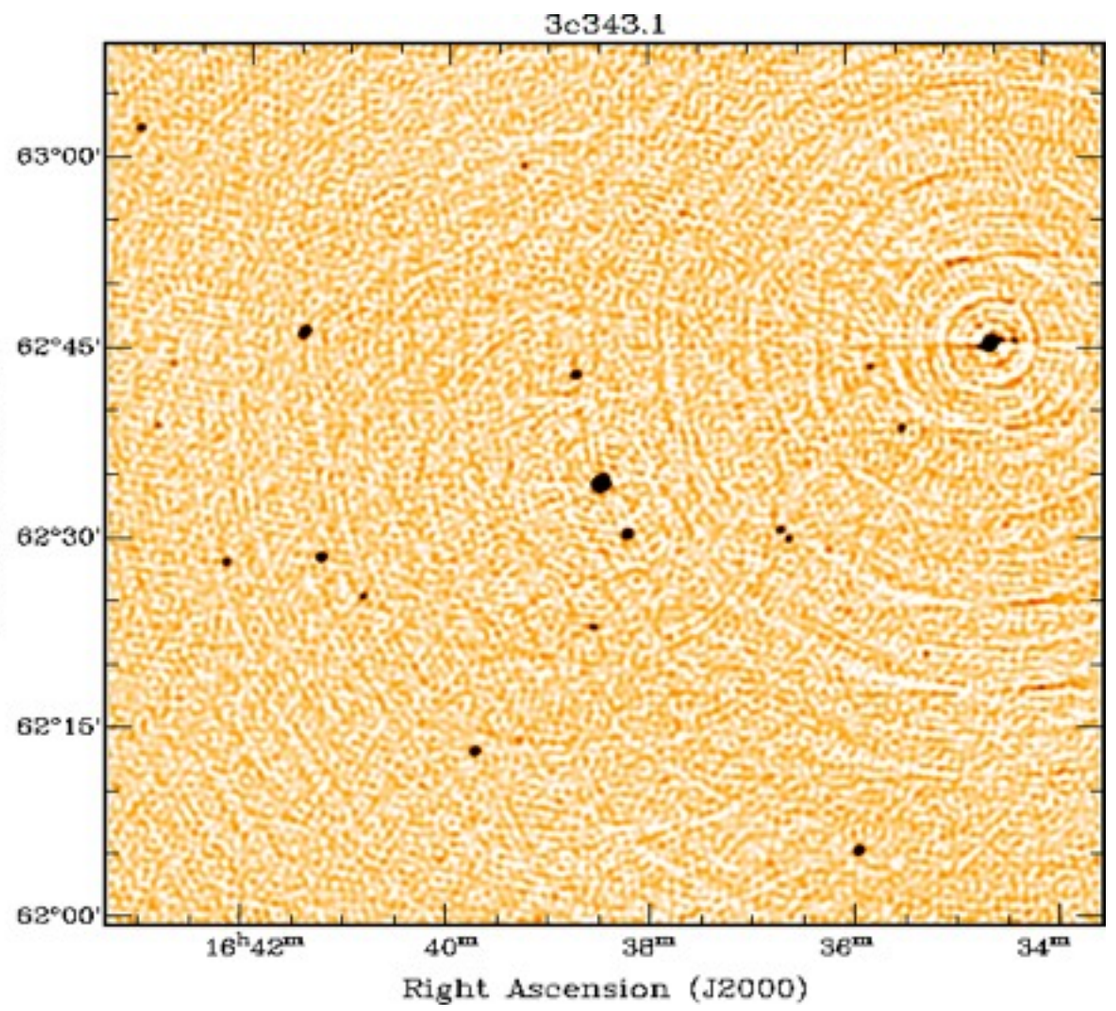

Apply corrections from off-axis source to the data - subtract out off-axis source from the data and undo corrections from off-axis source.

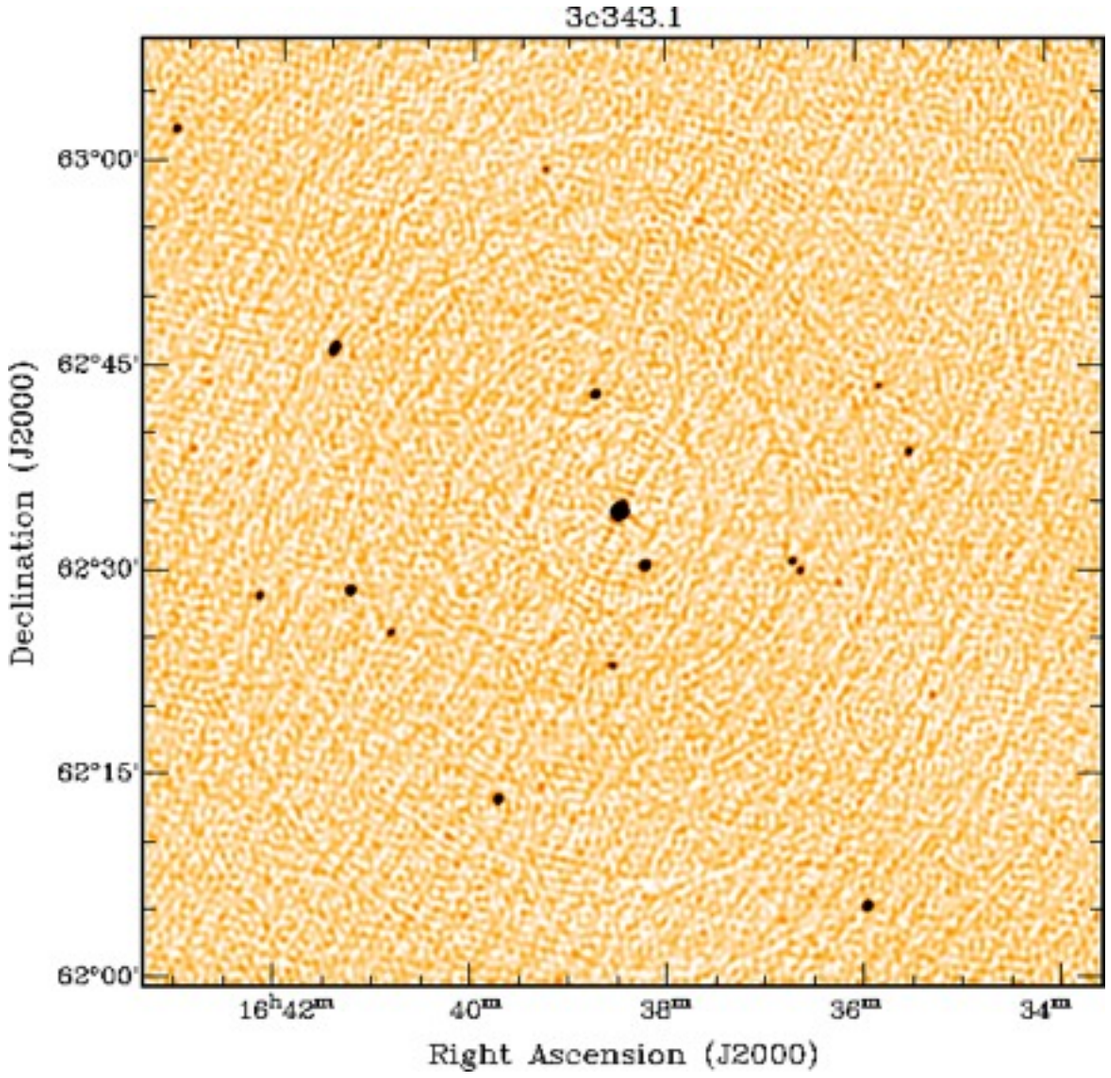

Make a new map - off-axis source is gone and its errors.

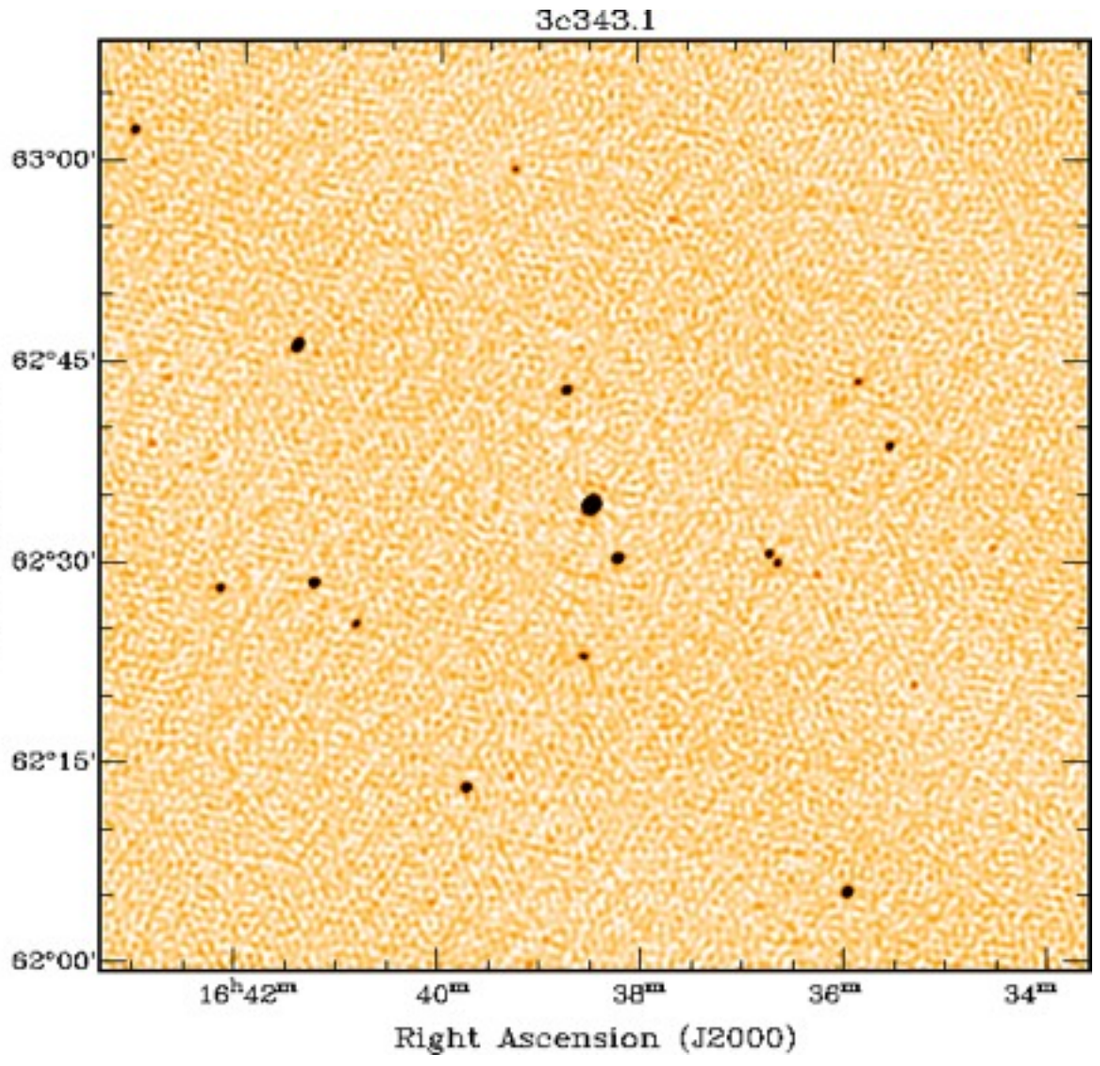

Self-cal data set, apply corrections and make new image

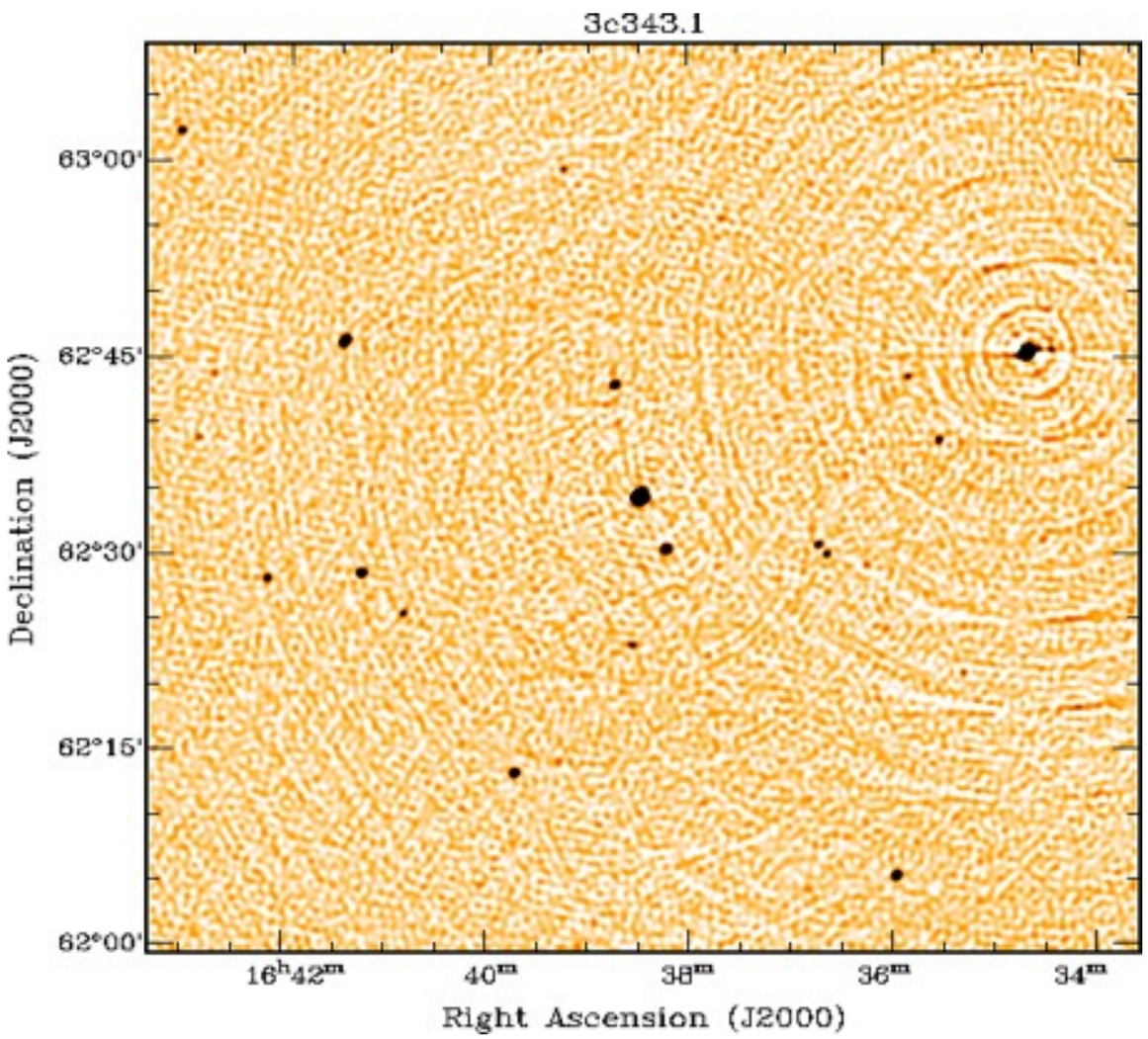

Original map of the field

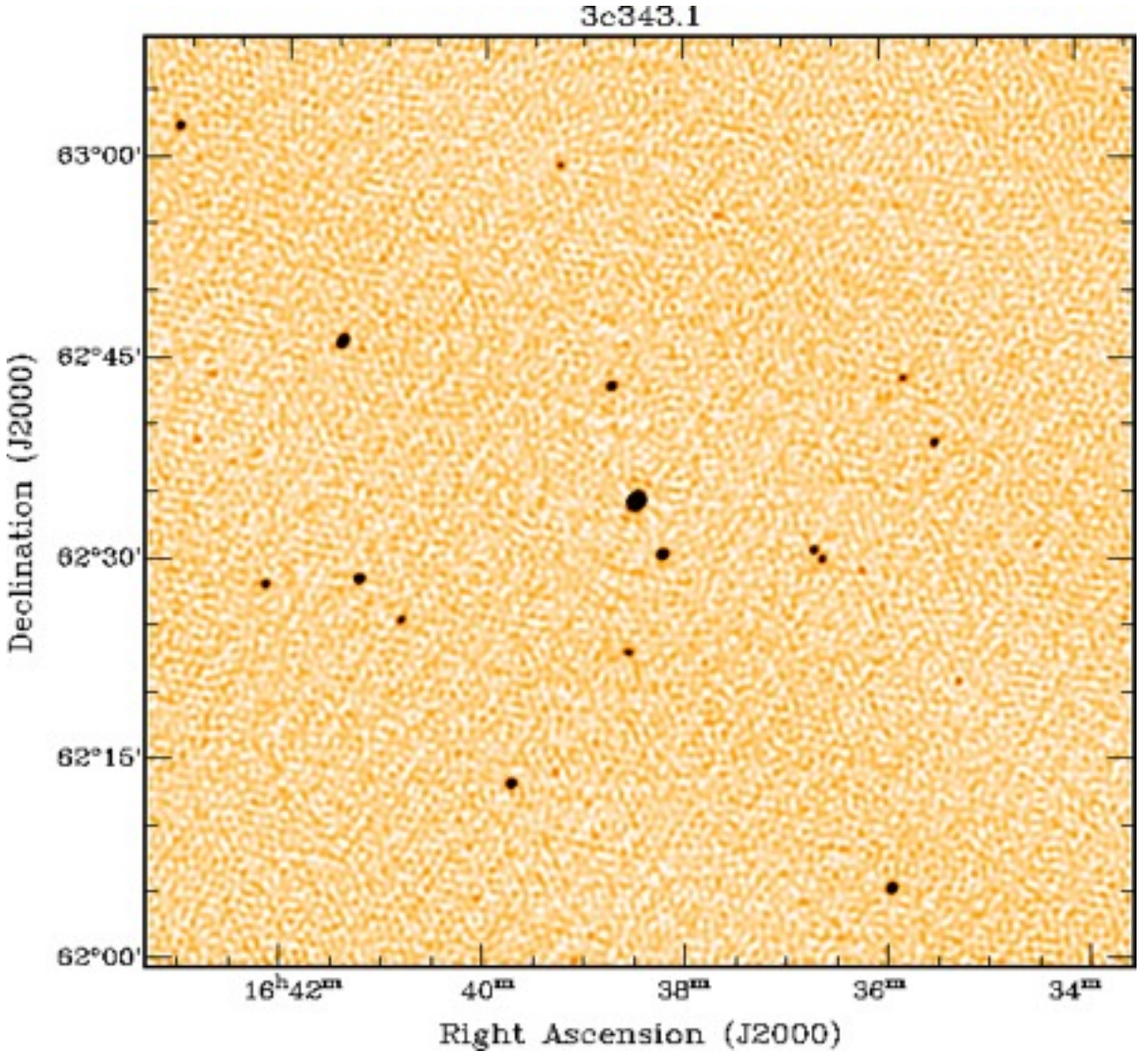

Final map after peeling

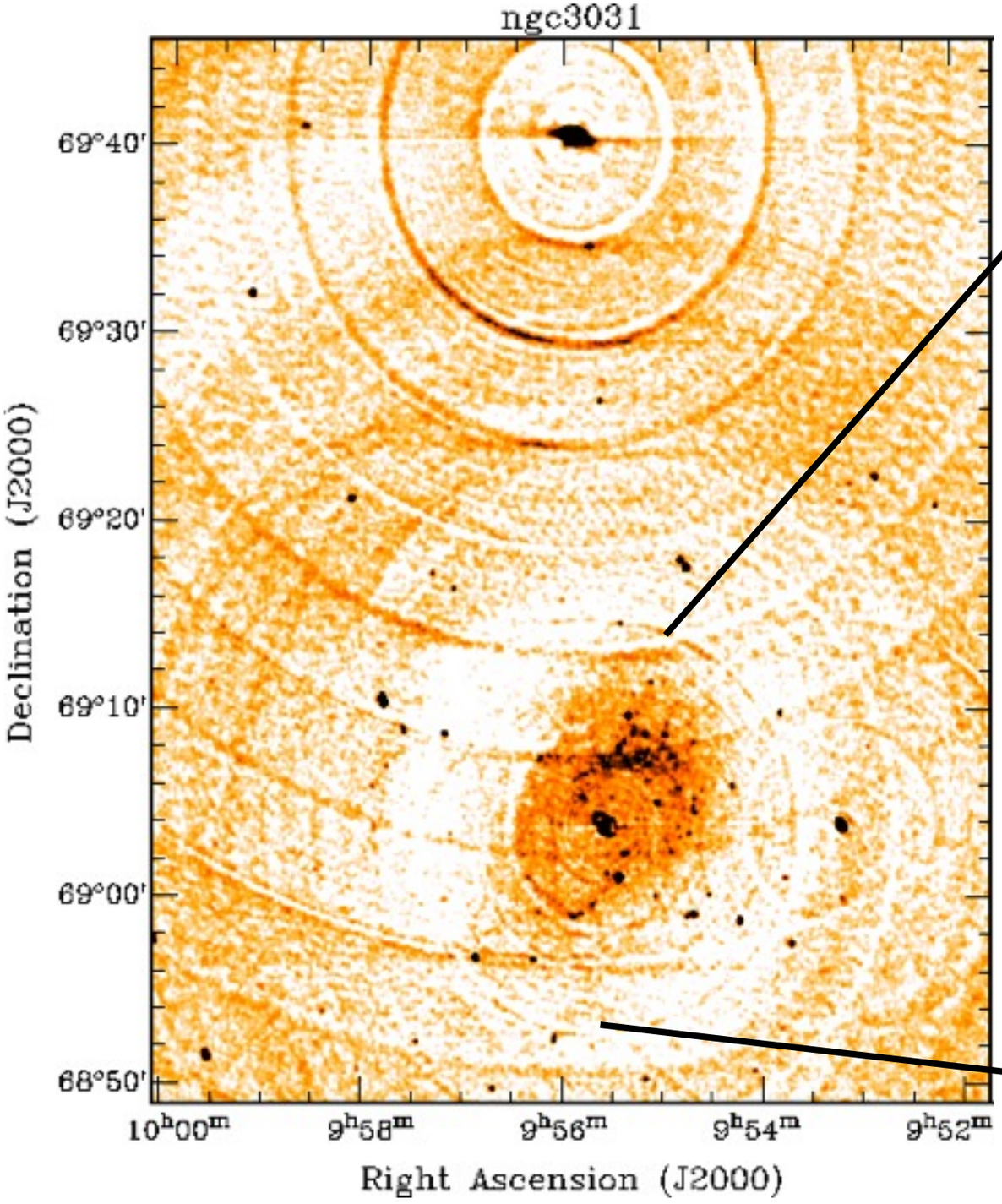

Original map of M82 and M81

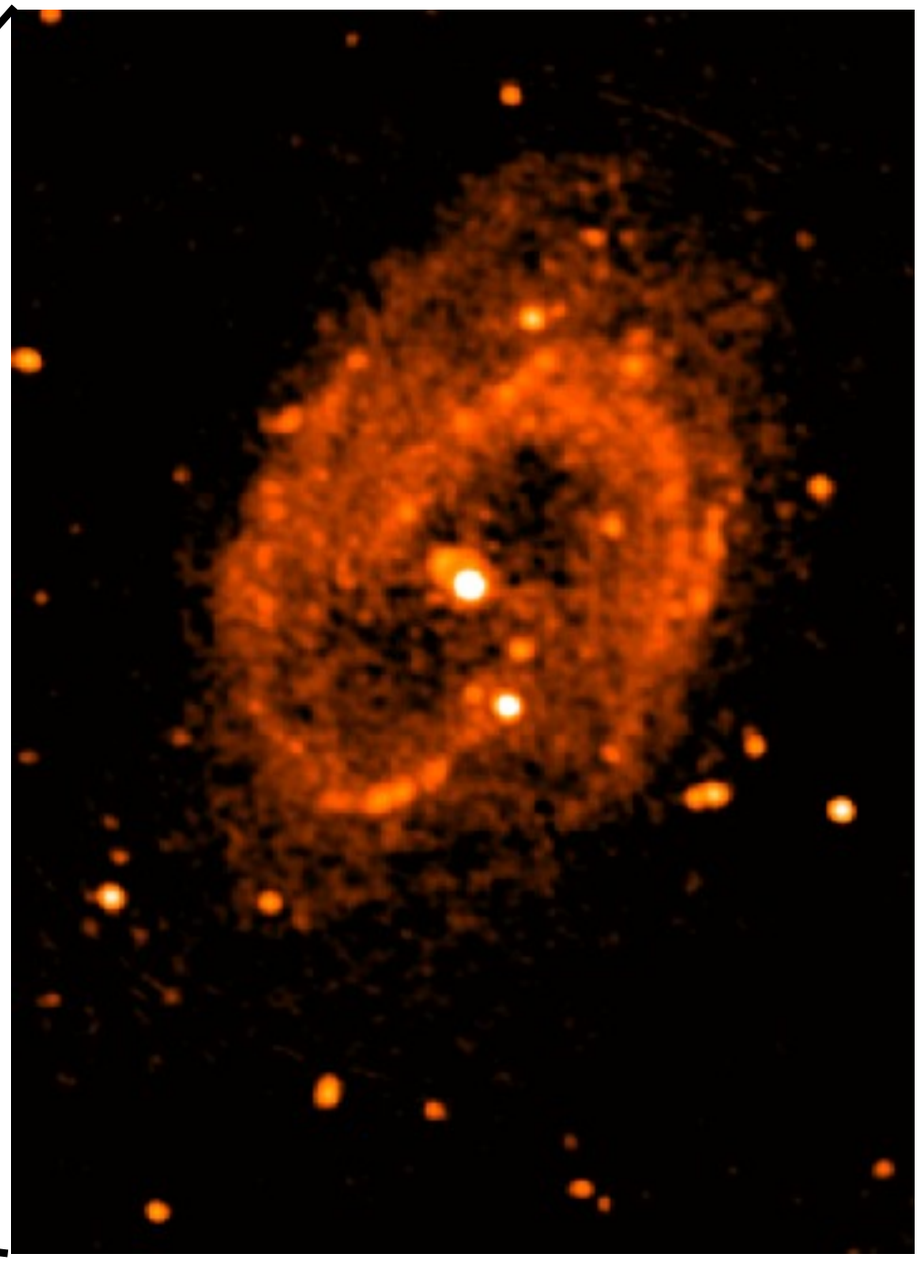

Final map of M81 after peeling - image reaches 15 microJy rms noise (~ expected thermal noise level).

All images courtesy of Tom Oosterloo